PHAM THI MAI PHUONG

STUDY ON THE IMPREGNATION PROCEDURES TO PREPARE CATALYTIC COMPLEXES FOR THE TREATMENT OF MOTORBIKE'S EXHAUST GASES

SUPERVISORS:
ASSOCIATED PROFESSOR. DOCTOR. LE MINH THANG
PROFESSOR. DOCTOR. ISABEL VAN DRIESSCHE

DOCTOR OF PHILOSOPHY THESIS: CHEMICAL ENGINEERING

Hanoi - 2013

Contents

LIST OF ABREVIATES

NO_x - Nitrogen oxide
THC - Total hydrocarbon
NMHC - Non-methane hydrocarbon
CO - Carbon monoxide
PM - Particulate matter
NO_2 - nitrogen dioxide
O_3 - ozone
PM10 - particulate matter less than 10 nm in diameter
SO_2 - sulfur dioxide
NO - nitrogen oxide
VOCs - volatile organic compounds
HC - Unburned hydrocarbons
TWCs - Three-way catalysts
A/F – Air to fuel
OSC - oxygen storage capacity
ACZ - $Al_2O_3 – CeO_2 – ZrO_2$ mixed oxides
CZ - $CeO_2 – ZrO_2$ mixed oxides
XRD - X-ray diffraction
BET - Brunauer, Emmett and Teller
SEM - Scanning electron microscopy
TGA - Thermogravimetric analysis
DTA - Differential thermal analysis
XPS - X-ray photoelectron Spectroscopy
CTAB - cetyl trimethyl ammonium bromide
SDS - sodium dodecyl sulfate
PEG - polyethylene glycol

CONTENT OF TABLES

CONTENT OF FIGURES

Acknowledgement

This Ph.D thesis has been carried out at the Department of Organic Synthesis and Petrochemistry, School of Chemical Engineering, Hanoi University of Science and Technology during the period July 2010 to September 2013. The work has been completed under the supervision of Assoc. Prof. Dr. Le Minh Thang and Prof. Isabel Van Driessche.

Firstly, I would like to express my deepest and most sincere gratitude to my promotors: Assoc. Prof. Dr. Le Minh Thang Prof. Isabel Van Driessche. They have been helping me a lot not only in the scientific work but also in my private life. Without their guidance, their encouragement, their enthusiastic and kind help, it would have been difficult to overcome the difficulties I met during the present work.

I want to thank my colleagues in the lab Environment friendly Materials and Technologies for their friendly attitude towards me and their help in my work.

I would like to thank all members of the Department of Inorganic and Physical Chemistry, especially the group of Solid State Chemistry for their support and guidance during the period I was in Belgium.

I am grateful to all the member in the Advanced Institute of Science and Technology for their help, and nice environment they created for me.

I especially want to express my sincere gratitude for the cooperation program between Flemish Interuniversity Council (VLIR) and Hanoi University of Technology (HUT) for the financial support for this study. I acknowledge to Prof. Isabel Van Driessche (Coordinator of the cooperation program) for the administrative help.

Finally, I lovingly thank my family for their love and encouragements during the whole long study period.

Summary

In this thesis the impregnation procedure to prepare catalytic complexes was studied to treat the motorbike's exhausted gases. Firstly, the substrate cordierite and different supports were prepared and characterized. Then, deposition methods were carried out to load support on substrates (cordierite and metal foils). From the best results, catalytic complexes was prepared and applied in motorbike.

With the aim of preparation of inexpensive catalytic complexes for Vietnam, the substrate cordierite was prepared from the domestic materials such as kaolin (exploited in Yen Bai), industrial MgO and Al_2O_3 and used three methods: solid-state reaction, conventional sintering and sol-gel. During calcinations at 1250^oC for 3 hour, the XRD patterns proved the formation of cordierite phase. However, the BET surface area and porosity of samples were not suitable for deposition. Thus, many additives as activated carbon, cellulose and dolomite were added to improve the disadvantages of cordierite substrates. Besides, the cordierite samples also were treated by acid solution before deposition for surface's improvement.

The support materials are one of the main components in the catalytic complexes' structure. For years, γ-Al_2O_3 has been used extensively in the catalyst application. Recently, $Ce_xZr_{1-x}O_2$ has been attracted attention of researchers in the world due to its excellent properties. And a new generation of support material Al_2O_3-CeO_2-ZrO_2 has been investigated. All three kinds of support materials were synthesized successfully and characterized by XRD, BET before the deposition process.

There are many methods to deposit the support material on the substrate, depending on the properties of the support and substrates, as well as the desired layer, the methods was chosen. For cordierite substrates, the deposition methods were in situ solid combustion, suspension, hydrid deposition secondary growth from seeding, double deposition consisted of wet impregnation and suspension; and for metal foils, dip-coating was used.

The last step of preparation the catalytic complex is loading the active phase on support/substrates by wet impregnation, and its catalytic activities were measured by micro-reactor connected with gas chromatography online.

For the application in motorbike, the cordierite was prepared in the form of honeycomb monolith. Then, the active phase was deposited on the substrate to produce the

catalytic complexes or three-ways catalysts. Afterward, they were installed into the exhaust tube of motorbike for the treatment of exhausted gases

Samenvatting

In deze thesis werd de synthese van katalysatoren voor de behandeling van uitlaatgassen van motorfietsen via een nieuwe impregnatiemethode bestudeerd. Eerst werden corderiet substraten en verschillende supports bereid en gekarakteriseerd. Daarna werden verschillende chemische depositiemethodes uitgetest om de support op de substraten (in huis gesynthetiseerde corderiet en commerciële metalen folies) aan te brengen. Op basis van deze resultaten, werden uiteindelijk volledig functionele katalysatoren gefabriceerd en getest in motorfietsen.

Vietnam, een ontwikkelingsland zijnde, met een enorm aantal, vaak oude, motorfietsen als belangrijkste vervoersmiddel, heeft nood aan goedkope katalysatoren om een drastische verbetering van de luchtkwaliteit, vooral in grote steden zoals Hanoi, te verzekeren. Daarom werd ervoor geopteerd om als substraat corderiet te gebruiken dat kan bereid worden vanuit materialen die allen in Vietnam zelf gemijnd worden : kaoline uit Yen Bai en industrieel MgO en Al_2O_3. Daartoe werden drie verschillende syntheseroutes verkend : Vaste stof reactie, conventioneel sinteren en sol-gel chemie. XRD analyse toont aan dat na sinteren voor 3 uur bij 1250 °C steeds de gewenste corderiet fase gevormd werd. Echter, het specifiek oppervlak van de verschillende samples bleek te laag. Daarom werden verschillende additieven zoals actieve kool, cellulose en dolomiet toegevoegd. Daarnaast werd het finale oppervlak van de samples ook behandeld met zuren om het oppervlak verder te verhogen.

Het support of drager materiaal is één van de belangrijkste componenten van een katalysator. Lange tijd werd vooral γ-Al_2O_3gebruikt. Recent echter werd heel wat onderzoek gevoerd naar het gebruik van $Ce_xZr_{1-x}O_2$ onder meer door de excellente zuurstof transport/opslag mogelijkheden van dit materiaal. Dit leidde tot de ontwikkeling van een nieuwe generatie drager materialen : Al_2O_3-CeO_2-ZrO_2. In deze thesis werden deze drie verschillende materialen succesvol gesynthetiseerd en volledig gekarakteriseerd XRD en BET analyse vooraleer ze aan te brengen op de geselecteerde substraten.

Erbestaan heel watverschillendemethodesomeendragermateriaal op eensubstraattecoaten. Voor de corderiet substraten werd geopteerd om via directe verbranding, suspensie routes, hybride routes via gecombineerde sol-gel en suspensie precursoren of meer geavanceerde depositiemethodes via bijvoorbeeld kiemgroei te werken. Voor de metalen folie substraten werd dipcoaten vanuit oplossingen gebruikt.

De laatste stap in de bereiding van de katalysatoren is dan het beladen met actieve fase (edelmetalen) via natte impregnatie. De katalytische activiteit van deze complexe structuren werd dan uiteindelijk bepaald via microreactor testen gekoppeld met online chromatografie.

Bij toepassing in motorfietsen wordt het corderiet meestal gebruikt als een honingraat monoliet. Ook op dergelijke structuren werd het substraat en de actieve fase afgezet om een werkzame driewegskatalysator te bereiden. Deze werden geïnstalleerd in de uitlaat van een motorfiets om de zuivering van uitlaatgassen onder reële omstandigheden te testen.

INTRODUCTION

Air pollution, especially from automobile exhaust gases, has become more and more serious problems over the world. In a developing country like Vietnam, with the tremendous increase of vehicles every year, it is urgent to control the emission which consisted of air pollutants as carbon monoxide (CO), nitrogen oxides (NO_x), unburnt hydrocarbon (HC), sulfur oxides (SO_x), volatile organic compounds (VOC),… for protection of air environment.

One of the most effective ways to control the vehicular pollution is catalytic converter which could treat simultaneously NOx, CO and HC. Most of catalytic converters contain three main components as substrate, support material and active phase. It is well-known that dispersion of rare metal as Pt, Pd, Rh on support material γ-Al_2O_3 had the best activity for the treatment of exhausted gases. Therefore, the commercial of catalytic converter has been produced with rare metals as active phase, γ-Al_2O_3 as support material and cordierite as substrate. Moreover, the addition of CeO_2 which has been proved to be an excellent promoter in the catalytic converters improved the catalytic activity for the treatment of NO_x, CO and HC.

However, the sensitive poisoning property and the cost of Pt-group is the reason for replacement of Pt-group by transition metals as active phase in catalytic converters. Many investigations both in the world and Vietnam proved the high ability of Co, Ni, Mn or Cu… for the conversion of CO, NO_x and HC. Thus, it is possible to prepare the inexpensive, effective catalytic converters for a developing country like Vietnam with the use of these transition metals.

The catalytic activity is influenced by not only the compositions of catalyst but also the deposition method for loading active phase, support material on substrates. It is obvious that the catalytic activity would be decreased sharply if the layer of active phase and support is detached from substrate's surface. Nevertheless, compared with the number of studies of catalyst's composition, the investigation on deposition method hasn't been attracted much attention. Thus, in this thesis, the method of impregnation process would be studied systematically to prepare the catalytic complexes.

The goal of this thesis is "**Study on the impregnation procedures to prepare catalytic complexes for the treatment of motorbike's exhaust gases**". The thesis includes three parts. The first part summarizes the aspects about the catalyst converter, and the preparation of catalyst in the literature. The second part describes the synthesis of separated components as substrate, supports, the method to prepare the complete catalyst and introduces basic principles of the physico-chemical methods used in the thesis.

The third part is focused on the characterization of prepared substrate, support, and the influence of different deposition method for loading support on substrates, the catalytic activity of catalysts.

Final is the general conclusions of the performed work.

1. LITERATURE REVIEW

1.1 Air pollution caused by vehicles emission

1.1.1 Over the world and in Vietnam

With the rapid growth of the number of vehicles in operation, the air pollutants emitted from these vehicles have contributed to urban air pollution in recent years, especially in large cities such as Sao Paulo, Detroit, and Tokyo…. In New York, the fine PM concentrations on mornings with traffic were 58% higher than mornings without traffic in 2011. A model simulation indicated that the contribution of NO_2 from vehicular sources accounted for a range of 9% to 39% of that concentration in atmosphere. In China, vehicle emissions in Beijing contributed to approximately 71%–85% of the total CO concentration, 67% –71% of the total NO_x concentration, and 26%–45% of total VOCs emission amount. NO_x emissions from vehicles accounted for 35.4% to 75.7% of the total emissions. The transportation sector has become a major source of urban air pollution. Therefore, it is necessary to control air pollutants emitted from vehicles [1].

Recently, the number of vehicles in Vietnam has increased tremendously. In 2013, there are 1 million and 500 thousands cars, over 37 million of two and three-wheels motorcycles, so annually, 100 thousand cars and 3 million motorcycles have been joined the traffic system, creating great pressure on air environment, especially in urban areas such as Hanoi, Ho Chi Minh City [2]. In regards to the air environment in urban areas, air pollution caused by traffic activities account for about 70% (Ministry of Transport, 2010). it is estimated that traffic activities contribute nearly 85% of CO emission and 95% of VOCs, 30% of NO_2. In consideration of different means of transport, the emission volume from motorcycles is quite low, being on average as little as a quarter of the emission volume of car transport. However, due to the higher number of motorcycles and their often poor quality, motorcycles are the main contributor of contaminants, especially of CO and VOC. Meanwhile, trucks and buses release larger volumes of SO_2 and NO_2 [3].

Therefore, it is urgent apply the European emission standard to control the emission of vehicles. European emission standards define the acceptable limits for exhaust emissions of new vehicles sold in European member states. So, emissions of nitrogen oxide (NO_x), total hydrocarbon (THC), non-methane hydrocarbon (NMHC), carbon monoxide (CO) and particulate matter (PM) are regulated for most vehicles, including cars, motorcycle, trucks ... For each vehicle type, different standards apply. Now, the Euro 5 has been applied with the limits of toxic emission from motorcylce as the following table 1.1 [4].

Table 1.1: European Emission Standard

Standard	Size	Wheel configuration	CO (g/km)	HC(g/km)	NO_x(g/km)
Euro 2	< 150 cc	2	5.5	1.2	0.3
	≥ 150 cc	2	5.5	1	0.3
Euro 3	< 150 cc	2	2.0	0.8	0.15
	≥ 150 cc	2	2.0	0.3	0.15
Euro 4		2	1.14	0.38	0.7

Euro 5		2	1	0.1	0.06

Vietnam's current emissions limits for two- and three-wheelers, referred to as Type 2 standards, are equivalent to Euro 2 standards. These regulations were implemented via Government Decision No: 249/2005/QĐ-TTg, 10 October 2005. Two- and three-wheelers must meet Euro 2 standards beginning 1 July 2007 [5].

Vietnam planned to apply future Policies as following:

- Type 3 - Standards (~Euro 3) are to be in place by 1 January 2017.
- Type 5 - Vietnam will skip Type 4 (~Euro 4) standards and move ahead to Type 5 (~Euro 5) Standards starting 1 January 2022.

At the present, emission standard for Vietnam vehicles in volume percentage are required as in table 1.2.

Table 1.2: Emission Standards for in-used vehicles in Vietnam

Toxic emission	Vehicle types					
	Cars			Motorcycles		
	Level 1	Level 2	Level 3	Level 1	Level 2	Level 3
CO (% vol):	4.5	3.5	3.0	4.5	3.5	2.5
HC (ppm vol):						
Four strokes	1200	800	600	1500	1200	800
Two strokes	7800	7800	7800	10000	7800	7800

- For the motorcycles has non-controlled exhaust emission treatment system
  - Level 1 for motorcycles with first registration date before 1 July 2008;
  - Level 2 for motorcycles with first registration date from 1 July 2008;
- For the motorcycles has controlled exhaust emission treatment system
  - Level 3 is applied.

1.1.2 Air pollutants from emission

The major criteria pollutants are carbon monoxide (CO), nitrogen dioxide (NO_2), ozone (O_3), particulate matter less than 10 nm in diameter (PM10), sulfur dioxide (SO_2), and lead (Pb). Ambient concentrations of NO_2 are usually controlled by limiting emissions of both nitrogen oxide (NO) and NO_2, which combined are referred to as oxides of nitrogen (NO_x). NO_x and SO_2 are important in the formation of acid precipitation, NO_x and volatile organic compounds (VOCs) can real react in the lower atmosphere to form ozone, which can cause damage to lungs as well as to property [6]. In addition, PM also affect the lung when inhaling. Carbon monoxide is mostly emitted from mobile sources (up to 90%). The high levels of carbon monoxide found in traffic congested areas (20 - 30 mg/m^3) can lead to levels of 3% carboxyhemoglobin. These levels can produce adverse cardiovascular and neurobehavioural effects and seriously aggravate the condition of individuals with ischemic heart disease. The toxic benzene, … in the VOCs cause cancer [7].

Due to incomplete combustion in the engine, there are a number of incomplete combustion products. Typical exhaust gas composition at the normal engine operating conditions is [8]:

• Carbon monoxide (CO, 0.5 vol. %);

- Unburned hydrocarbons (HC, 350 vppm);
- Nitrogen oxides (NO_x , 900 vppm);
- Hydrogen (H_2, 0.17 vol. %);
- Water (H_2O, 10 vol. %);
- Carbon dioxide (CO_2, 10 vol. %);
- Oxygen (O_2, 0.5 vol. %);
- Sulfur dioxides (SO_2 0.01% vol):
- Particulate matter (PM10 0.05% vol).

HC, CO and NO_x are the major exhaust pollutants. HC and CO occur because the combustion efficiency is <100% due to incomplete mixing of the gases and the wall quenching effects of the colder cylinder walls. The NO_x is formed during the very high temperatures (>1500 ◦C) of the combustion process resulting in thermal fixation of the nitrogen in the air which forms NO_x [8].

1.1.3 Solutions for air pollution

Because of the large vehicle population, significant amounts of HC, CO and NO_x are emitted to the atmosphere, it is extremely urgent to treat the exhaust gases before emission to the environment. There have been many ways to convert these toxic compounds to harmless ones, such as treating separated pollutants by catalyst or simultaneously by three-ways catalyst.

1.1.3.1 Separated treatments for pollutants

i. CO treatments

Method 1: Carbon monoxide can be converted by oxidation:

$CO + O_2 \longrightarrow CO_2$

The catalysts base on noble metals [9, 10]. Moreover, some transition metal oxides (Co, Ce, Cu, Fe,W, Mn) can be used for treating CO [11, 12].

Method 2: water gas shift process can converted CO with participation of steam:

$CO + H_2O \longrightarrow CO_2 + H_2 \quad \Delta H^0_{298K} = -41.1$ kJ/mol

This reaction was catalyzed by catalysts base on precious metal [13].

Method 3: NO elimination:

$NO + CO \longrightarrow CO_2 + ½ N_2$

The most active catalyst is Rh [14]. Besides, Pd catalysts were applied [15]

ii. VOCs treatments

Some control technologies were used to treat VOCs as thermal oxidizers by passing organic compounds through high-temperature environments in the presence of oxygen, or adsorption which rely on a packed bed containing an adsorbent material to capture the VOCs. Condensers are also used to reduce the concentrations of VOCs by lowering the temperature of the emission stream, thereby condensing these compounds. Another method is bio-filters relying on microorganisms to feed on and thus destroy the VOCs. And catalytic oxidizers use a catalyst to promote the reaction of the organic compounds with oxygen, thereby requiring lower operating temperatures and reducing the need for

supplemental fuel. Destruction efficiencies are typically near 95%, but can be increased by using additional catalyst or higher temperatures (and thus more supplemental fuel) [16].

iii. NO_x treatments

NO_x formed by the combustion of fuel in air is typically composed of greater than 90% NO, with NO_2 making up the remainder. Unfortunately, NO is not amenable to flue gas scrubbing processes, as SO_2 is. An understanding of the chemistry of NO_x formation and destruction is helpful in understanding emission-control technologies for NO_x.

Because the rate of NO_x formation is so highly dependent upon temperature as well as local chemistry within the combustion environment, NO_x is ideally suited to control by means of modifying the combustion conditions. There are several methods of applying these combustion modification NO_x controls, ranging from reducing the overall excess air levels in the combustor to burners specifically designed for low NO_x emissions [16]. NO_x can be treated by some reductions occurred in exhaust gas such as CO, VOCs or soot with using noble metal, perovskite catalysts and metallic oxide systems [17, 18,19].

1.1.3.2 Simultaneous treatments of three pollutants

i. Two successive converters

It can be treated simultaneously three pollutants (NO_x, CO, HC) by designing successive oxidation and reduction converters. The main reactions in treatment process are:

Reduction reaction: $NO \rightarrow \frac{1}{2} N_2 + \frac{1}{2} O_2$

Oxidation reactions: $CO + \frac{1}{2} O_2 \rightarrow CO_2$

$C_xH_y + (x+y/4) \rightarrow x\, CO_2 + y/2\, H_2O$

Steam formed in process reacts with CO to form CO_2 and H_2. Thus, some by-reactions occur:

$CO + H_2O \rightarrow CO_2 + H_2$

$NO + 5/2\, H_2 \rightarrow NH_3 + H_2O$

$NH_3 + 5/4\, O_2 \rightarrow NO + 3/2\, H_2O$

In this method, reduction converter only operates well in excess fuel condition. Furthermore, NH_3 can be formed in reduction condition. This pollutant will be converted into NO-another pollutant in oxidation media [20].

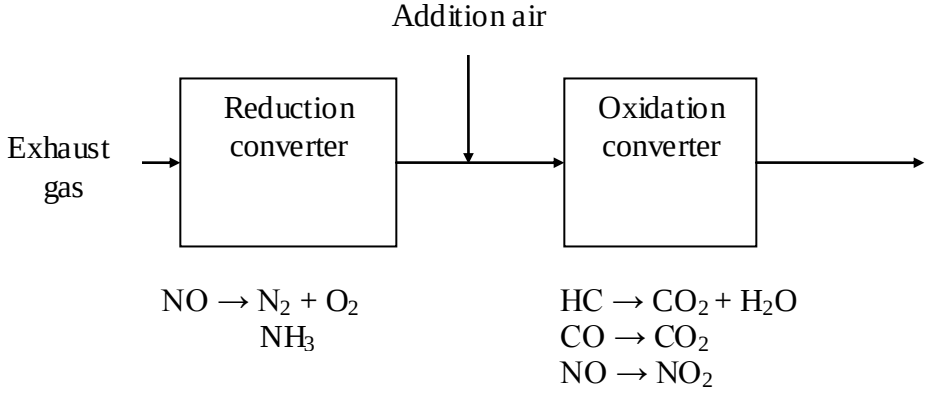

Fig.1.1: Scheme of successive two converter model [20]

ii. Three-way catalytic (TWC) systems

The basic reactions for CO and HC in the exhaust are oxidation with the desired product being CO_2, while the NO_x reaction is a reduction with the desired product being N_2 and H_2O. A catalyst promotes these reactions at lower temperatures than a thermal process giving the following desired reactions for HC, CO and NO_x:

Oxidation:

$C_yH_n + (1+ n/4)O_2 \rightarrow yCO_2 + n/2\ H_2O$

$CO + ½\ O_2 \rightarrow CO_2$

$CO + H_2O \rightarrow CO_2 + H_2$

Reduction:

$NO\ (or\ NO_2) + CO \rightarrow ½\ N_2 + CO_2$

$NO\ (or\ NO_2) + H_2 \rightarrow ½\ N_2 + H_2O$

$(2 + n/2)\ NO\ (or\ NO_2) + C_yH_n \rightarrow (1+n/4)\ N_2 + yCO_2 + n/2\ H_2O$

There are some common components, which represent the state-of-art of the composition:

• Cordierite ceramic or metal foil as popular substrate.

• Alumina, which is employed as a high surface area support. CeO_2–ZrO_2 mixed oxides, principally added as oxygen storage promoters. Barium and/or lanthanum oxides as stabilizers of the alumina surface area

• Noble metals (Rh, Pt and Pd) as active phases [8].

1.2 The catalytic converter

The three-way catalytic monolith converter for abatement of automobile emissions operated inherently in a transient regime is the most common multifunctional reactor. Here oxidation of CO and hydrocarbons and reduction of nitrogen oxides (NO_x) take place simultaneously in the complex porous structure of catalytic washcoat layer, which is formed by γ -Al_2O_3 support (alumina) with dispersed crystallites of noble metals (typically Pt and Rh) as catalytic sites, particles of oxygen storage materials (CeO_2 or mixed Ce-Zr oxides) and stabilizers of surface structure (e.g. oxides of Ba and La). Storage (deposition) and release of different exhaust gas components, reaction intermediates and products take place concurrently with reactions on specific sites on the washcoat surface. Not only chemisorption of gas components on noble metal sites (Pt, Rh), but also oxygen storage on ceria and zirconium compounds, CO_2 and HC adsorption on γ-Al_2O_3 support and other adsorption processes participate in TWC operation. They become important in the transient regime, when inlet flow rate, temperature and concentrations of components vary with time (e.g. city driving) [21, 22].

The three-ways catalysts have three main components as substrates, support materials and active phase as following figure.

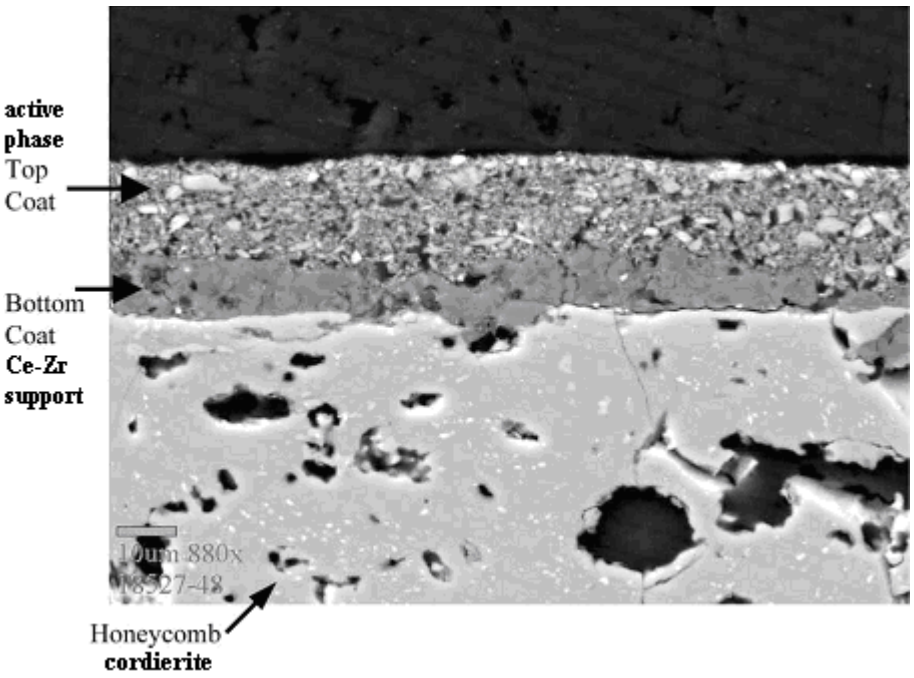

Fig.1.2: Structure of three-ways catalyst

The top of the catalyst is the catalytic phase where the reactions happen. The rare metallic elements such as Pt, Pd and Rh has been used for a long time for the application of catalyst, but now, peroskite, and transition metals (Cu, Ni, Mn, Co…) has attracted the attention for its high efficiency and low cost. As mentioned above, the γ-Al_2O_3 plays an important role of dispersion noble metals' crystallite as catalytic sites. Thus, γ-Al_2O_3 has been used as the most popular support material for years. However, the excellent properties of CeO_2 or $Ce_xZr_{1-x}O_2$ make this substance plays not only as the support material but also a part of active phase. The essential component of three-ways catalyst is monolith. This monolith has been prepared in the form of honeycomb for the low pressure drop. Cordierite and metal foil were chosen to produce monolith because they have high mechanical strength, can stand high temperatures and temperature shocks, and has a low thermal expansion coefficient.

1.2.1 Substrates

The first success of the monolithic catalyst was in the automobile exhaust treatment. After that, other applications became available, the environmental ones being by far those most demanded. The following environmental applications have been listed as: three-way catalysts; diesel catalysts for the abatement of liquid particulate (soluble organic fraction) and CO, HC; O_3 abatement in aircraft; … [23]. The monolithic reactors have clear advantages over the conventional slurry and fixed-bed reactors, especially in application of automobile exhaust treatment, because of low pressure drop, high thermal stability, easy preparation…. [24]

1.2.1.1 Ceramic monoliths

First, the (most commonly used) porous ceramic material is easier to use as a catalyst support than the metal of the conventional structured packings (the bonding of the catalyst to the support material is more facile). When coating metal supports with a catalyst

or catalyst support material, an intermediate layer of a ceramic material is often used for a better binding. Second, the cost of monolithic supports is relatively low, mainly due to the large-scale production for the automotive industry. The cost for a basic monolithic structure can be as low as US$ 3 per dm^3, mainly due to the relatively simple production method (i.e. via an extrusion process) [24].

In the application of a monolithic catalyst, one should first determine what the requirements for the support are. The most common material for monolithic structures is cordierite (a ceramic material consisting of magnesia, silica, and alumina in the ratio of $2MgO.2Al_2O_3.5SiO_2$), because this material is very well suited for the requirements of the automotive industry. The main reasons for this are that it has a high mechanical strength, can stand high temperatures and temperature shocks, and has a low thermal expansion coefficient [24].

Other materials whose ceramic monolith structures are commercially available are mullite (mixed oxide of silica and alumina, ratio 2:3) and silicon carbide. Disadvantages of all these materials are that, similar to cordierite, they have a low specific surface area (e.g., for cordierite, typically 0.7 m^2/g), they are rarely used as support materials for conventional catalysts, and the metal – support interaction is usually very low. Monolithic elements out of carbon, silica, and γ-alumina are available as research samples and can be produced once a significant demand exists. For these materials, surface areas of 200 m^2/g are easily available; the mechanical strength, however, is significantly lower than that of cordierite. The most important characteristics of ceramic monoliths are listed in table 1.3 [24].

Table 1.3: Characteristic properties of Cordierite

Cell density (cpsi)	25 - 1600
Pore volume (Hg porosimetry, mL/g)	0.19
Pore volume (N_2 BET, mL/g)	-
Surface area (N_2 BET, mL/g)	≤4

As the cordierite mineral is not abundant, for industrial production usually it has to be synthesized. Thus, there are many raw materials that may be used for the preparation of cordierite monoliths where the employment of aluminum silicates, such as kaolin or clays, and the use of talc together with alumina is frequent. The simplest composition is a mixture of kaolin and talc that can be kneaded with the aid of a dispersant (sodium lignosulfate), an agglomerant (polyvinyl alcohol) and a lubricant (water). The paste is extruded, dried and subsequently calcined at 1300◦C for 2h. Nevertheless, in the majority of the procedures described in patents over the preparation of monoliths from mixtures of precursors and their posterior cordierisation, three or more components are utilized in proportions that are adequate to obtain a SiO_2:Al_2O_3:MgO ratio equal to 51.4:34.9:13.7 (ratio of weight), that is close to that corresponding to cordierite, the most frequently used being mixtures of talc + kaolin or clay + aluminum hydroxide [23].

Talc is present in the composition described in most patents. The contribution of magnesium in some procedures is made by the addition of magnesium hydroxide. The second component (kaolin or clay) contributes with the silica and some of the alumina. The same effect may be obtained with the addition of halloysite or saponite. The third

component (aluminum hydroxide) is used to provide the aluminum necessary to complete the cordierite composition, although the use of mixtures of this hydroxide with alumina is also frequent [23].

Generally, the multi-component mixtures are prepared for extrusion with the aid of an agglomerant and water. Once extruded, the monolith is dried and then calcined at 1200–1450◦C for 2–3 h.

Sometimes, the overall composition is designed to obtain cordierite plus other materials such as spinel, mullite or similar, in order to improve the thermal shock resistance of the monolith. It is also very important to control the particle size of the raw materials to achieve a good contact between the solids that take part in the reactions during this process [23].

1.2.1.2 Metallic monoliths

Beside the initial pellet beds and cordierite monoliths, metallic monoliths were soon proposed due to their higher mechanical resistance and thermal conductivity, the possibility of thinner walls allowing higher cell density and lower pressure drop. But additional advantages of the metallic substrate were soon discovered, in particular, the easy way to produce different and complicated forms adapted to a wide variety of problems and uses [23].

Many different metals and alloys have been proposed for the manufacture of monoliths in search for mechanical, chemical and thermal stability, availability in thin foils and good surface adherence of the catalytic coating. In addition to some Ni and Cr alloys, steel is the most widely used alloy, in particular ferritic alloys containing Al (5 – 7%) that can produce alumina protecting coatings with excellent properties for anchoring the catalytic coating. It is important to note that during the high temperature use of the alloy, the alumina protective layer continues growing until the aluminum is consumed. Breakdown of this thermally grown alumina would lead to breakaway oxidation conditions and rapid component failure. This is especially important for the new ultra-thin foils (20 μm) available for the high cell density monoliths (1600 cpsi). Reducing the thickness from 70 to 20 μm means that the component life will be reduced. However, it is quite difficult and usually uneconomical to increase the Al concentration to a value more than 5 mass%, because such an alloy is brittle, hence inducing difficulty during production or lowering productivity. It is generally easier to produce the thin foil or even the monolith from an alloy having low Al content and hence good mechanical and manufacturing properties, and subsequently to treat it to increase the Al content. In addition to the main components of these ferritic steels, chromium (17–22%) and other reactive elements are present in small quantities because they are fundamental to improve the oxidation resistance of the alloy and to aid oxide adhesion [23].

The new stricter emission limits for car exhausts all around the world demand more effective catalytic solutions. Metal catalyst substrates offer a variety of solutions for all combustion engine applications:

- Significant reductions of all emissions (HC, CO, NO_x and PM) can be achieved for both spark ignition and diesel engines.

- New, high cell density, ultra-thin foil substrates further increase catalyst efficiency.

The formation of a self-healing protective "skin" of alumina allows the ultra-thin steel to withstand the high temperatures and corrosive conditions in auto exhaust and other environmental uses. These materials also have high thermal shock resistance and high melting and softening points and facilitate the development of high cell densities with very low-pressure losses [23].

1.2.2 Supports

The first and important role of support materials in the three-ways catalyst is a host of active phase, mostly noble metals. Without support material, it is extremely difficult for the dispersion of crystallite of noble metals, which act as catalytic sites in the reactions. It is well-known that γ-Al_2O_3 has been used as the support for Pt, Rh in the application of catalysis because of its high surface area, and strong structure under high temperature. Since the beginning of 1980s, the researchers have focused on the CeO_2- based materials or it has been called the oxygen storage material, which can improve the catalytic activity. This material has been used not only as the support but also as a part of active phase. Recently, a new generation of materials as Al_2O_3-CeO_2-ZrO_2 was investigated. With the aim of combination the advantages of alumina and $Ce_xZr_{1-x}O_2$, this material is expected to become the optimal support for the catalytic application.

1.2.2.1 Alumina

In 1950, Stumpf et al. reported that apart from α-Al_2O_3(corundum), another six crystal structures of alumina occur: γ, δ, κ, η, θ, χ-Al_2O_3 .The sequence of particular type formation under the thermal processing of gibbsite, bayerite, boehmite and diaspore is as follows [25]:

$$\text{Gibbsite } (Al(OH)_3) \xrightarrow{250^oC} \chi\text{-}Al_2O_3 \xrightarrow{900^oC} \kappa\text{-}Al_2O_3 \xrightarrow{1200^oC} \alpha\text{-}Al_2O_3$$

$$\text{Bayerite } (Al(OH)_3) \xrightarrow{230^oC} \eta\text{-}Al_2O_3 \xrightarrow{850^oC} \theta\text{-}Al_2O_3 \xrightarrow{1200^oC} \alpha\text{-}Al_2O_3$$

$$\text{Boehmite } (AlOOH) \xrightarrow{450^oC} \gamma\text{-}Al_2O_3 \xrightarrow{600^oC} \delta\text{-}Al_2O_3 \xrightarrow{1050^oC} \theta\text{-}Al_2O_3 \xrightarrow{1200^oC} \alpha\text{-}Al_2O_3$$

$$\text{Diaspore} \xrightarrow{450^oC} \alpha\text{-}Al_2O_3$$

Fig.1.3 : The formation of various alumina during calcination

The temperature of aluminum hydroxide formation is the basis of this system of classification. The two groups of alumina are: low-temperature aluminas: Al_2O_3. nH_2O ($0<n<6$) obtained by dehydrating at temperatures not exceeding 600^{o}C (γ-group). This group belongs to: γ, η, χ-Al_2O_3, high-temperature aluminas: nearly anhydrous Al_2O_3 obtained at temperatures between 900 and 1000^{o}C (δ-group). This group belongs to: κ, θ and δ-Al_2O_3.

All these structures are based on a more or less close-packed oxygen lattice with aluminum ions in the octahedral and tetrahedral interstices. Low-temperature alumina is characterized by cubic close-packed oxygen lattices; however, high-temperature alumina is

characterized by hexagonal close-packed lattices. In terms of catalytic activity, high-temperature alumina is less active than low-temperature alumina. This results from not only lower surface area (higher order and larger particle size) but also the different population of surface active sites of high-temperature alumina when compared to low-temperature ones [25].

The most common form of alumina used for catalyst support is γ form, which is its surface area more than 300 m^2/g, pore size ranged from 30 to 120 Å and pore volume from 0.5 ÷ 1 cm^3/g. The structure of γ-Al_2O_3 is built from single layers of packing spheres, the layers have the ionic O^{2-} at position 1. The spheres of the second layer sit in half of the hollows of the first layer. There are two cases for the distribution of third layer, but in case of γ-Al_2O_3, the third layer was distributed on the hollows of the first one, following the number: 1,2,3,1,2,3 …. Therefore, cation Al^{3+} was placed in the space between these layers of oxide anion packing. The structure of γ-Al_2O_3 was illustrated in the figure 1.4:

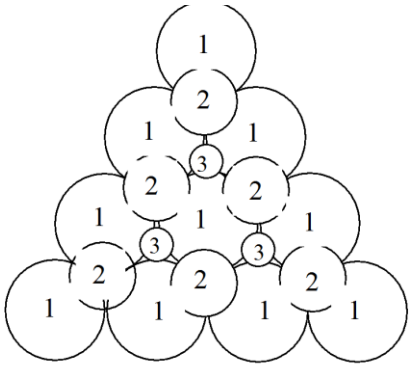

Fig.1.4: Structure of γ-Al_2O_3
1 – layer 1; 2 – layer 2; 3 – layer 3

Because of γ-Al_2O_3's octahedral cubic crystallite, the structure includes octahedral and tetragonal Al. The structure of γ-Al_2O_3 is psedo-spinen differing only in oxide anion packing density. The surface of γ-Al_2O_3 contains both Bronsted and Lewis active sites, which plays important role in catalytic reaction [14].

In conclusion, γ-Al_2O_3 has been used extensively in the application of automobile exhaust catalyst because of its normal inexpensiveness, workability, long life criteria, are those allowing the greatest activity of the active catalytic agent, namely high specific surface and adequate porosity on one hand, and on the other hand that of the highest structural stability [26].

1.2.2.2 $Ce_xZr_{1-x}O_2$

Since the beginning of the 1980s, the use of CeO_2 in the automotive pollution control has become so broad to represent today the most important application of the rare earth oxides. Ceria is a very useful support in three-way automobile catalyst mainly due to its oxygen storage capacity that allows effective catalyst operation under conditions with oscillating oxygen concentration. Because Ce^{4+} in the CeO_2 lattice is readily converted to Ce^{3+} due to its nonstoichiometric behavior, the addition of CeO_2 promotes dynamic performance in purifying CO, NOx and HC under conditions of rich–lean ratio air to fuel

(A/F) in automotive exhaust, which is called oxygen storage capacity (OSC). CeO_2 provides oxygen for oxidizing CO and HC under rich A/F conditions and removes it from the exhaust gas phase for reducing NO under lean A/F. However, the surface of CeO_2 is collapsed under elevated temperature; the addition of Zr can not only prevent this phenomenon but also improve the oxygen mobility in the CeO_2 lattice. For years, the phase of $Ce_xZr_{1-x}O_2$ is still a huge argument between many researchers in the world. Besides the oxygen storage capacity (OSC), ceria exhibits metal support interaction with precious metals such as Pt, Pd or Rh enhancing their catalytic activity [27]. These effects are noticeable as long as a high surface area, and consequently low temperature reduction features are present in the CeO_2-based catalysts. Accordingly, the research activity in the 1990s has been focused mainly on the improvement of the surface area stability in the CeO_2 promoter. Among different systems tested, ZrO_2 appeared to be the most effective thermal stabilizer of CeO_2, particularly when it forms a mixed oxide with ceria. This material has been investigated since the early 1990 and is now generally known that the incorporation of zirconium into the ceria lattice creates a higher concentration of defects improving, thus, the O_2 mobility; such mobility would explain the outstanding ability to store and release oxygen [28].

Many researchers have reported the phase diagrams of promoters for TWC, phase diagram of $Ce_xZr_{1-x}O_2$ is present in fig.1.5. In the Ce-rich region of the diagrams, a cubic solid solution of $Ce_xZr_{1-x}O_2$ appears, while tetragonal and monoclinic solid solutions form in the tight regions of the Zr-rich region.

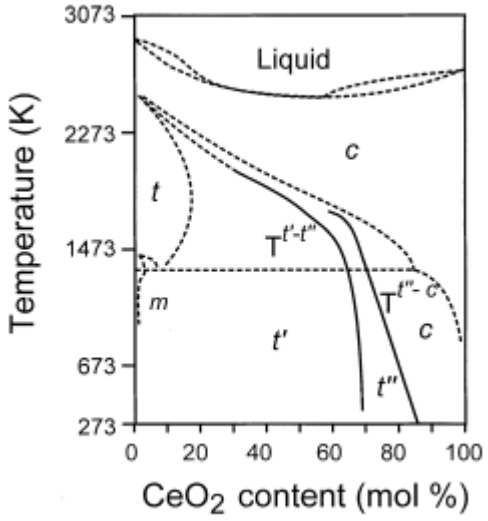

Fig. 1.5: Phase diagram of the CeO_2 –ZrO_2 system
(*m*: monoclinic, *t*, *t'*, *t''* : tetragonal, *c*: cubic) [29]

CeO_2-ZrO_2 system exhibited following properties:

- Inhibiting sintering:

CeO_2 powder readily sinters at elevated temperatures, although it is a good refractory oxide with a high melting point. The addition of zirconium, especially the formation of CeO_2-ZrO_2 mixed oxides, is effective in the inhibition of the sintering of ceria. Simple experiments indicate that Zr modification of CeO_2 powder, followed by solid state reactions, has the effect of improving the thermal stability of CeO_2 promoter [30]. For

examples, Eduardo L. Crepaldi et al. prepared the crystalline phase of $Ce_xZr_{1-x}O_2$ which was stable at temperature above 800°C and no phase segregation [31].

- Redox properties:

Oxygen evolution and/or uptake originate from the nonstoichiometry and oxygen diffusion in the surface and lattice of $Ce_xZr_{1-x}O_2$. The OSC promoter should satisfy two factors: a wide operation range for redox between Ce^{3+} and Ce^{4+} in reducing and oxidizing atmospheres, and a high reaction rate over the modified CeO_2 particles. The redox behavior and catalytic activity of five different CeO_2-ZrO_2 mixed oxides and CeO_2 were investigated using a series of temperature programmed experiments. Samples containing at least 50 mol% ceria were reduced at similar temperatures as 581–598°C, while samples with lower ceria content were reduced at significantly higher temperatures as 666–690°C [32].

- High performance of precious metal given by high oxygen storage capacity:

The activities of precious metallic (Pt, Rh) catalysts were enhanced by the presence of $Ce_xZr_{1-x}O_2$. Temperature-programme reduction in a H_2/Ar mixture of Rh-loaded CeO_2-ZrO_2 solid solution with a ZrO_2 content varying between 10 and 90% mol was carried out. It is shown that incorporation of ZrO_2 into solid solution with CeO_2 strongly promotes bulk reduction of the Rh-loaded solid solution in comparison to a Rh/CeO_2 sample. In the reaction of reduction NO by CO, bulk oxygen vacancies play an important role of in promoting NO conversion over metal-loaded CeO_2-ZrO_2. An oxygen vacancy gradient is indicated as the driving force for NO dissociation, suggesting that it may be responsible for the enhanced NO and CO conversions [33, 34].

The CeO_2-ZrO_2 mixed oxide was also a part of active phase as $Ce_{0.98}Pd_{0.02}O_{2-\delta}$ for the oxidation of major hydrocarbons in exhaust gases. Hydrocarbon oxidation over the monolith catalyst is carried out with a mixture having the composition, 470 ppm of both propene and propane and 870 ppm of both ethylene and acetylene with the varying amount of O_2. Three-way catalytic test is done by putting hydrocarbon mixture along with CO (10000 ppm), NO (2000 ppm) and O_2 (15000 ppm). Below 350°C full conversion is achieved [27].

In order to improve the CeO_2-ZrO_2 mixed oxide, the element such as La, Y was added to Ce-Zr-O system. HU Chunming et al. prepared $Ce_{0.55}Zr_{0.35}Y_{0.05}La_{0.05}O_2$ by co-precipitation. This material calcined at 600ºC has surface area of 131.5 m^2/g, pore volume of 0.23 ml/g, mean pore diameter of 8.5 nm, and OSC of 478 μmol/g; after 1000ºC aging for 5 h, still has surface area of 44.4 m^2/g, pore volume of 0.11 ml/g, mean pore diameter of 16.8 nm, and OSC of 368 μmol/g [36]. Another example is $Ce_{0.35}Zr_{0.55}Y_{0.10}$ which was prepared by Guo Jiaxiu et al. $Ce_{0.35}Zr_{0.55}Y_{0.10}$ had cubic structure similar to $Ce_{0.5}Zr_{0.5}O_2$ and its specific surface area can maintain higher than $Ce_{0.5}Zr_{0.5}O_2$ after 1000°C calcinations for 5h [37]. Thus, these materials are suitable to prepare a motorcycle catalyst that can work at high space velocities and larger fluctuations of the air-to-fuel ratio.

1.2.2.3 $Al_2O_3 – CeO_2 – ZrO_2$ materials

Recently the support of three-ways catalyst is directed to the combination between the high surface area Al_2O_3 and the effective oxygen storage capacity (OSC) material Ce-Zr-O_2. This material has attracted the attention of many researchers.

The $Al_2O_3 – CeO_2 – ZrO_2$ (ACZ) samples with alumina contents 10, 25, 50, 75 wt%, were prepared by co-precipitation method (the atom ratio of Ce to Zr is 1:1). For all of the fresh samples with 10–75 wt% Al_2O_3, only the single CeO_2 fluorite structure phase was observed and no Al_2O_3 diffraction pattern was detected. As alumina contents increase, the peak intensities of the ACZ samples become weaker and the 2θ values of these peaks show no shift. The reasons maybe ACZ compounds form homogeneous solid solutions and the highly dispersed alumina in ACZ solid solutions can-not be detected by XRD. Based on the calculation of lattice parameters by the Scherrer formula, the lattice parameters of ACZ samples are larger than that of the $CeO_2 – ZrO_2$ (CZ) sample and increase with Al_2O_3 content increasing, which indicates that alumina enters into the crystal lattice of CZ and makes lattice parameter become larger. However, after calcination at 1273 K, the increase degree of lattice parameter of the ACZ samples is less than that of the CZ sample. It is plausible that the CeO_2, ZrO_2 and Al_2O_3 are well dispersed at the nanometer level and can serve as a barrier to each other and thus sintering is impeded [38].

$Al_2O_3 – CeO_2 – ZrO_2$ –support exhibits the following properties:

- Texture properties

Specific surface area and pore volume both increase with Al_2O_3 content increasing and are larger than that of CZ. It means Al_2O_3 doped into CZ mixed oxides can stabilize and improve their textural properties. The textural properties such as surface area, pore volume and average pore diameter, play an important role in the performance of catalytic supports, especially for the catalytic supports used in high space velocity, which requires the supports to have larger surface area, pore volume and good pore diameter distribution. Compared with CeO_2 oxides, CZ solid solutions are widely employed in TWCs, due to their excellent redox behaviour and higher thermal stability. However, CZ mixed oxides still have drawbacks in stability of structure, especially in thermal stability of texture, which obviously need be improved as catalytic supports employed in high space velocity. Since ACZ samples exhibit excellent thermal stability in structure and texture, they should be more suitable as catalytic carriers and can be employed in high space velocity [39] .

- Reduction behaviour and oxygen storage capability

The H_2-TPR of the ACZ samples indicated their reduction peaks also shift to lower temperature to some extent, which is attributed to an increase of oxygen mobility in the bulk induced by solid solution sintering. The results indicate that these materials have more stable reduction performance at high temperature.

After oxygen uptakes measurements, with alumina contents increasing, it can be seen that the OSC of the fresh ACZ sample increases from 439.5 to 728 $\mu molg^{-1}$, and the OSC of the aged sample, which were calcined in air at 1000^oC for 5h, increases from 351.5 to 700 $\mu molg^{-1}$. This indicates that the surface area of ACZ sample becomes larger and the ratio of utilizable cerium also increases correspondingly with Al_2O_3 content increasing [40].

Akia Morikawa et al. proved the beneficial effect of Al to the mixed oxide $Ce_{1-x}Zr_xO_2$. It was the improvement of the desorption rate of oxygen (OSC-r) in the fresh catalyst and inhibition of the decrease in the OSC-r after durability testing were achieved by suppression of particle growth of $(Ce,Zr)O_2$ in ACZ by introducing Al_2O_3 as a diffusion barrier with resultant inhibition of sintering of Pt particles [41]. This material was used as the support for hosting the active phase. For example, Pt was dispersed on $Al_2O_3 – CeO_2 – ZrO_2$ to make a catalyst in the reaction of partial oxidation of methane [42]. It is also to be applied in the three way catalyst as well [43, 44].

Trivalent La^{3+} has been used to promote the thermal stability and oxygen mobility (ionic conductivity) of CeO_2-ZrO_2 solid solution and to restrict the phase transformation of γ-Al_2O_3 to α-Al_2O_3 at high temperature. Therefore, the introduction of lanthanum into the systems of ACZ composite oxide was expected to improve the thermal stability and oxygen storage capacity, and then its use as the support of Pd catalyst. Pd supported on Ce-Zr-La-Al_2O_3 was used for transforming CO, C_3H_8, NO. With these fresh catalytic systems, the conversions are 100% at above 240, 300, 340^0C for CO, NO, C_3H_8 respectively. Operating temperatures for aged catalysts, which were calcined at 1000^oC for 5h, are higher [6]. Furthermore, palladium catalysts were prepared by impregnation on ACZ and CeO_2-ZrO_2-Al_2O_3-La_2O_3 for CH_4, CO and NO_x treatment in the mixture gas simulated the exhaust from natural gas vehicles operated under stoichiometric condition was investigated by Xiaoyu Zhang [45].

1.2.3 Active phase

The primary precious metals for a TWC were Pt and Rh with the latter being mostly responsible for reduction of NO_x and the former for oxidation of CO and HC. Palladium is less resistant to deactivation by poisons such as Pb and S versus Pt and Rh. With 0.5 – 1 %w.t of precious loading on substrates, the catalysts still exhibit completely conversion of CO, HC and NOx. However, the noble metals were limited by cost and sensitivity to poisoning, especially by chlorine/chloride products. Thus composite mixed oxides, mostly with perovskite-type structure (ABO_3 or A_2BO_4), can be seen as interesting alternatives as they are low-cost materials and stable even at above 1000^oC. Another alternative way is transition metals as Mn, Co, Cu, V, … which are inexpensive, high activity and resistance to poisoining.

1.2.3.1 Noble metals:

Noble metal catalysts have received considerable attention for more than 20 years for used in automotive emission control systems, essentially base on Pt, Pd, Rh over supports. Supports can be CeO_2- ZrO_2, Al_2O_3, mixtures of some oxides. Catalyst based on noble metal exhibited high catalytic activity in pollutant treatment and these catalysts were used extensively [46, 47].

Containing Pd catalyst was researched by Jianqiang Wang et al.[48]. For fresh catalyst it can be observed that both Pd/ $Ce_{0.67}Zr_{0.33}O_2$ and Pd/$Ce_{0.67}Zr_{0.33}Sr_{0.03}O_{2.03}$ show the almost same oxidation activity for CO, the conversion of which can reach almost 100% under $\lambda > 1$ conditions, but descend as decreasing λ -value under $\lambda < 1$ conditions (λ: the theoretical stoichiometric value and λ can be calculated $\lambda = (2O_2+NO)/(10C_3H_8+CO)$.

U. Lassi indicated that catalytic activity of catalyst base on Rh depends on the nature of ageing atmosphere and temperature. These catalysts reach their maximum conversions (100%) by the temperature of 400◦C [49].

Sudhanshu Sharma showed that catalytic activity of cordierite honeycomb by a completely new coating method for the oxidation of major hydrocarbons in exhaust gas. Weight of active catalyst can be varied from 0.02 wt% to 2 wt% which is sufficient but can be loaded even up to 12 wt% by repeating dip dry combustion. Adhesion of catalyst to cordierite surface is via oxide growth, which is very strong [27].

Binary metallic activity is higher than single one. Furthermore, some metals are added to promote activity or reduce price but properties preserving or increase activity.

Ana Iglesias et al. studued the behaviors of a series of Pd–M (M as Cr, Cu and Ni) bimetallic catalysts for CO oxidation and NO reduction processes has been tested and compared with that of monometallic Pd references. The catalytic properties display a strong dependence on the degree of interaction which exists between the metals in the calcinations state. For CO oxidation with oxygen, the second metal plays no significant role except in the case of Pd-Cu/ $Ce_{0.5}Zr_{0.5}O_2$ [50].

Hyuk Jae Kwon investigated the light-off temperature of the oxidations of CO and C_3H_6 over a commercial TWC was shifted to a lower temperature by the addition of water to the feed stream. The formation of carboxylate and carbonate by a reaction between adsorbed CO and OH on the catalyst surface was observed during the course of the reactions. The catalysts are containing Pd only and Pt-Rh/Ce catalysts [51].

In Vietnam, the catalyst with the dispersion of Pd on γ- Al_2O_3 for the treatment of exhaust gases was investigated by Tran Van Nhan with co-worker since 2000 [20].

Other noble metals were also studied in Vietnam, Le Thi Hoai Nam studied on Au-ZSM-5 catalysts for carbon monoxide oxidation to carbon dioxide. The result showed that catalytic activity can be affected at very low temperature. Catalytic activity increases when temperature increases and it is more preeminent than some systems (Au/α-Fe_2O_3 Au:Fe=1:19) [52]. Nanoparticles gold was also loaded on support Co_3O_4 in the investigation of Tran Que Chi and her co-workers. This material was prepared by co-precipitation. The products had sphere shape and the size about 1 – 3 nm, the BET surface area of 69 m^2/g. The catalytic activity was studied on the oxidation reaction of CO and C_3H_6, the results showed that the complete conversion of CO was at ambient temperature (27^oC), and total conversion of C_3H_6 was at 200^oC [53].

1.2.3.2 Perovskite:

Perovskite-type mixed oxides have been widely studied for the last four decades. These materials present an ABO_3 formula, with the tolerance factor defined by Goldschmidt as: $t = (r_A + r_O)/ \sqrt{2} (r_B + r_O)$, where r_A, r_B and r_O are the ionic radii for the ions A, B and O. Perovskite structures are obtained at $0.8 < t < 1$. Their high catalytic activity was reported for a wide set of reactions and particularly for oxidation reactions of hydrocarbons and volatile organic compounds. Cobalt- and manganese-based perovskites were usually reported as the two most efficient structures in oxidation reactions and they were even proposed as an alternative to noble metal supported catalysts since they present

similar activities in oxidation and a lower synthesis cost. However the low specific surface area generally displayed by these solids is still the major impediment to their use [54].

D. Fino and colleague realized that the $LaMn_{0.9}Fe_{0.1}O_3$ catalyst was found to provide the best performance of combustion of methane. Further catalyst development allowed to maximize the catalytic activity of this compound by promoting it with CeO_2 (1:1 molar ratio) and with 1 wt% Pd. This promoted catalyst was lined on cordierite monoliths in a γ-Al_2O_3-supported form [55].

Following L. Forni's investigation, series of $La_{1-x}Ce_xCoO_{3+\delta}$ perovskite-type catalysts, with x ranging from 0 to 0.20**,** showed to be quite active for reduction of NO by CO and for oxidation of CO by air oxygen at temperatures ranging from 373 to 723 K [56].

Hirohisa Tanaka et al. showed that one of the most important issues of automotive catalysts is the endurance of fluctuations between reductive and oxidative (redox) atmospheres at high temperatures exceeding 1173 K. The catalytic activity and structural stability of $La_{0.9}Ce_{0.1}Co_{1-x}Fe_xO_3$ perovskite catalysts (x = 0, 0.2, 0.4, 0.6, 0.8 and 1.0), both in powder and monolithic forms, were investigated after aging treatments in real and simulated "model" automotive exhaust gases [57].

In Vietnam, Tran Thi Minh Nguyet studied $deNO_x$ properties of $La_{1-x}Sr_xCoO_3$ perovskite/complex oxides. The results showed that catalyst with molar ratios La:Sr:Co=0.4:0.6:1; a single phase perovskite exhibited only an oxidation function, while the product with three phases realized three functions of $DeNO_x$ reaction. The conversion was 40% [58]. In 2011, she and coworkers prepared nanoparticles of perovskite $La_{1-x}Na_xCoO_3$ by sol-gel using citric acid. The obtained materials had sphere shape, the particles size about 30 – 40 nm, surface area in the range 12 – 14 m^2/g. Catalyst $La_{1-x}Na_xCoO_3$ exhibited maximum activity with x as 0.2 – 0.3 by the total conversion temperature of CO and diesel soot was 215^{o}C and 400^{o}C, respectively [59].

1.2.3.3 Transition metallic oxides:

The high price of noble metals and their sensitivity to higher temperatures have long motivated investigators to search for substitute catalysis. Metal oxides are an alternative to noble metals as catalysts for complete oxidation. They are less active at low temperatures, but at higher temperatures their activity is similar to that of the noble metals. The most active single metal oxides for combustion of VOCs are the oxides of Cu, Co, Mn, and Ni. Among all metal oxides studied, manganese and cobalt containing catalysts are low cost, environmentally friendly and relatively highly active for VOC combustion. The catalytic properties of MnO_x-based catalysts are attributed to the ability of manganese to form oxides of different oxidation states and to their high oxygen storage capacity (OSC) [39].

Selective catalytic reduction of NO by propene was investigated on Cu, Co, Ni and Mn ion-exchanged ZSM-5 and mordenite in the presence of excess of oxygen by A. De Lucas et al. Cobalt, nickel and manganese were present in the form Co^{2+} and Co^{3+} ,Ni^{2+} ,Mn^{3+} and Mn^{4+}, respectively. The catalytic activity showed for all the catalysts increased with increasing metal content reaching a maximum of NO_x conversion, and then decreased at higher contents. In turn, NO_x conversion increased with the reaction temperature passing through a maximum, and then decreased at higher temperatures, due to the combustion of

the hydrocarbon. NO TOF for all the catalysts here prepared was analyzed at 375–425◦C [60].

In Vietnam, the role of oxygen in selective reduction of NO_x by C3H6 in the presence of oxygen over Cu/ZSM-5 catalyst was investigated by Tran Van Nhan and co-worker. It was found that oxygen enhances the oxidation of NO by C_3H_6 to NO_2, but also consumes C_3H_6 as an oxidative agent casing a decrease in the decomposition of NO_x [61].

Moreover, catalysts on the basis of CuO, Cr_2O_3 were investigated for CO oxidation in a microflow reactor by Hoang Tien Cuong et al. At 180°C, 100% of CO was treated completely by catalyst 10%CuO + 10% Cr_2O_3 loaded on γ-Al_2O_3 [62].

The influence of Mn loading on the support Ba/Al on the Nox decomposition activities in the presence of an excess of oxygen was investigated by Le Phuc Nguyen et al. The maximum conversion NO_x on xMnBa/Al samples (x is molar ratio of Mn/Ba) was obtained as 55% with 0.5MnBa/Al sample. Lower and higher Mn loading resulted in a significant loss of the overall efficiency of NO_x conversion. The lower NO_x conversion at lower Mn loading (x = 0.1) demonstrated that manganese oxide was the catalytic site. The loss in efficiency at higher Mn loading is attributed to the lower dispersion of Ba on the surface, which chould decrease the NO_x storage ability, and the lower BET surface [63].

Nano oxides Co_3O_4, ZrO_2 and Co_3O_4- ZrO_2 were prepared by citrate sol-gel method and dispersed on the cordierite as a carrier in the study of Tran Thi Minh Nguyet et al. The catalytic activities was studied for the oxidation of CO. Co_3O_4 had high catalytic activity byt less durability, while ZrO_2 oxide was thermally stable but exhibited limitative catalytic activity. However, Co_3O_4 dispersed on the surface of ZrO_2 carried by cordierite had the highest activity and more durability. The complete conversion of CO was at 170°C [64].

1.3 Kinetic modelling of transient experiments of automotive exhaust gas catalyst

Detailed non-stationary kinetics of reactions in catalytic monolith reactors for car exhaust gases with specific storage properties has become available only recently. Hence steady-state or simplified semi-empirical kinetics is still most often used in transient analysis of catalytic monoliths [65]. Experiments on the non-stationary kinetics of typical reactions on Pt/Rh/Ce/γ-Al_2O_3 three-way catalyst were performed, for example, by Harmsen et al. [66, 67], who also evaluated the results in the form of detailed micro-kinetic schema, including number of reaction steps and intermediates for important components of exhaust gases (Table 1.4). All the kinetic sub-models (CO and C_2H_2 oxidation, oxygen storage on CeO_2 and NO_x transformation) have been proposed and evaluated by the same research group for a typical TWC washcoat, so that the TWC reaction scheme and the values of kinetic parameters are consistent

Table 1.4: TWC microkinetic scheme used in the model

No	Reaction step	Note
1	$CO + * \rightleftarrows CO*$	The reaction subsystems are employed: for
2	$O_2 + 2* \rightarrow 2O*$	- CO (reactions 1–5) and C_2H_2 (reactions 6–11) oxidation on noble
3	$CO + O* \rightarrow CO_2 + 2*$	
4	$CO + O* \rightleftarrows OCO*$	

5	$OCO^* \rightarrow CO_2 + *$	metal (* = Pt, Rh),
6	$C_2H_2 + * \rightleftarrows C_2H_2^*$	- O_2 storage and release (reactions 12–14) on ceria (s),
7	$C_2H_2^* + 2^* \rightleftarrows C_2H_2^{***}$	- CO_2 storage (reaction 15) on γ-Al_2O_3 (γ)
8	$C_2H_2^* + 3O^* \rightarrow 2CO^* + H_2O + 2^*$	- and NOx transformation (reactions 16–23) on noble metals (* = Pt, Rh)
9	$C_2H_2^{***} + 3O^* \rightarrow 2CO^* + H_2O + 4^*$	
10	$C_2H_2 + O^* \rightleftarrows C_2H_2O^*$	
11	$C_2H_2O^* + 2O^* \rightarrow 2CO^* + H_2O + *$	
12	$O_2 + 2s \rightarrow 2O^s$	
13	$CO^* + O^s \rightarrow CO_2 + * + s$	
14	$C_2H_2^* + 3O^s + * \rightarrow 2CO^* + H_2O + 3s$	
15	$CO_2 + \gamma \rightleftarrows CO_2^{\gamma}$	
16	$NO + * \rightleftarrows NO^*$	
17	$NO^* + * \rightarrow N^* + O^*$	
18	$NO^* + N^* \rightarrow N_2O^* + *$	
19	$N_2O^* \rightarrow N_2O + *$	
20	$N_2O^* \rightarrow N_2 + O^*$	
21	$N^* + N^* \rightarrow N_2 + 2^*$	
22	$NO + O^* \rightleftarrows NO_2^*$	
23	$NO_2^* \rightleftarrows NO_2 + *$	

This model of CO treatment consists of three different pathways: (1) adsorption of carbon monoxide and oxygen on noble metal, followed by a Langmuir - Hinselwood surface reaction; (2) adsorption of carbon monoxide on an oxygen-covered site, with subsequent carbon dioxide desorption from so-called OCO species; and (3) reaction between carbon monoxide adsorbed on the noble metal and oxygen adsorbed on ceria.

For the treatment of two acetylene surface species, the work was followed: (1) μ acetylene, adsorbed on one catalytic site (atop), is the most unstable and therefore most reactive species; (2) di-δ + μ acetylene, triangular adsorbed, is stable and therefore refractory towards oxidation.

Thus, the reversible adsorption of acetylene (step 6) leads to μ acetylene on the surface and is first order in the vacant sites. Step 7 describes the reversible conversion of the two types of adsorbed acetylene into each other. The conversion of π acetylene to di-δ + μ acetylene requires two vacant sites, making the latter species less abundant when acetylene is in the gas phase. The rate of this step is second order in the fraction of vacant sites. The direct partial combustion of both acetylene species to adsorbed carbon monoxide is described by steps 8 and 9, i.e. reaction paths A and B.

Although not elementary, the first and rate-determining step is assumed to be the oxygen-assisted abstraction of the weakest bonded hydrogen atom, whereupon oxidation to carbon monoxide occurs instantaneously. Decomposition of acetylene on the surface is unlikely because of the small number of vacant sites, and the relatively large molar flow rates in the reactor. Steps 10 and 11 show an Eley-Rideal type of reaction for the combustion of acetylene. Acetylene is able to adsorb on an oxygen-covered surface to yield oxidation products immediately. Therefore, the species formed in step 10 is believed to be highly unstable and will react rapidly through step 11 to adsorbed carbon monoxide. Step 14, finally, describes the influence of ceria in the catalyst on the oxidation of

acetylene. Only the reaction between the π acetylene and the ceria oxygen has been used in the model.

For the treatment of NO, initially NO remains fully adsorbed. At 548 K, CO slowly desorbs, leaving vacant sites onto which NO can adsorb (step 16). The production of N_2O requires the dissociation of NO, which involves extra vacant sites (step 17) then N_2O is then formed by step 18, and subsequence desoption in step 19. Nitrogen can be produced in two different ways, where the first (step 20) is known to be more important at low temperature than step 21. And finally, NO_2 was form by the reaction between NO and oxygen adaptom (step 22 and 23).

Besides the above reaction kinetic of three-ways catalyst researched by Harmsen et al, the kinetic model based on Langmuir-Hinderwood was investigated by Hyuk Jae Kwon et al. [68]. The reaction kinetics has been developed on the basis of the following assumptions: (i) all reaction steps are assumed to be a first-order reaction with respect to each of the reactants involved, (ii) all reactants except CO_2 adsorb on the catalyst surface, (iii) oxygen and hydrogen adsorb dissociatively on the catalyst surface, (iv) the surface reaction is a rate-determining step and described by a dual-site Langmuir–Hinshelwood mechanism. Table 1.5 shows the surface reaction mechanism considered in the present study. First, it has been assumed that all reactants are adsorbed reversibly on the active reaction site, S, as reactions (1)–(8). And then, the adsorbed species can react through reactions (9)–(24), mainly occurring in the commercial automotive catalytic converter. For the H2 oxidation, it has been reported that the reaction proceeds via H· S + OH· S as illustrated in reaction (14) after forming OH · S from the H · S + O · S reaction. On the other hand, water and hydrogen enhanced the activity of the reactions involving CO by moderating the self-poisoning of CO adsorbed on the catalyst surface. The enhancement effects of water and hydrogen have been accounted for in reaction (15), which involves the reaction intermediate, OH · S, derived from water dissociation and the H · S + O · S reaction. Note that the water–gas shift and steam reforming reactions have not been explicitly considered in the model, in view of their relatively small contributions to TWC kinetics at low reaction temperatures. The reduction of NO to N_2O and N_2 can be described by reactions (16)–(18) and (23). Moreover, the reaction (19) was included since hydrogen-assisted NO dissociation plays an important role during NO reduction by H_2. NH_3 formed via reaction (20) can be consumed by the reaction of oxidation and reduction of NO as illustrated in reactions (21)–(23).

Table 1.5: Surface and kinetic reaction of Pt/Rh/γ-Al2O3

No	Reaction
1	$CO + S \leftrightarrow CO \cdot S$
2	$C_3H_6 + S \leftrightarrow C_3H_6 \cdot S$
3	$H_2 + 2\,S \leftrightarrow 2H \cdot S$
4	$O_2 + 2S \leftrightarrow 2O \cdot S$
5	$NO + S \leftrightarrow NO \cdot S$
6	$H_2O + S \leftrightarrow H_2O \cdot S$
7	$NH_3 + S \leftrightarrow NH_3 \cdot S$
8	$N_2O + S \leftrightarrow N_2O \cdot S$
9	$H_2O \cdot S + S \rightarrow OH \cdot S + H \cdot S$

10	H_2O . S + O . S → 2OH . S
11	H . S + O . S → OH . S + S
12	CO . S + O . S → CO_2 + 2S
13	C_3H_6 . S + 9 O . S → 3 CO_2 + 3 H_2O . S + 7S
14	H . S + OH . S → H_2O . S + S
15	CO . S + 2OH . S →CO_2 + H_2O . S + 2S
16	NO . S + S →N . S + O . S
17	NO . S + N . S → N_2O . S + S
18	NO . S + N . S → N_2 + O . S + S
19	NO . S + H . S → N . S + OH . S
20	N . S + 3H . S → NH_3 . S + 4S
21	2NH_3 . S + 5O . S →2NO . S + 3H_2O . S + 2S
22	2NH_3 . S + 3O .S → N_2 + 3H_2O . S + 2S
23	2NH_3 . S + 2NO . S + O . S → 2N_2 + 3H_2O . S + 2S
24	N_2O . S → N_2 + O . S

In conclusion, the latter kinetic reaction model reveals four typical reactions as oxidation of CO, HC, reduction of NO and water-gas shift which not indicated in the former model. However, both models was investigated on catalysts based on noble metals (Pt, Rh, Pd), therefore, there is consistent between the modeling of oxidation CO and reduction of NO. In the exhaust gases of internal combustion engine, C_3H_6 is the main pollutant, but the first model didn't discuss, while the second one didn't explain more detail.

1.4 Preparation the catalytic converters

The cordierite and metal substrates have many excellent properties such as high mechanical strength, low thermal expansion constant, resistant to pressure shock, but they have disadvantages on surface as low surface area. Therefore, it is essential to coat the support material on substrates. Then, the active phase should be deposit later. The advantage of using the coating technique is that the catalyst is used more efficiently, because the diffusional distance toward the active species will be small.

1.4.1 Coating a monolith with a catalysis support material

For deposition the support material on substrate, there are many methods can be used depending on the properties of support and substrate. In cases of cordierite and metal foil, the deposition methods were investigated as direct synthesis techniques [69, 70], suspension, hydrid deposition, and sol-gel.

1.4.1.1 Direct synthesis techniques

Direct combustion synthesis has already proved to be an efficient, quick, cheap and straightforward preparation process, suitable for producing a layer of catalyst which excellent adherence on ceramic substrates. The catalytic loading content (up to 10%) and thickness of the catalyst layer are dependent on the concentration of the mother solution.

However, surface areas of the catalysts remain small although an improvement compared to the original ceramic is observed.

When the coating layer is zeolite (ZSM-5), the in-situ crystallization method was chosen, in which zeolite can be deposited by direct crystallization from a gel on substrates placed together with the gel in an autoclave. The thickness of the layer varied from 70-100 μm. For the samples with a dense layer of zeolite, the adhesion was good but in some case, less dense films were formed, which showed crystal detachments [69]. Some modifications of the in-situ crystallization method have been reported [70], where a seeding step was performed prior to the in-situ crystallization of ZSM-5 by hydrothermal synthesis. According to this report, after the first synthesis, the cordierite substrate gained 28 wt.%, and 11 wt.% more after the second. The porosity of the final coated cordierite was 16%.

1.4.1.2 Suspension

All methods based on the dispersion of a finished material (catalyst support or catalyst itself) have been gathered under the term ‘‘suspension method’’. It is the most largely used method, namely for ceramic monoliths. Powder (catalyst support or catalyst itself), binder, acid and water (or another solvent) are the standard ingredients. The concentration of all ingredients depends on the nature of the surface to coat and on the desired layer thickness [72].

The slurry method has also been applied to coat different powders such as γ-Al_2O_3, ZrO_2, TiO_2, CeO_2 on cordierite ceramics. It was proved that a homogeneous and good adhesive coating layer on the ceramic could be obtained with small particle sizes (d_{90} < 2μm) [73]. γ-Al_2O_3 was also deposited on cordierite from sols of γ-Al_2O_3 itself [75], by a sol-gel method. The viscosity of the solution, which was adjusted by binders and sol concentration, influenced significantly the loading content and thickness of the layer (5μm) [74]. Compared with boehmite precursors, the wash coating of cordierite monoliths with γ-Al_2O_3 suspensions of suitable particle size allows a higher alumina loading, and the deposition of a homogeneous wash coat layer with good adhesion properties and surface areas of about 50 m^2/g [75]

Zapf et al. [76] prepared the suspension with 20g Al_2O_3 (3μm particles), 75 g water, 5g polyvinyl alcohol and 1g acetic acid and obtained a very adherent Al_2O_3 layer on stainless steel microchannels.

In the case of Pfeifer et al., the suspension contained a cellulose derivative (1 wt% of hydroxy ethyl (or propyl cellulose) and a solvent (water or isopropyl alcohol). The nanoparticles (20 wt% in the suspension) of CuO, ZnO and TiO_2 or Pd/ZnO catalyst were mixed together with this solution. The cellulose derivative was found to efficiently avoid the particles agglomeration. The resulting suspension was filled into microchannels, dried and calcined at 450°C. A complete burn off of the polymer was obtained [77, 78].

Liguras et al. prepared a dense suspension of catalyst (Ni/La_2O_3) powder in de-ionized water. A simple immersion of ceramic substrates in the suspension followed by drying at 120°C and calcinations (550°C and 1000°C) allowed obtaining the catalytic material [79].

L.F. Liotta et al. deposited the support over cordierite by suspension. Commercial cordierite with a cell density of 400 cpsi was cut to obtain samples with 25 channels on the

cross-section and different lengths up to 40 mm. In order to obtain a washcoat layer of ceria–zirconia onto the cordierite surface, highly dispersed pseudobohemite alumina powder was used as a binder. The monoliths were dipped in a slurry composed of diluted nitric acid solution (1.4 wt%) and appropriate amounts of finely grounded ceria–zirconia and pseudobohemite powders in order to obtain a final washcoat composition of ceria–zirconia (80 wt%)- γ-Al_2O_3 (20 wt%). Several dips were needed to obtain the desired amount of washcoat loading (25% of the total weight). In each cycle the excess slurry was removed by blowing air through the channels and then the samples were dried at 120°C for 1 h and calcined at 550°C for 3 h for binder decomposition and γ-Al_2O_3 stabilization. The deposition over the cordierite doesn't produce any structural modification [80].

1.4.1.3 Hybrid method between suspension and sol-gel deposition

This method was the between suspension and sol-gel method. The process was carried out following sol-gel method. But the difference is a sol acts as the binder, and also participates in the chemical and textural properties of the final deposited layer. For example, to obtain a silica layer, metallic monoliths have been dipped in a suspension of silica powder (0.7–7 μm) with a silica sol. The layer obtained after drying and calcination steps is 20–50 mm thick [72].

In order to obtain thicker films, A. Rouge et al. added γ-alumina powder to an aqueous suspension of boehmite, the boehmite acting as a binder for the particles. In the washcoating procedure, an aqueous suspension containing 15% boehmite, 15% γ-alumina, 1% acetic acid and 4% polyvinylalcohol was used. In this way, considerable thicker films consisting of an agglomerate of particles instead of a homogeneous layer were obtained [81].

L. Villegas also used boehmite as the binder in the suspension of alumina for washcoating. The washcoating procedures were developed with 230 and 400 cpsi cordierite monoliths with square channels. The boehmite and one γ-Al_2O_3 (3 mm average particle size powder) were used for the washcoat preparation. The boehmites have been used with HCl as the dispersant. The γ-Al_2O_3 powder was dispersed by HNO3. After vigorous stirring for 15 h at room temperature, the suspensions were used for washcoating. The monoliths were dipped vertically into the suspension for 2 min, then removed and the excess suspension was evacuated from the channels by a flow of compressed air. The monoliths were dried at 100°C for 1.5 h and weighted. The procedure was repeated until a 13–15 wt.% increase was obtained. The washcoated monoliths were calcined in air at 800oC for 4h. The use of γ-Al_2O_3 suspensions of suitable particles size allows a faster alumina loading and the deposition of a washcoat layer with better adhesion properties than those obtained with boehmite precursors [74].

1.4.2 Deposition of active phase on monolithic support

The simplest way to deposit a metal on a monolith is by impregnation. For conventional catalyst supports, "wet" and "dry" (also called pore volume or incipient wetness) impregnations are possible. For a large structure, however, dry impregnation is difficult, as it is hard to supply the monolith with exactly the amount of liquid corresponding to its pore volume, as the liquid will have to travel a long distance to reach

all the pores. The center of the monolith can then easily remain dry while the external part of the monoliths contains excess liquid, causing an uneven distribution. In this procedure, the monolith is allowed to suck up the liquid by capillary forces, and after 5 min, the excess liquid is allowed to drip out of the channels. [24]

In the case of wet impregnation, first the amount of liquid a monolith will adsorb must be determined. The metal precursor is dissolved so that the concentration of metal in the liquid to be taken up by the monolith will produce the desired metal loading. A dry monolith is immersed in this solution, removed, and excess liquid blown out. To prevent an uneven distribution of metal, especially if the metal precursor shows a significant interaction with the support, the dipping procedure should be carried out in as short a time as is practically feasible to prevent an excess of metal adsorbing on the support. Because drying can also result in maldistribution, it is important to continue immediately with this step, because many solvents will start evaporating immediately after the monolith is removed from the liquid. If, out of practical considerations, this is not possible, the wet monoliths should be kept in a horizontal position while continuously being rotated to prevent gravity from causing the liquid to flow to one side of the monolith [24].

L. Villegas deposited Ni on alumina support by wet impregnation. The alumina-washcoated monoliths were dipped into a stirred aqueous solution of 0.5M $Ni(NO_3)_2.6H_2O$ for 2 h. After removal, the excess solution in the channels was evacuated with an air flow. The wet impregnated monoliths were dried by three different methods: (i) in a ventilated oven at 100°C for 2 h; (ii) at room temperature and pressure for 2 weeks; (iii) in a microwave oven operating at 200W for 50 min. The monoliths were then calcined at 550°C for 4 h in air. The Ni distribution is strongly influenced by drying method applied to wet-impregnated monoliths. At a macroscopic scale, the Ni distribution is more homogeneous after microwaves or room temperature drying. At a microscopic scale, there is a surface enrichment of the washcoat in Ni, whatever the drying method applied. In all catalysts, the Ni is present in two forms: it is predominantly incorporated in a Ni-alumina spinel phase, but some large metal particles (10–20 nm) are also present, in a larger extent in the monoliths dried by microwaves and oven procedures [74]

L.F. Liotta et al investigated the prepared monolithic alumina supported ceria–zirconia sample impregnated with platinum (1 wt% with respect to the ceria–zirconia weight content) by using a solution of $Pt(acac)_2$ in toluene at 70°C, then calcined at 400°C for 5 h. The resulting catalyst had homogeneous distribution of the active components over $Ce_{0.6}Zr_{0.4}O_2$. [80]

1.5 The aim of the thesis

TWCs to treat the automobile exhaust gases have been investigated for many years. The investigations mainly focus on the factors which influence on the catalytic performances of noble metals. However, noble TWCs are expensive and not suitable to apply in Vietnam. Therefore, the overall objective of this project is to study and find out optimal non-noble catalysts for treatment of motorcycle exhaust gases in developing country like Vietnam. The expected catalysts should have better activity to treat exhaust gases, longer lifetime, low cost, be able to operate at low temperature and require very little modification of motorcycle's design.

The first purpose of this thesis is to produce the substrates of the three-ways catalyst as cordierite ceramic. For the aim of inexpensive catalytic complex, we utilize the materials which can exploit in Vietnam. Kaolin was the initial option because its compositions. Although kaolin contains variety of elements such as Ca, Na, K, Fe, Al, Mg, Si …., the content of Al_2O_3, MgO and SiO_2, which are the main substances of cordierite, is very high. Therefore, kaolin could be mixed with suitable amount of MgO, Al_2O_3 to get the stoichiometric ratio of cordierite. Finding a suitable method to prepared cordierite ceramic is a task of this study since a lot of preparation methods such as : conventional sintering, extrusion, solid-state reaction, sol-gel … have been used to prepare cordierite. In order to chose the best way of producing cordirerite, three methods: conventional sintering from kaolin, solid-state reation of Al_2O_3, MgO, SiO_2, and sol-gel would be tested and compared. Moreover, surface area of synthesized cordierite would be studied to improve by using additives or acid treatment. Improvement of cordierite's surface area is a new research direction in Vietnam.

Another substrate for catalytic complex is metal foil. With the high thermal stability, easy to produce different shapes, metal foil has been applied in catalytic complex for vehicles emission since 1990s. For the preparation of support on metal substrates, firstly a FeCr alloy would be studied for surface treatment to increase the wetness of the impregnated solution. Afterward, impregnation would be studied to produce support on the substrate.

The preparation of support materials is the second purpose of this thesis. With the important role of hosting the active phase, the support needs to have high surface area for better distribution of active phase, thermal stability for the application of treating exhaust gases, and also ability to react with the emission gases (not important). Over the years, the γ-Al_2O_3 has been used as the support of three-ways catalyst because of its inexpensiveness, ability for dispersion of rare metallic elements such as Pt, Pd, Rh …, high surface area and high structure stability. Thus, it can be a good option for preparation of catalytic complex for Vietnam. Another material should be considered as CeO_2 – based mixed oxide, the support exhibited wonderful property of oxygen storage capacity. In this thesis, $Ce_{0.2}Zr_{0.8}O_2$ would be prepared due to its ability of nano-structure formation, and high thermal stability. Moreover, the new material Al_2O_3-CeO_2-ZrO_2 can get the best properties as high surface area, high structure stability, and also oxygen storage capacity. This material would also be studied in this work. The investigation of different support materials in this work would lead to compare their properties and select the suitable one to prepare complete TWCs.

Thirdly, we study the methods to deposit supports on substrates. Consistent with the appearance of the substrate, the deposition has been investigated widely. There are many methods to load the support on the substrates such as ceramic and metal foil, but depending on the properties of each material, the methods should be adapted. For preparation of supports on cordierite substrate, suspension, hydrid deposition … methods would be compared with the aim to select an optimal method for a stable film of support on cordierite and metal monoliths.

The final aim is also the most important part in this thesis, the preparation of a complete catalyst including active phase of mixed oxides/ support/ substrates would be. As we

mention above, the purpose on this thesis is seeking for the efficient and inexpensive catalytic complex for treatment of emission pollution in Vietnam, thus, the active phase was transition metallic oxides instead of precious metals such as Pt, Pd, Rh … The catalyst of Ni, Co, Ce and Mn has been studied in treatment of CO, NO_x or hydrocarbon in many research, and the results proved its efficient activities, that's the reason why we chose these metallic elements as components of the active phase. The simple wet impregnation method would be used to deposit the active phase on system of support-substrate to produce a complete catalytic complex. The catalytic activities of the prepared complete catalyst complex are then proposed to be investigated by both micro-line reactor set up and in real motorbike.

2. EXPERIMENTS

2.1 Preparation the substrates

2.1.1 Preparation of the Cordierite substrate

2.1.1.1 Preparation of the cordierite by solid-state reaction of the metal oxides

The metal oxides (MgO, Al_2O_3, and SiO_2) were produced by sol-gel method prior to use. They were ground, and then mixed in the following proportion: 13.7 wt.% MgO, 34.9 wt.% Al_2O_3, 51.37 wt.% SiO_2 to get a stoichiometric ratio of cordierite $2MgO.2Al_2O_3.5SiO_2$. Pellets of Cordierite were made using a Carver hydraulic presser with a pressed force 10^5N for 5 minutes. These pellets were calcined at 1250^{o}C for 3 hours with a heating rate 5^{o}C per minute. The products have a diameter of 1.2 cm and a height of 0.3 cm.

2.1.1.2 Preparation of the cordierite by conventional sintering from kaolin

Vietnamese kaolin exploited from Yen Bai province was used. Because kaolin contains the additional oxides and impurities, the material was activated in order to remove unexpected substances. The activation process includes:

i. Eliminating the sand by settling and filtering.

ii. Activation of the kaolin to get rid of iron oxides:

+ In hydrochloric solution 36% wt for 3 hours,

+ In hydrochloric solution 10% wt for 1 day, and

+ In hydrochloric solution 10% wt for 5 days.

iii. Wash activated kaolin until Cl^- ion was removed completely from kaolin

After activation, the kaolin was dried at 105^{o}C for 5 hours. The composition of the kaolin after activation is listed in table 2.1.

Table 2.1: The content (weight %) of main metal oxides in kaolin after activation

Metal oxides	SiO_2	Al_2O_3	MgO	Fe_2O_3
Content	51.47	29.53	0.44	1.01

As can be seen from table 2.1, the contents of Cordierite's components (SiO_2, Al_2O_3, and MgO) in kaolin are not present in the correct stoichiometric amount to form Cordierite, thus for each 20 gram of activated kaolin, 2.542 gram MgO and 1.0914 gram Al_2O_3 was added. Afterward, the components were ground, mixed, and dried before making pellets. The slurry of precursor powder was mixed thoroughly by magnetic stirring for 3 hour. Cordierite pellets were made using a cylinder with a pressed force 500 N for 5 minutes. The pellets were calcined at 1250^{o}C for 3 hours. The products have a diameter of 0.5 cm and a height of 0.3 cm.

2.1.1.3 Preparation of the cordierite by the sol-gel method

Cordierite was synthesized by a sol – gel method from $Al(NO_3)_3$. $9H_2O$ (99%, China), $Mg(NO_3)_2$. $6H_2O$ (99%, China), and TEOS (Merk, Germany). 55.4ml TEOS was

put into a beaker which contained 15 ml ethanol and 450 ml distilled water. The mixture was stirred at room temperature for 2 hours.

Separately, 37.5 gram $Al(NO_3)_3$. $9H_2O$ and 31.8gram $Mg(NO_3)_2$.$6H_2O$ were dissolved completely in 100 ml distilled water under stirring conditions. 84.164 gram citric acid was dissolved completely in 300 ml distilled water under stirring conditions.

$Mg(NO_3)_2$ and citric acid solutions were poured stepwise to the $Al(NO_3)_3$ solution. The mixture was stirred until a homogenous solution was obtained. Then, this solution was put slowly into the TEOS solution. The final mixture was stirred at 60 – 80°C until a white gel was formed. The gel was dried at 120°C for 5 hours to form a white powder. Finally, the powder was ground, and calcined as mentioned previously.

2.1.2 Preparation of Cordierite using additives

In some experiments, activated carbon and cellulose additives were added to the precursor mixed powder prepared by conventional sintering and sol-gel methods with the aim to increase the surface area and porosity of cordierite.

The cellulose and activated carbon were added to the powder according to the ratio 5, 10, 15 wt.%. The slurry of mixture containing precursor mixed powder (above) and additives were stirred by a magnetic stirrer for 3 hours. Afterward, the dough was put into the drier set up at 80°C. When the water was vaporized completely, each 1 gram precursor powder was pressed by a hydraulic presser under pressure 25.10^4 N for 10 minutes to make a pellet with the diameter 1.2 cm, and height 0.3 cm. The pellets were calcined at 1250°C for 3 hours.

2.1.3 Preparation of cordierite with the addition of dolomite

In some experiments, dolomite ($CaMg(CO_3)_2$) was added in the precursor powder containing kaolin, $Mg(OH)_2$ and industrial $Al(OH)_3$. The use of dolomite and industrial $Al(OH)_3$ aimed to reduce the cost of cordierite. Moreover, other oxides (CaO, Fe_2O_3) existed in the dolomite and industrial $Al(OH)_3$ which will be removed by further acid treatment may help to increase surface area of cordierite product. Table 2.2 lists the composition of different cordierite samples synthesized with the addition of dolomite and industrial $Al(OH)_3$.

The slurry of precursors in water were mixed by magnetic stirrer for 3 hour, then dried it at 120°C for 30 minute to get the optimal humidity. Afterward, the dough was pressed into cylinder to produce the pellet with 0.5 cm diameter and 0.3 cm thickness. These pellets were calcined at 1250°C for 3 hour to yield cordierite phase.

2.1.4 Surface treatment of prepared Cordierite

Cordierite pellets were immersed in 100 ml of boiling oxalic acid solution (40 wt%, China, A grade) for 2, 4, 7 hours. The treated pellets were thoroughly washed with distilled water until a pH value of 7 is reached and then dried at room temperature. For extended treatments, the acid solution was replaced with a fresh solution every hour.

Cordierite pellets was also treated with HCl 36 wt.% solution (A grade, China) using the same procedure.

2.1.5 Surface treatment of FeCr alloy substrate

In this work, FeCr alloy was also used as substrates. Prior to used, surface of the metallic substrate must be treated in order to increase wetting ability of the samples. Metallic foils which are 2 cm in length, and 1 cm in width were stored in ethanol solution before treatment. There are two steps of cleaning process as chemical etching and thermal treatment. The chemical etching included treating the metal foil in chemical solution such as NaOH 10 wt.% solution, HNO_3 10 wt.% solution, oxalic acid 1.5 wt.% solution, peroxide 1 wt.% solution. Next, the obtained metal foils were calcinated at 800^oC for deep treatment. Finally, all the treated metal samples were stored in the ethanol solution for preventing from impurities in atmospheres.

In order to find the optimal process of treatment, we changed the order of two steps. For the first group (A), we treated the metal foil in chemical solutions before thermal treatment. And for the second group (B), we reversed the process.

All the samples of prepared substrates were listed in table 2.2.

Table 2.2: Synthesis condition of substrates samples

No	Symbol	Precursors	Synthesis condition	Desired product
1	SSR-0	MgO, Al_2O_3 and SiO_2	Solid-state reaction method, calcination at 1250^oC	Cordierite
2	SG-0	$Al(NO_3)_3$. $9H_2O$, $Mg(NO_3)_2$. $6H_2O$ and TEOS.	Sol-gel method, calcination at 1250^oC	Cordierite
3	CV-0	kaolin, commercial MgO, Al_2O_3	Conventional sintering method, calcination at 1250^oC	Cordierite
4	CV-5, 10 AC	kaolin, commercial MgO, Al_2O_3, addition of 5, 10 wt.% of activated carbon	Conventional sintering method	Cordierite
5	SG-5AC	$Al(NO_3)_3$. $9H_2O$, $Mg(NO_3)_2$. $6H_2O$ and TEOS, addition of 5 wt.% of activated carbon	Sol-gel method	Cordierite
6	CV-0-Ox2, 4, 7	CV-0	Treatment in oxalic acid solution at 90^oC for 2, 4, 7 hour	Cordierite
7	CV-0-HCl2, 4, 6, 8, 10, 12, 14	CV-0	Treatment in HCl solution at 90^oC for 2, 4, 6, 8, 10, 12, 14 hour	Cordierite
8	TD1	Kaolin, $Mg(OH)_2$, industrial $Al(OH)_3$, Dolomite: 8.69	Conventional sintering method, calcinations at 1250^oC	Cordierite

		wt.%		
9	TD2	Kaolin, $Mg(OH)_2$, industrial $Al(OH)_3$, Dolomite: 16.27 wt.%	Conventional sintering method, calcinations at 1250^oC	Cordierite
10	TD1.1	TD1	Treatment in HCl solution at 90^oC for 8 hour	Cordierite
11	TD2.1	TD2	Treatment in HCl solution at 90^oC for 8 hour	Cordierite
12	FeCr alloy	FeCr alloy	original	FeCr alloy
13	A1	FeCr alloy	Chemical treatment in NaOH 10 wt.% solution at 60^oC for 10 minute, then in solution of HNO_3 10 wt.%, H_2O_2 1 wt.%, oxalic acid 1.5 wt.% for 5 min. Afterward, thermal treatment at 800^oC for 3 hour.	FeCr alloy
14	A2	FeCr alloy	Similar to A1, but differ in 15 min immersion in acid solution	FeCr alloy
15	A3	FeCr alloy	Similar to A1, but differ in absence of HNO_3 in acid solution	FeCr alloy
16	A4	FeCr alloy	Similar to A3, but differ in 15 min immersion in acid solution	FeCr alloy
17	A5	FeCr alloy	Similar to A1, but differ in absence of oxalic acid in acid solution	FeCr alloy
18	B0	FeCr alloy	Thermal treatment at 800^oC for 3 hour, without any chemical etching.	FeCr alloy
19	B1	B0	NaOH 5 wt.% solution at 60^oC for 10 minute	FeCr alloy
20	B2	B0	NaOH 10 wt.% solution at 60^oC for 10 minute	FeCr alloy
21	B3	B0	NaOH 20 wt.% solution at 60^oC for 10 minute	FeCr alloy
22	B4	B0	solution of H_2O_2 1wt.%, oxalic acid 1.5 wt.% solution at 60^oC for 5 minute	FeCr alloy
23	B5	B0	NaOH 10 wt.% solution at 60^oC for 10 minute, next in solution of HNO_3 10 wt.%, H_2O_2 1 wt.%, oxalic acid 1.5 wt.% for 5 min	FeCr alloy
24	B6	B0	NaOH 10 wt.% solution at 60^oC for 10 minute, next in solution of H_2O_2 1 wt.%, oxalic acid 1.5 wt.% for 5	FeCr alloy

			min	

2.2 Preparation the supports

2.2.1 γ-Al_2O_3

250 ml distilled water and 50g $Al(NO_3)_3$. 9H2O were put into beaker and stirred thoroughly until a homogeneous solution was obtained. Then solution NaOH 25 w.t% was added gradually to get pH over 12. At this moment, precipitate appeared. It is necessary for the precipitate to accumulate at the bottom of the beaker after one night. Next, the alumina solution was filtered to remove precipitate of hydroxide of other metals. The obtained alumia solution was heat to 80 – 85°C. Then, liquid H_2SO_4 15 wt.% was dropped to the solution alumina under vigorous stirring. The pH of the obtained solution was 8.5. The beohmite precipitate was filtered by Bucher filter and washed by hot distilled water until SO_4^{2-} ion was eliminated completely. The boehmite was dried at 80°C for 8 hour and then 120°C for 4 hour.

Finally, beohmite was calcined at 550°C for 3 hour to get γ-alumina.

2.2.2 $Ce_{0.2}Zr_{0.8}O_2$ mixed oxides

Mesoporous $Ce_{0.2}Zr_{0.8}O_2$ mixed oxide was prepared by hydrothermal route. $Ce(NO_3)_3$. $6H_2O$ and ZrOCl2. $8H_2O$ were used as the precursors.

According to the ratio of Ce and Ze in the mixed oxide $Ce_{0.2}Zr_{0.8}O_2$, 1.6 mmol $Ce(NO_3)_3$. $6H_2O$ and 6.4 mmol $ZrOCl_2$. $8H_2O$ were put together in the beaker. Next, 16 mmol urea was added to that mixture. Water was added to get the total volume as 80 ml.

In case of using the surfactant, 100 ml solution of 3 mmol CTAB (cetyl trimethyl ammonium bromide -(($C_{16}H_{33}N(CH_3)_3Br$) was added to the above obtained solution.

Afterward, the obtained solution was stirred until completely dissolved. The solution was poured into an autoclave. The autoclave was put in a warm oven at 160°C for 24 hours. Then, the obtained light-yellow precipitate was then washed by distilled water to pH as 7. The solid was dried at 80°C, and calcined at 500°C for 4h

2.2.3 $AlCe_{0.2}Zr_{0.05}O_2$ mixed oxides

The method to prepare the mixed oxides of Al, Ce, Zr is co-precipitation. The precursors $Al(NO_3)_3$. $9H_2O$, $Ce(NO_3)_3$. $6H_2O$ and $ZrO(NO_3)_2$. xH_2O from Aldrich-Sigma were used. The molar ratio of Al : Ce : Zr is 20 : 4 : 1 for all experiments. Thus, 20 mmol $Al(NO_3)_3$. $9H_2O$, 4 mmol $Ce(NO_3)_3$. $6H_2O$ and 1 mmol $ZrO(NO_3)_2$. xH_2O were dissolved in 150 ml distilled water. Then they were mixed under thorough mixing for 1 hour. In these experiments, we used three kinds of surfactants, SDS (sodium dodecyl sulfate – $CH_3(CH_2)OSO_3Na$), CTAB (cetyltrimethylammoniumbromide -(($C_{16}H_{33}N(CH_3)_3Br$), and PEG (polyethylene glycol – H-(O-CH_2-CH_2)$_n$-OH). 2.5 mmol SDS (or CTAB, or PEG) was dissolved in 100 ml distilled water. After 1 hour, the solution of Al, Ce, Zr was mixed with the surfactant solution. To get the best diffusion of the all composition, the mixture was mixed for 3 hour before adding the precipitant. The pH was adjusted to 9 by adding KOH, NH_4OH or NH_4HCO_3. At this moment, the solution was turned to white due to precipitate. The obtained solution was poured to the autoclave. The autoclave was set up at high temperature (90 or 160°C) for 20 hour. After ageing, the solid was settled at the bottom of the autoclave, then it was filtered by ethanol and distilled water until the pH

unchanged as 7. Finally, the as-synthesized sample was dried overnight at 60^{o}C, and then calcined at 550^{o}C for 3 hour.

In order to investigate the influence of the precipitants, the ageing temperature, and the surfactants to the mixed oxides, these factors were changed in each experiment.

All the prepared supports were listed in table 2.3

Table 2.3: Synthesis conditions of supports samples

No	Symbol	Precursors	Synthesis condition	Desired product
1	Boehmite	$Al(NO_3)_3.9H_2O$	Precipitation	AlOOH
2	γ-Al_2O_3	Boehmite	Calcined at 550^{o}C for 3 hour	γ-Al_2O_3
3	CZ28-non template as-prepared	$Ce(NO_3)_3$. $6H_2O$, $ZrOCl_2$. $8H_2O$, urea	Hydrothermal synthesis method	$Ce_{0.2}Zr_{0.8}O_2$ uncalcined
4	CZ28-non template	CZ28-non template as-prepared	calcined at 550^{o}C	$Ce_{0.2}Zr_{0.8}O_2$
5	CZ28-CTAB as prepared	$Ce(NO_3)_3$. $6H_2O$, $ZrOCl_2$. $8H_2O$, CTAB, urea	Hydrothermal synthesis method	$Ce_{0.2}Zr_{0.8}O_2$ uncalcined
6	CZ28-CTAB	CZ28-CTAB as prepared	calcined at 550^{o}C	$Ce_{0.2}Zr_{0.8}O_2$
7	ACZ08	$Al(NO_3)_3$. $9H_2O$, $Ce(NO_3)_3$. $6H_2O$ and $ZrO(NO_3)_2$. xH_2O, NH_4HCO_3	Co-precipitation	$AlCe_{0.2}Zr_{0.05}O_2$
8	ACZ09	$Al(NO_3)_3$. $9H_2O$, $Ce(NO_3)_3$. $6H_2O$ and $ZrO(NO_3)_2$. xH_2O, NH_4OH	Co-precipitation	$AlCe_{0.2}Zr_{0.05}O_2$
9	ACZ10	$Al(NO_3)_3$. $9H_2O$, $Ce(NO_3)_3$. $6H_2O$ and $ZrO(NO_3)_2$. xH_2O, KOH	Co-precipitation	$AlCe_{0.2}Zr_{0.05}O_2$
10	ACZ11	$Al(NO_3)_3$. $9H_2O$, $Ce(NO_3)_3$. $6H_2O$ and $ZrO(NO_3)_2$. xH_2O, NH_4HCO_3	Co-precipitation, aging at 90^{o}C	$AlCe_{0.2}Zr_{0.05}O_2$
11	ACZ12	$Al(NO_3)_3$. $9H_2O$, $Ce(NO_3)_3$. $6H_2O$ and $ZrO(NO_3)_2$. xH_2O, NH_4HCO_3	Co-precipitation, aging at 160^{o}C	$AlCe_{0.2}Zr_{0.05}O_2$

12	ACZ13	$Al(NO_3)_3$. $9H_2O$, $Ce(NO_3)_3$. $6H_2O$ and $ZrO(NO_3)_2$. xH_2O, NH_4HCO_3, SDS	Co-precipitation, aging at 160°C	$AlCe_{0.2}Zr_{0.05}O_2$
13	ACZ14	$Al(NO_3)_3$. $9H_2O$, $Ce(NO_3)_3$. $6H_2O$ and $ZrO(NO_3)_2$. xH_2O, NH_4HCO_3, CTAB	Co-precipitation, aging at 160°C	$AlCe_{0.2}Zr_{0.05}O_2$
14	ACZ15	$Al(NO_3)_3$. $9H_2O$, $Ce(NO_3)_3$. $6H_2O$ and $ZrO(NO_3)_2$. xH_2O, NH_4HCO_3, PEG	Co-precipitation, aging at 160°C	$AlCe_{0.2}Zr_{0.05}O_2$

2.3 Deposition methods of support on cordierite substrate

2.3.1 Direct combustion

Acid treated cordierite pellets, which were taken out from an oven at 120°C and 420°C, were immediately impregnated by immersion in an aqueous solution, containing $Ce(NO_3)_3$ and $ZrOCl_2$ with the Ce/Zr molar ratio of 2/8. Concentration of this solution is 200 gram of expected formed $Ce_{0.2}Zr_{0.8}O_2$ in a litre of the solution, which was proved as the best value to get the highest loading [82]. After the immersion, each cordierite pellet was withdrawn using a tweezer, thus allowing the removal of excess solution. Subsequently, they were immediately placed into the oven maintained at 120°C or 420°C. Afterwards, samples were blown with air in order to remove the $Ce_{0.2}Zr_{0.8}O_2$ particles which were not perfectly bonded to the substrate.

2.3.2 Hydrid deposition

In this method, a sol of $Ce(NO_3)_3$ and $ZrOCl_2$ acts as a binder to attach previous formed $Ce_{0.2}Zr_{0.8}O_2$ powders on cordierite substrate.

A sol of $Ce(NO_3)_3$ and $ZrOCl_2$ was prepared by dissolving 0.868g $Ce(NO_3)_3.6H_2O$ and 2.578g $ZrOCl_2.8H_2O$ with 1 ml nitric acid. 5 ml of the sol was mixed with 0.117 g of as prepared $Ce_{0.2}Zr_{0.8}O_2$ powder (section 2.2.2), resulting in a slurry. After thoroughly stirring, acid treated - cordierite pellets were dip-coated into the prepared slurry. After drying for 6h, the pellets were calcined at 550°C for 3hour.

2.3.3 Suspension

The treated-cordierite pellets were immersed in a slurry which contains 1 g of as-prepared $Ce_{0.2}Zr_{0.8}O_2$ powder (section 2.2.2) having BET surface area of 200 m^2/g, 1 ml Brij 56 ($C_{16}H_{33}(OCH_2CH_2)_nOH$, n~10, SIGMA), 3 ml distillated water and 1 ml solution HNO_3 65 wt.% in a total 5ml of slurry. The concentration of as-prepared $Ce_{0.2}Zr_{0.8}O_2$ powder is thus calculated as 200g/l. The mixing time of the slurry was 24h. The treated ceramic was maintained immersed in this slurry for 5 minutes, afterward dried at 120°C for 1h. This step was repeated 5 times. After each immersion, the air was blown to eliminate the excess liquid and achieve the homogenously thick film of $Ce_{0.2}Zr_{0.8}O_2$ powder on the ceramic surface. Finally, the samples were calcined at 550°C for 4 hours.

For the deposition Al_2O_3, 2 g boehmite (section 2.2.1) was mixed with 0.75 ml HNO_3 65% and 75 ml distilled water to prepared sol beomite. The treated cordierite was immersed in the slurry of boehmite for 3 min at 60°C, then was put into the oven at 95°C for 30 minute until formation of gel layer. The process was repeated 3 times before calcinations at 550°C for 2h.

2.3.4 Secondary growth

– Seeding procedure

The cordierite pellets were firstly seeded with $Ce_{0.2}Zr_{0.8}O_2$ powder according to the above described direct combustion procedure at 420°C. This procedure was repeated 2 times.

– Hydrothermal synthesis step

The seeded substrates were put into a 80ml solution containing of 6.4 mmol $ZrOCl_2$. $8H_2O$, 1.6 mmol $Ce(NO_3)_3.6H_2O$ and 16 mmol urea in an autoclave. After ageing at 180°C for 3 hour, the solid was removed from the autoclave, washed with distillated water, dried at 80°C, and calcined at 550°C for 4 hour.

2.3.5 Double depositions

The first deposition was performed by the wet impregnation of the cordierite pellets in the solution containing stoichiometric quantities of $ZrOCl_2$. $8H_2O$, 1.6 mmol $Ce(NO_3)_3$. $6H_2O$ (corresponding to Ce/Zr molar ratio of 2/8). The total concentration of the solutes was 200g/l. After 5 minutes of immersion, the cordierite pellets were dried at 120°C for 15 minutes. The immersion was repeated ten times. Afterwards, the coated cordierite was calcined at 300°C for 2 hour

The second deposition was performed following the above described suspension method with the following condition: 0.5 ml Brij56, mixing time of the slurry is 24h, the procedure is repeated 5 times. The as prepared $Ce_{0.2}Zr_{0.8}O_2$ powder (prepared according to section 2.2.2) used for this deposition possesses BET surface area of 117 m^2/g.

For the deposition of Al_2O_3, the aluminate solution was prepared by 2g $Al(NO_3)_3$ dissolved in 10 ml distilled water. The immersion was repeated 3 times.

The second deposition was performed following the above described suspension method with the following condition: 2g boehmite (section 2.2.1), 5ml distilled water, 6ml HNO_3, 0.5 ml Brij56, mixing time of the slurry is 24h, the procedure is repeated 2 times.

For the deposition of $AlCe_{0.2}Zr_{0.05}O_2$, the solution containing stoichiometric quantities of 7.5g of $Al(NO_3)_3.9H_2O$, 0.322 g of $ZrOCl_2$. $8H_2O$, and 1.73 g of $Ce(NO_3)_3$. $6H_2O$ (corresponding to Al/Ce/Zr molar ratio of 20/4/1) was prepared.

The second deposition was performed following the above described suspension method with the following condition: 2g ACZ13 as-prepared, 5ml distilled water, 6ml HNO_3, 0.5 ml Brij56, mixing time of the slurry is 24h, the procedure is repeated 5 times. The as-prepared ACZ13 powder (prepared according to section 2.2.3) was used for this deposition. Other steps was followed the double depositions procedure.

All the support deposited on substrates samples were listed in table 2.4

Table 2.4: Synthesis conditions of supports deposited on substrates samples

No	Symbol	Precursors	Synthesis condition	Desired product

1	SC-120	$Ce(NO_3)_3$ and $ZrOCl_2$, CV-0-HCl8	Direct combustion at 120°C	$Ce_{0.2}Zr_{0.8}O_2$/treated cordierite
2	SC-420	$Ce(NO_3)_3$ and $ZrOCl_2$, CV-0-HCl8	Direct combustion at 420°C	$Ce_{0.2}Zr_{0.8}O_2$/treated cordierite
3	HD	$Ce(NO_3)_3$ and $ZrOCl_2$, CZ28-CTAB as prepared, CV-0-HCl8	Hydrid deposition	$Ce_{0.2}Zr_{0.8}O_2$/treated cordierite
4	Su-CZ	CZ28-CTAB as prepared, CV-0-HCl8	Suspension	$Ce_{0.2}Zr_{0.8}O_2$/treated cordierite
5	Su-A	$Al(NO_3)_3.9H_2O$, boehmite, CV-0-HCl8	Suspension	γ-Al_2O_3/ treated cordierite
6	Seed	$Ce(NO_3)_3$ and $ZrOCl_2$, SC-420	Second growth seeding	$Ce_{0.2}Zr_{0.8}O_2$/treated cordireite
7	DD-CZ	$Ce(NO_3)_3$ and $ZrOCl_2$, CZ28-CTAB as prepared, CV-0-HCl8	Double depositions	$Ce_{0.2}Zr_{0.8}O_2$/treated cordierite
8	DD-A	$Al(NO_3)_3.9H_2O$, boehmite, CV-0-HCl8	Double depositions	γ-Al_2O_3/ treated cordierite
9	DD-ACZ	$Al(NO_3)_3.9H_2O$, $Ce(NO_3)_3$ and $ZrOCl_2$,ACZ13-as prepared, CV-0-HCl8	Double depositions	$AlCe_{0.2}Zr_{0.05}O_2$/ treated cordierite
10	SG-A	$Al(NO_3)_3.9H_2O$, CV-0-HCl8	Sol-gel	γ-Al_2O_3/ treated cordierite

2.4 Deposition of support on metal substrates

The support materials was deposited on the best treated metal substrate samples by dip-coating. The samples was dipped in the mother solution of support, then dried at 60°C for 4 hours, then 120°C for next 4 hour. The process was repeated 5 times. The coated samples were calcined at 550°C for 3 hour.

The mother solution of γ-Al_2O_3 support was prepared by 3.84 g $Al(NO_3)_3$. $9H_2O$ was dissolved in 8 ml distilled water mixing with 2.92 g etylen diamin tetraacetic acid - EDTA (Merck), 10 ml H_2O and 2.5 ml etylen amin - EA (Merck), the pH was adjusted to 7 by adding EA.

The mother solution of $AlCe_{0.2}Zr_{0.05}O_2$ was prepared by mixing the separated solution of $Ce(NO_3)_3$, $ZrOCl_2$ and $Al(NO_3)_3$ according to molar ration of Al: Ce: Zr = 20:4:1. The cerium solution, and zirconium solution were prepared as the same as aluminium solution but the amount of $ZrOCl_2$ and $Ce(NO_3)_3$ as 3.44g and 4.34g, respectively.

2.5 Deposition of active catalytic phase on support/substrate

Different active phases (MnO_2-NiO-Co_3O_4, MnO_2-Co_3O_4-CeO_2) were deposited on support/substrates by wet impregnation method using starting materials are $Co(NO_3)_2$.

$6H_2O$, $Ni(NO_3)_2.6H_2O$ (99.0 wt.%, Merck), $Mn(NO_3)_2$ solution (58 wt.%, Merck) and $Ce(NO_3)_3.6H_2O$ (99.0 wt.%, Merck). The support/substrate samples were dried at 120oC for 30 min prior to the deposition of the active phase.

For MnO_2-NiO-Co_3O_4 catalyst, the prepared support /substrate ($Ce_{0.2}Zr_{0.8}O_2$/cordierite) was immersed in the solution of $Mn(NO_3)_2$, $Ni(NO_3)_2$ and $Co(NO_3)_2$ with the content as 747 g/l. Then, the complete catalyst was dried at 120°C for 30 min. The process was repeated 5 times before calcinations at 550°C for 3 hour.

The active phase including MnO_2-Co_3O_4-CeO_2 mixed oxides (the mole ratio was 21:63:16, respectively) was also deposited on the substrates by wet impregnation. The prepared support/ substrates with different supports such as γ-Al_2O_3, $Ce_{0.2}Zr_{0.8}O_2$ and $AlCe_{0.2}Zr_{0.05}O_2$ were immersed in the solution of active phase which had the concentration of 850g/l. Next, the complete catalysts were removed from the solution and dried at 120°C for 30 min. The process was repeated 5 times before calcinations at 550°C for 3 hour. For metal substrate, the same procedure was carried out by dip-coating to make complete catalyst.

2.6 Preparation of the real catalytic converter

A catalyst monolith (100 cpsi) module of cross section 5 x 5 cm, and length 7.5 cm was used to prepared a real catalytic converter to set up to the exhaust tube of motorbike. The support material and active phase were deposited on monolith by wet impregnation. Firstly, the treated monolith was impregnated in the solution of Al^{3+}, Ce^{3+} and Zr^{4+} prepared from 22,5 g $Al(NO_3)_3.9H_2O$, 6,51 g $Ce(NO_3)_3.6H_2O$ and 4,85 g $ZrOCl_2.8H_2O$ dissolved completely in 100 ml distilled water. After immersion in 5 min, the monolith was dried at 120°C for 30 min in the oven. The process was repeated 5 times before calcinations at 550°C for 3 hour. For the loading of active phase, the coated monolith was impregnated in solution of Mn^{2+}, Co^{2+} and Ce^{3+}, that was prepared by 29,367g solution $Mn(NO_3)_2$ 50 wt.%, 215,578g $Co(NO_3)_2.6H_2O$ và 27,125g $Ce(NO_3)_3.6H_2O$ dissolved completely in 80 ml distilled water. The immersion, drying and calcinations was carried out the same as the support deposition process. The loaded support material and active phase on cordierite were 5 wt% and 5.7 wt%, respectively.

Table 2.5: Synthesis conditions of catalyst samples

No	Symbol	Precursors	Synthesis condition	Desired product
1	Ca.2	$Co(NO_3)_2$. $6H_2O$, $Ni(NO_3)_2.6H_2O$ $Mn(NO_3)_2$, CV-0-HCl8	Prepared by wet impregnation	MnO_2 – NiO – Co_3O_4 / cordierite
2	Ca.3	$Co(NO_3)_2$. $6H_2O$, $Ni(NO_3)_2.6H_2O$ $Mn(NO_3)_2$, DD-CZ	Prepared by wet impregnation	MnO_2 – NiO – Co_3O_4/ $Ce_{0.2}Zr_{0.8}O_2$/ cordierite
3	Ca.4	$Co(NO_3)_2$. $6H_2O$, $Mn(NO_3)_2$ solution $Ce(NO_3)_3.6H_2O$, CV-0-HCl8	Prepared by wet impregnation	MnO_2 – Co_3O_4-CeO_2/ cordierite
4	Ca.5	$Co(NO_3)_2$. $6H_2O$, $Mn(NO_3)_2$	Prepared by	MnO_2 – Co_3O_4-

		solution $Ce(NO_3)_3.6H_2O$, DD-A	wet impregnation	CeO_2/Al_2O_3/cordierite
5	Ca.6	$Co(NO_3)_2$. $6H_2O$, $Mn(NO_3)_2$ solution $Ce(NO_3)_3.6H_2O$, DD-CZ	Prepared by wet impregnation	MnO_2 – Co_3O_4-CeO_2/ $Ce_{0.2}Zr_{0.8}O_2$/cordierite
6	Ca.7	$Co(NO_3)_2$. $6H_2O$, $Mn(NO_3)_2$ solution $Ce(NO_3)_3.6H_2O$, DD-ACZ	Prepared by wet impregnation	MnO_2 – Co_3O_4-CeO_2/ $AlCe_{0.2}Zr_{0.05}O_2$/cordierite
7	Ca.8	$Co(NO_3)_2$. $6H_2O$, $Mn(NO_3)_2$ solution $Ce(NO_3)_3.6H_2O$, B2	Prepared by wet impregnation	MnO_2 – Co_3O_4-CeO_2/FeCr foil
8	Ca.9	$Co(NO_3)_2$. $6H_2O$, $Mn(NO_3)_2$ solution $Ce(NO_3)_3.6H_2O$, $Al(NO_3)_3$. $9H_2O$, B2	Prepared by wet impregnation	MnO_2 – Co_3O_4-CeO_2/Al_2O_3/ FeCr foil
9	Ca.10	$Co(NO_3)_2$. $6H_2O$, $Mn(NO_3)_2$ solution $Ce(NO_3)_3.6H_2O$, $Al(NO_3)_3$. $9H_2O$, $ZrO(NO_3)_2$, B2	Prepared by wet impregnation	MnO_2 – Co_3O_4-CeO_2/ $AlCe_{0.2}Zr_{0.05}O_2$/ FeCr foil
10	Ca.11	$Co(NO_3)_2$. $6H_2O$, $Mn(NO_3)_2$ solution $Ce(NO_3)_3.6H_2O$, $Al(NO_3)_3.9H_2O$, $Ce(NO_3)_3.6H_2O$, $ZrOCl_2.8H_2O$, honeycomb monolith CV-0-HCl8	Prepared by wet impregnation	MnO_2 – Co_3O_4-CeO_2/ $AlCe_{0.2}Zr_{0.05}O_2$/cordierite

2.7 Catalyst characterization

2.7.1 X-ray diffraction (XRD)

X-ray diffraction is one of the oldest and most frequently applied techniques in catalyst characterization. It is used to identify crystalline phases inside catalysts by means of lattice structural parameters, and to obtain an indication of particle size.

A conventional X-ray source consists of a target (Cu or Co… metal) that is bombarded with high energy electrons. From this, narrow lines such as the Cu $K\alpha$ line, with a specific energy (8.04 keV) and a specific wavelength (0.154 nm) arises.

X-ray diffraction is the elastic scattering of X-ray photons by atoms in a periodic lattice. X-rays scattered by atoms in an ordered lattice interfere constructively in directions given by Bragg's law :

$$n\lambda = 2d \sin\theta;\ n = 1, 2\ldots \qquad \text{(Eq. 2.1)}$$

where

λ is the wavelength of the X-rays

d is the distance between two lattice planes

θ is the angle between the incoming X-rays and the normal to the reflecting lattice plane

n is an integer called the order of the reflection

The XRD pattern of a powdered sample is measured with a stationary X-ray source (usually Cu Kα) and a movable detector, which scans the intensity of the diffracted radiation as a function of the angle 2θ between the incoming and the diffracted beams. When working with powdered samples, an image of diffraction lines occurs because a small fraction of the powder particles will be oriented such that by chance a certain crystal plane is at the right angle θ with the incident beam for constructive interference. Rotation of the sample during measurement enhances the number of particles that contribute to diffraction.

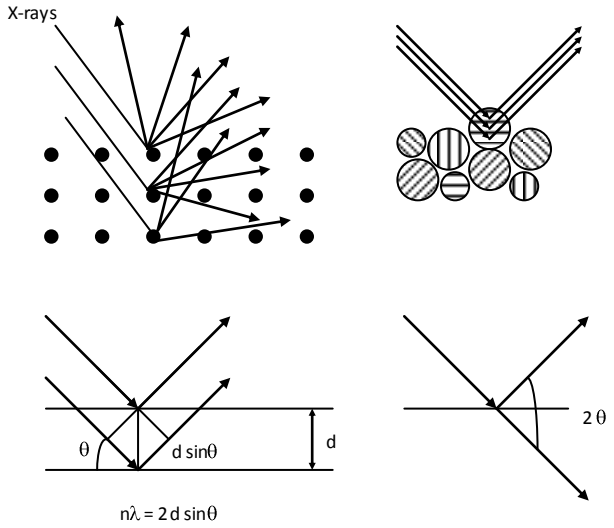

Fig.2.1: Diffraction of X-rays by crystal planes allows one to derive lattice by using Bragg relation.

In catalyst characterization, diffraction patterns are mainly used to identify the crystallographic phases that are present in the catalyst.

XRD has serious disadvantages as well. Because the technique is based on the interference between reflecting X-rays from lattice planes, it requires samples that possess sufficient long-range order. Amorphous phases and small particles give either broad and weak diffraction lines or no diffraction at all, with the consequence that if catalysts contain particles with a large size distribution, XRD may only detect the larger ones. XRD at synchrotrons greatly improves the possibilities for studies of small particles. Finally, the surface region is where catalytic activity resides, but this part of the catalyst is virtually invisible to XRD [84].

In this work, XRD patterns were mainly recorded using a D8 Advance Bruker device (Faculty of Chemistry, Hanoi University of Science, Vietnam). The diffractometer has a Cu source with Cu Kα radiation (λ = 0.154 nm), step scan=0.03.

2.7.2 Characterization of surface properties by physical adsorption

BET theory (has been introduced by Brunauer, Emmett and Teller)aims to explain the physical adsorption of gasmolecules on a solidsurface and serves as the basis for an important analysis technique for the measurement of the specific surface area of a material. BET theory is based on the following assumptions:

- the surface of adsorbent is flat.
- the adsorption process terminates at multilayer coverage.

- all adsorption sites are energetically equivalent.

- there is no mutual interaction between the adsorbed molecules or atoms (no lateral interactions)

- in the first adsorbed layer the heat of adsorption is assumed to be higher than in all other adsorbed layers, where the heat of adsorption is set equal to the latent heat of condensation of the adsorbed gas.

BET equation is expressed as following:

$$\frac{1}{v\left[P_o / P - 1\right]} = \frac{C - 1}{V_m C}\left(\frac{P}{P_0}\right) + \frac{1}{V_m C} \qquad \text{(Eq.2.2)}$$

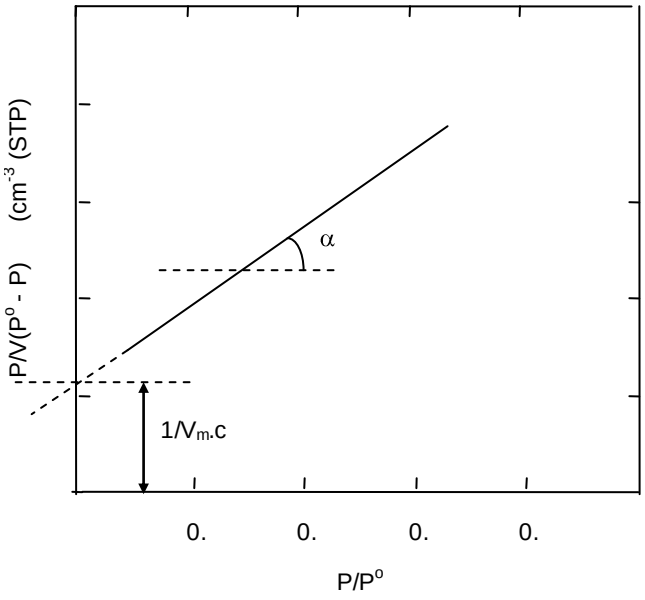

Fig. 2.2: BET plot

P and P_0 are the equilibrium and the saturation pressure of adsorbates at the temperature of adsorption, v is the adsorbed gas quantity (for example, in volume units), and V_m is the monolayer adsorbed gas quantity. C is the BET constant, which is expressed by (Eq.2.3):

$$C = \exp\frac{E_1 - E_L}{RT} \qquad \text{(Eq.2.3)}$$

E_1 is the heat of adsorption for the first layer, and E_L is that for the second and higher layers and is equal to the heat of liquefaction.

Equation (2.2) is an adsorption isotherm and can be plotted as a straight line with $1 / v[(P_0 / P) - 1]$ on the y-axis and $\varphi = P / P_0$ on the x-axis according to experimental results. This plot is called a **BET plot**. The linear relationship of this equation is maintained only in the range of $0.05 < P / P_0 < 0.35$. The value of the slope A and the y-intercept I of the line are used to calculate the monolayer adsorbed gas quantity v_m and the BET constant c. The following equations can be used:

$$v_m = \frac{1}{A + I} \qquad \text{(Ea.2.4)}$$

$$C = 1 + \frac{A}{I} \qquad \text{(Eq. 2.5)}$$

A total surface area S_{total} and a specific surface area$S$ are evaluated by the following equations:

N: Avogadro's number,

$$S_{BET,total} = \frac{(v_m N s)}{V} \qquad \text{(Eq.2.6)}$$

s: adsorption cross section,
V: molar volume of adsorbent gas
a: molar mass of adsorbed species

$$S_{BET} = \frac{S_{total}}{a} \qquad \text{(Eq. 2.7)}$$

Brunauer, Demming, Demming and Teller, based upon an extensive literature survey, found that all adsorption istherms fit into one of the six types shown in figure 2.3.

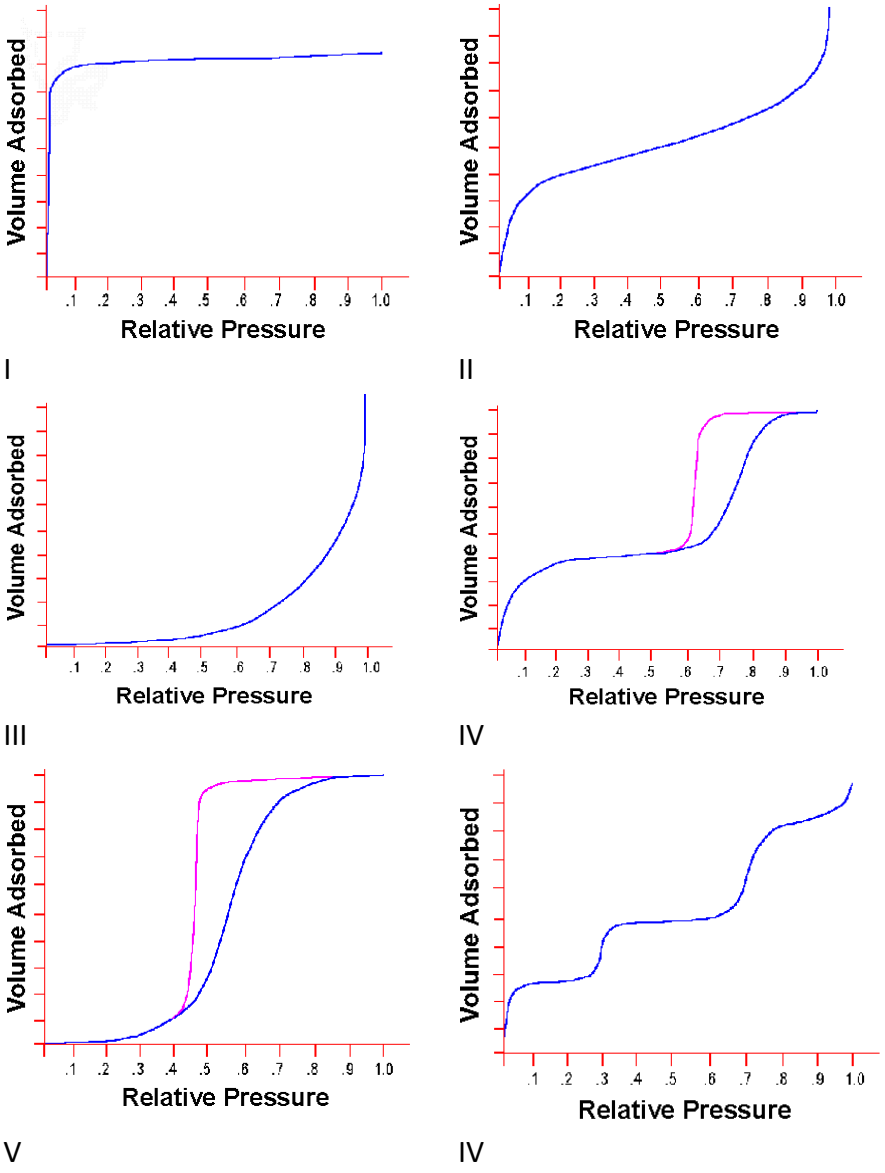

Fig.2.3: Isotherm adsorption

Type I isotherms are encountered when adsorption is limited to, at most, only a few molecular layers. This condition is encoutered in chemisorption, where the asymptotic approach to a limiting quantity indicates that all of the surface sites are occupied. In the case of physical adsorption, type I isotherms are encountered with microporous powders whose pore size does not exceed a few adsorbate molecular diameters. A gas molecule,

when inside pores of these small dimensions, encounters the overlapping potential from the pore walls which enhances the quantity adsorbed a low relative pressures. At higher pressures, the pores are filled by adsorbed or condensed adsorbate leading to the plateau showing little or no addition adsorption after the micropores have been filled. Physical adsorption that produces the type I isotherm indicated that the pores are microporous.

Type II isotherms are most frequently encountered when adsorption occurs on non-porous powders or on powders with pore diameters larger than micropores. The inflection point or knee of the isotherm usually occurs near the completion of the first adsorbed monolayer and, with increasing relative pressure, second and higher layers are completed until, at saturation, the number of adsorbed layers becomes infinite.

Type IV isotherms occur on porous adsorbents possessing pores in the radius range of approximately 2 - 100 nm. The slote increasing at higher elevated pressures indicates an increased uptake of adsorbate as the pores are being filled. As is true for the type II isotherms, the knee of the type IV isothem generally occurs near the completion of the first monolayer.

Generally, a type IV adsorption isotherm will exhibit hysteresis. The presence of the hysteresis loop introduces a considerable complication, in that within the region of the hysteresis loop, there are two relative pressure values corresponding to a given quantity adsorbed with the lower value always residing on the desorption isotherm.

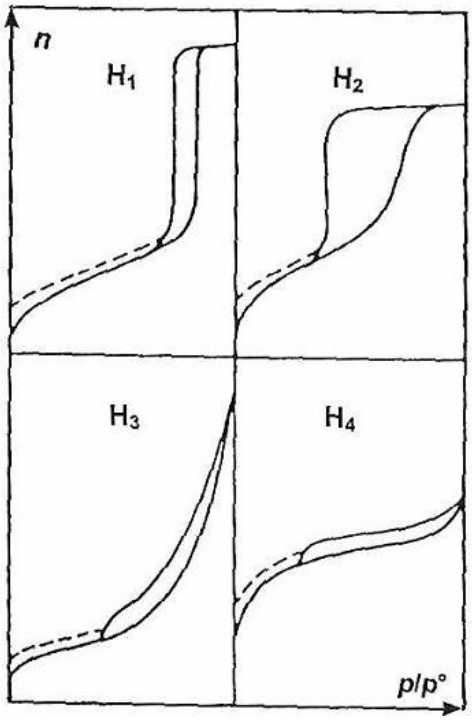

Fig.2.4: IUPAC classification of hysteresis loops (revised in 1985)

Figure 2.4 shows the four types of hysteresis loops. This is the new IUPAC classification, that overtook in 1985 the older De Boer classification. Type H1-hysteresis is due principically to cylindrical pores, open at both ends. Type H2-hysteresis results from so-called ”‘bottleneck”’ or ”‘inktbottle”’ pores. In pores of this shape, emptying of the wide portion will be delayed during desorption until the narrow neck can evaporate. Therefore, the desorption curve exhibits a small slope at high relative pressures and a large

slope where the wide part of the pores evaporates. Type H3-hysteresis and type H4-hysteresis is associated with slit-shaped pores or the spaces between parallel plates [84].

In this thesis, physical adsorption was measured using nitrogen gas as absorbed gas, the nitrogen adsorption isotherm being measured at the boiling point of nitrogen, 77.4 K. The surface area, adsorption isotherm and pore distribution were measured using device: Gemini VII Micrometics in Advanced Institute of Science and Technology, Hanoi, Vietnam.

2.7.3 Scanning electron microscopy (SEM)

SEM belongs to the group of electron microscopy, which is a fairly straightforward technique to determine the size and shape of supported particles, which can also reveal information on the composition and internal structure of the particles, for example by detecting the characteristic X-rays that are produced by the interaction of the electrons with matter, or by analyzing how the electrons are diffracted.

Scanning electron microscopy (SEM) is carried out by rastering a narrow electron beam over the surface and detecting the yield of either secondary or backscattered electrons as a function of the position of the primary beam (Fig2.5). Contrast is caused by the orientation, parts of the surface facing the detector appear brighter than parts of the surface with their surface normal pointing away from the detector. The secondary electrons have mostly low energies (in the approximate range 5-50 eV) and originate from the surface region of the sample. Backscattered electrons come from deeper regions and carry information on the composition of the sample, because heavy elements are more efficient scatters and appear brighter in the image.

An electron microscope offers additional possibilities for analyzing the sample. Diffraction patterns (spots from a single-crystal particle and rings from a collection of randomly oriented particles) enable one to identify crystallographic phases as in XRD. Emitted X-rays are characteristic of an element and allow for a determination of the chemical composition of a selected part of the sample. This technique refers to as energy dispersive X-ray analysis (EDX, EDAX) [84].

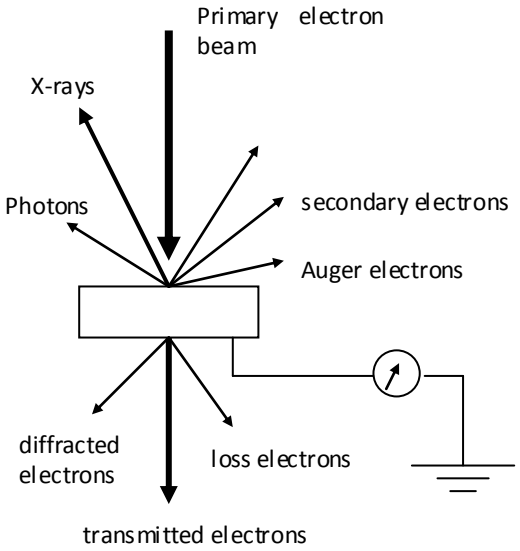

Fig. 2.5: SEM principles: The interaction between the primary electron beam and the sample in an electron microscope leads to a number of detectable signals [84]

SEM images were obtained using a JEOL JSM– 5410– LV scanning electron microscope (National Institute of Hygiene and Epidemiology, Hanoi, Vietnam).

2.7.4 Thermal Analysis

Thermal analysis (TA) is a group of techniques in which a property of the sample is monitored against time or temperature while the temperature of the sample in a specified atmosphere, is programmed.

The following is two techniques which is most common used in TA [84]:

Technique	Abbreviation	Property	Use
1. Thermogravimetric analysis	TGA	Mass	Decompositions Dehydrations Oxidaton
2. Differential thermal analysis	DTA	Temperature difference	Phase changes Reactions

In differential thermal analysis (DTA), the difference in temperature between the sample and an inert reference is measured during a programmed temperature change. The temperature difference between sample and reference should be the same until some thermal event, such as melting, decomposition or change in crystal structure, occurs, in which case the sample temperature either lags behind (if the change is endothermic) or leads (if the change is exothermic) the reference temperature. The arrangement used in DTA is shown in fig.2.6 a. Sample and reference are placed side by side in a heating block which is heated or cooled at a constant rate, identical thermocouples are placed in each and are connected 'back to back'. When the sample and reference are at the same temperature, the net output of this pair of thermocouples is zero. When a thermal event occurs in the sample, a temperature difference ΔT exists between sample and reference which is detected by the net voltage of the thermocouples. A third thermocouple is used to monitor the temperature of the heating block and the results are presented as ΔT against temperature (b). A horizontal baseline, corresponding to $\Delta T = 0$, occurs and superposed on this a sharp peak due to the thermal event in the sample. The temperature of the peak is taken either as the temperature at which deviation from the baseline begins, T_1, or as the peak temperature, T_2. While it is probably more correct to use T_1, it is often not clear where the peak begins and therefore, it is more common to use T_2. The size of the ΔT peak may be amplified so that events with very small enthalpy changes may be detected.

DTA cells are designed for maximum sensitivity to thermal changes, but this is often at the expense of losing a calorimetric response, thus peak areas or peak heights are only qualitatively related to the magnitude of the enthalpy changes occurring [84].

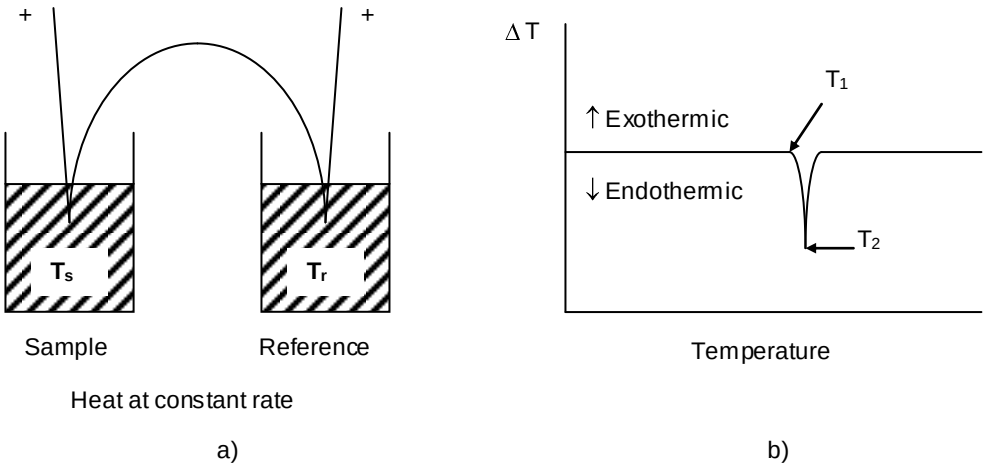

Fig.2.6: The DTA method. **(b) a typical DTA trace, results from the arrangement shown in (a)**

TGA detect changes in mass of the samples due to reaction, vaporization, etc… The results appear as a continuous record as shown in fig. 2.7. The sample is heated at a constant rate and has a constant mass M_i, until it begins to decompose at temperature T_i. Under conditions of dynamic heating, decomposition usually takes place over a range of temperatures, T_i to T_f, and a second constant mass plateau is observed above T_f, which corresponds to the mass of the residue M_i. The masses M_i and M_f and the difference ΔM are fundamental properties of the sample and can be used for quantitative calculations of compositional changes, etc. By contrast, the temperatures T_i and T_f depend on variables such as heating rate, the nature of the solid (e.g. its particle size) and the atmosphere above the sample. T_i and T_f pertain to the particular experimental conditions and do not necessarily represent equilibrium decomposition temperature [84].

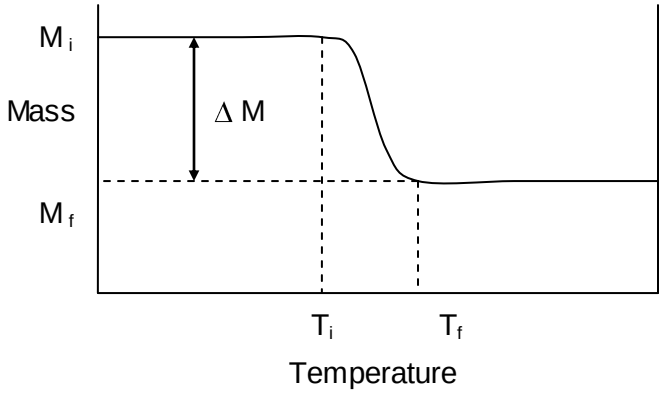

Fig.2.7: Schematic TGA curve for a single step decomposition reaction

TGA-DTA spectra in this thesis were recorded using a NETZSCH STA 409 PC/PG (School of Chemical Engineering, Hanoi University of Science and Technology, Vietnam)

2.7.5 X-ray photoelectron Spectroscopy (XPS)

XPS is among the most frequently used techniques in catalysis. It yields information on the elemental composition, the oxidation state of the elements and in favorable cases on the dispersion of one phase over another. When working with flat layered samples, depth-selective information is obtained by varying the angle between sample surface and the analyzer.

XPS is based on the photoelectric effect, in which an atom absorbs a photon of energy hν, next a core or valence electron with binding energy E_b is ejected with kinetic energy (Eq. 2.8, fig.2.8):

$$E_k = h\nu - E_b - \varphi \qquad \text{(Eq. 2.8)}$$

Where E_k is the kinetic energy of the photoelectron
h is Planck's constant
ν is the frequency of the exciting radiation
E_b is the binding energy of the photoelectron with respect to the Fermi level of the sample
φ is the work function of the spectrometer

Routinely used X-ray sources are Mg Kα (1253.6 eV) and Al Kα (1486.3 eV). In XPS one measures the intensity of photoelectrons N(E) as a function of their kinetic energy. The XPS spectrum however, is usually a plot of N(E) versus E_k, or, more often, versus the binding energy E_b [84].

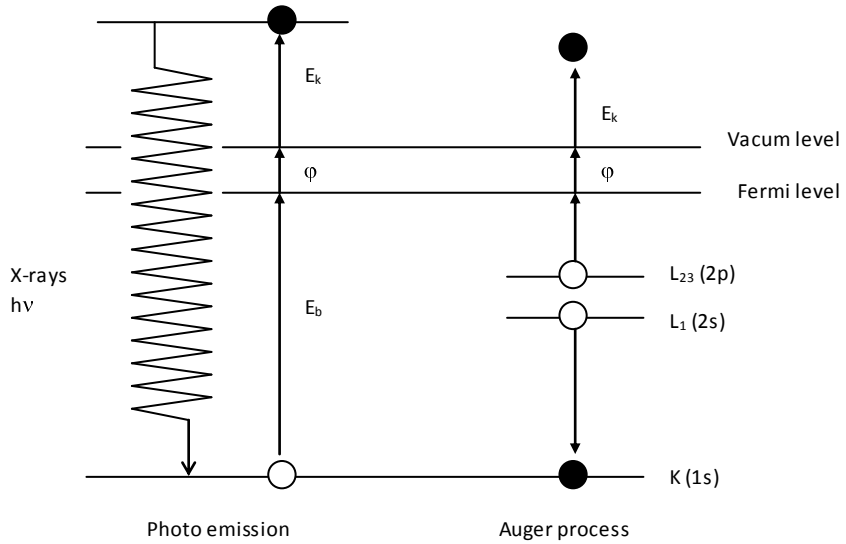

Fig.2.8: Photoemission and the Auger process. Left: An incident X-ray photon is adsorbed and a photoelectron emitted. Measurement of its kinetic energy allows one to calculate the binding energy of the photoelectron. The atom stays behind as an unstable ion with a hole in one of the core levels. Right: The excited ion relaxes by filling the core hoel with an electron from a higher shell. The energy released by this transition is taken up by another electron, the Auger electron, which leaves the sample with an element-specific kinetic energy. In Auger spectroscopy a beam of energetic (2-5 keV) electrons creates the initial core hole [84].

In this work, XPS spectra were recorded using an ESCA Phi 600 spectrometer (Department of Solid State Sciences, Ghent University, Belgium) equipped with an Al anode (hν = 187.850 eV).

2.8 Catalytic activity measurement

2.8.1 Measurement of catalytic activity in the micro-reactor connected with GC online.

In order to measure the catalytic activities in the laboratory scale, we used the micro-line reaction. The catalyst pellets with 5 mm in diameter, 3 mm in thickness were put in a reaction tube made from quart. And the metallic foils were cut into the small pieces to fit the diameter of the tube. Each samples had the weight of 0.42 g.

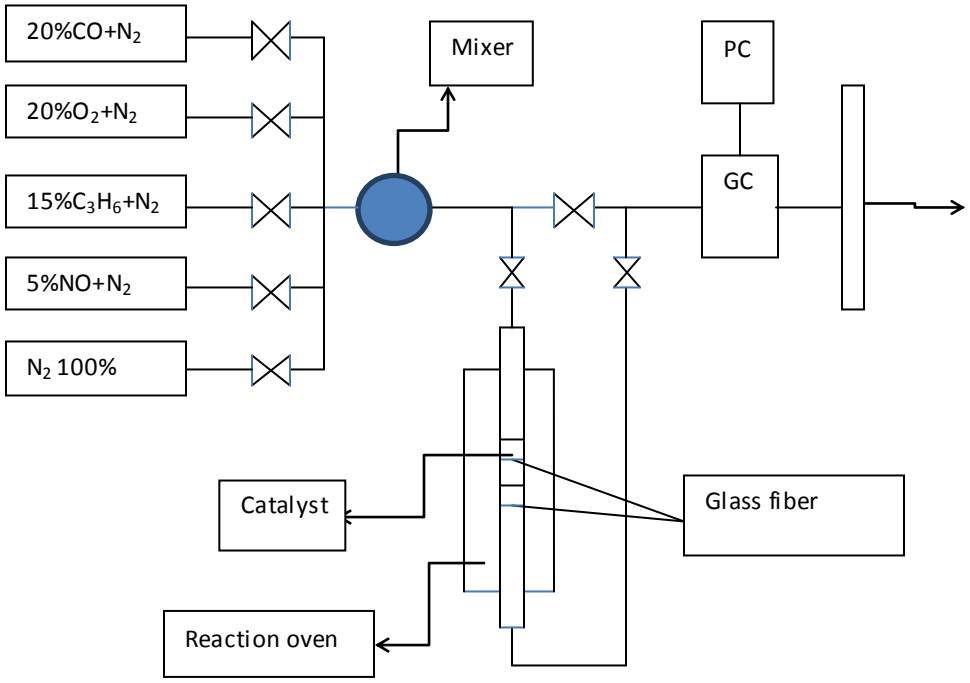

Fig.2.9 : Schema of micro-reactor set up

All the reactions were run at the temperature from 100 to 500°C because this temperature window is suitable with operation condition of catalyst in the reality. a total gas flow of 184.7 ml/min (approximately 30000 h^{-1}) at a pressure of 1 atm. The volume composition of the gas flow was 2.6% CO, 7.7% O_2, 1.5% C_3H_6, 1.9%NO. The products were detected online by gas chromatography FOCUS GC–Thermo Scientific equipped with two detectors Thermo conductivity detector (TCD) and Flam ionization detector (FID). NOx and C_3H_6 were detected with a column of 80/100 chromosorb and a column of carbowax 20M in series while CO_2, CO, O_2 were detected with a column of 60/80 carboxen and a column of 80/100 porapak in series.

+ Catalytic activity was determined through conversion:

- *with* C_3H_6

$$C = \frac{A_{C_3H_6 bypass} - A_{C_3H_6 saupu}}{A_{C_3H_6 bypass}}$$

$A_{C3H6bypass}$: Intensity of C_3H_6 peak before reaction (bypass peak)

$A_{C3H6saupu}$: Intensity of C_3H_6 peak after reaction

CO and NOx conversion were calculated similarly.

2.8.2 Measurement of exhausted gases

Before installing to the exhaust tube of motorbike vespa Lx-125 ie, the catalysis complexes were covered by a stainless crust and then set up as the figure below:

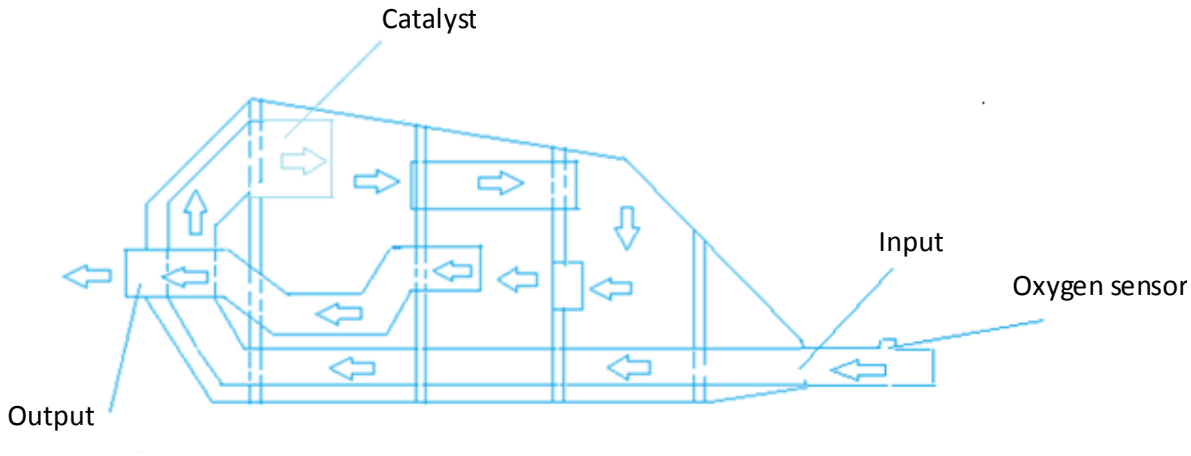

Fig. 2.10: Schema of exhaust tube

After installing the exhaust tube into the motorbike, the composition of exhaust gases was measured by Automotive emission Analyzer, model HG-520. In this equipment, CO, CO_2, HC were analysized by Non Dispersive InfraRed method, O_2, NO_x were analysized by electrochemistry method. The HG-520 device was connected with the motorbike exhaust pipe as demonstrated in fig.2.11.

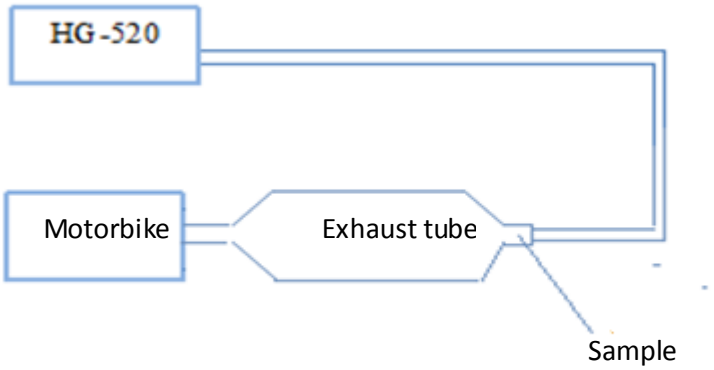

Fig. 2.11 : Schema of measuring motorbike's exhaust gases

The motorbike Vespa LX-125 ie, has been used for 2 years and has been running about 10800 km so far. When testing, the engine was in idle mode in 5 minute, then the results were recorded in next 60 seconds.

Fig. 2.12: Automotive emission Analyzer HG- 520.

3. RESULTS AND DISCUSSION

3.1 Synthesis of cordierite substrate

3.1.1 Influence of synthesis methods on the preparation of cordierite

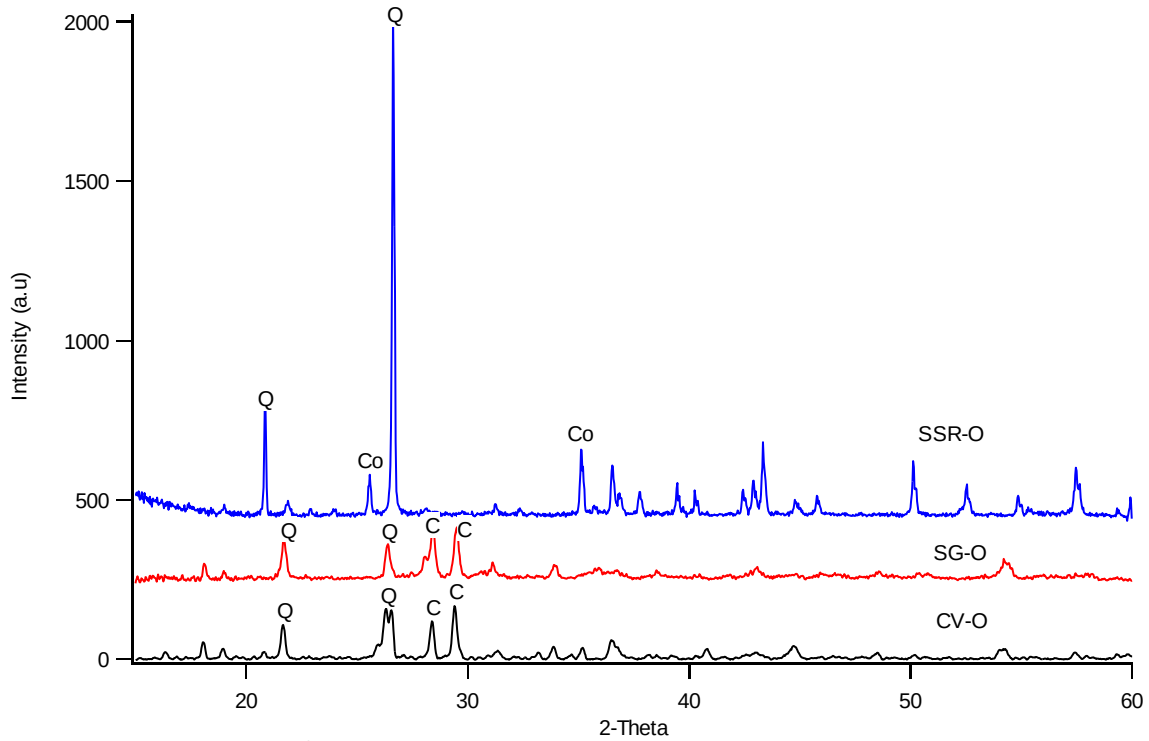

Fig.3.1: XRD patterns of Cordierite samples prepared by various methods as solid-state reaction (SSR-O), sol-gel (SG-O), and conventional sintering (CV-O) (Q: quartz, C: cordierite)

Cordierite was prepared by different methods as solid-state reation of metallic oxides; sol-gel method using $Al(NO_3)_3$, $Mg(NO_3)_2$ and TEOS as the precursors; and conventional sintering using kaolin and commercial MgO, Al_2O_3. XRD patterns of Cordierite samples prepared by different methods are shown in fig. 3.1. It was observed that solid-state reaction method hasn't resulted in high amount of Cordierite. A local enrichment of silica and other metal oxides was inside the pellets. The sample, however, exhibited a higher surface area (table 3.1) than those of other methods since surface area of quartz was known higher than that of cordierite.

Based on the strongest intensity for the cordierite reflections at 2θ of 29.5^o compared to the strongest intensity of other phases (quartz and mullite), the content of cordierite in the samples was estimated, as shown in table 3.1. It is thus clear that sol-gel method resulted in the highest composition of cordierite due to the better mixing of precursor components at atomic scale.

The sol-gel method also produced the cordierite with higher surface area, although it is still low due to the calcination at rather high temperature. Mechanical strength limit of cordierite body prepared using sol-gel method is also higher than that of cordierite prepared by conventional sintering; however, the high cost and difficulty of the preparation may lead to limit the application of this method in large scale production of this monolith.

Table 3.1: Properties of cordierite samples synthesized from different methods

No	Samples	Content of Cordierite (wt%) (*)	S_{BET} (m^2/g)
1	SSR-0	0	2.57
2	CV-0	55.26	0.2
3	SG-0	75.23	0.57

(*) estimated based on the equation: $C_{cordierite} = \frac{I_{Cordierite}}{\sum_1^n I} \times 100\%$ (wt.%)

With: $C_{cordierite}$: content of cordierite phase (wt.%)

$I_{cordieriter}$: Intensity of the strongest peak of Cordierite (a.u)

$\sum_1^n I$: Total of intensities of the strongest peaks of other phases (a.u).

SEM image of cordierite prepared by conventional sintering and sol-gel was demonstrated on fig. 3.2. There was not the big difference of the morphology of Cordierite samples produced from conventional sintering and sol-gel method. Grains of about 5 - 10 μm are found in a good sintering appearance. Nevertheless, the surface of the products prepared by sol-gel method had the smoother surface than the one prepared by conventional sintering method (Fig.3.2). It is because the function of acid citric as a complexing agent to make the Cordierite's compositions combine better.

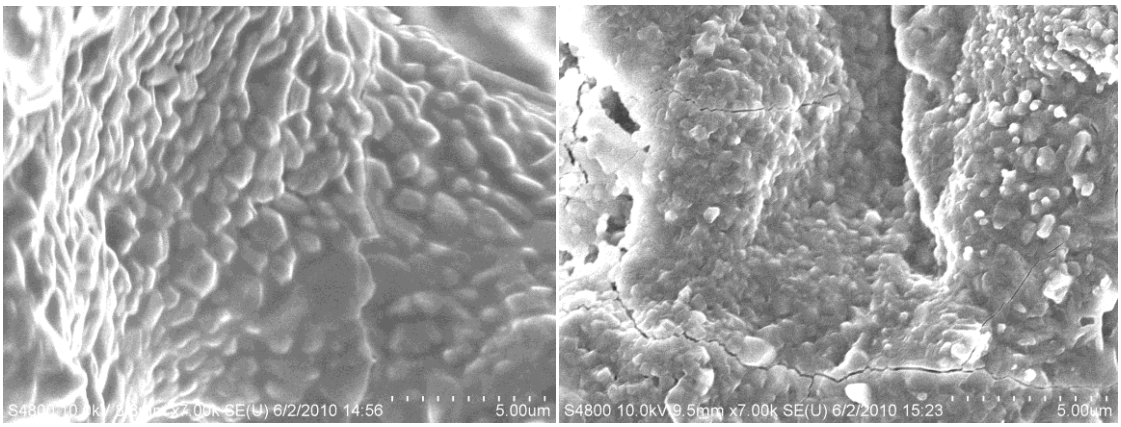

(a) *(b)*

Fig.3.2: SEM image of Cordierite produced by sol-gel processing: SG-0 (a) and conventional sintering of kaolin: CV-0 (b)

Calcination temperature also influences on the formation of cordierite. As seen from TGA-DSC diagram of the precursors (fig.3.3), the formation of cordierite occurs at 1108°C and hasn't completed yet at 1250 °C. Thus cordierite sample was calcined at higher temperature 1400°C with the expectation to obtain more cordierite content. XRD of sample calcined at 1400°C show 100% cordierite phase (fig. 3.4).

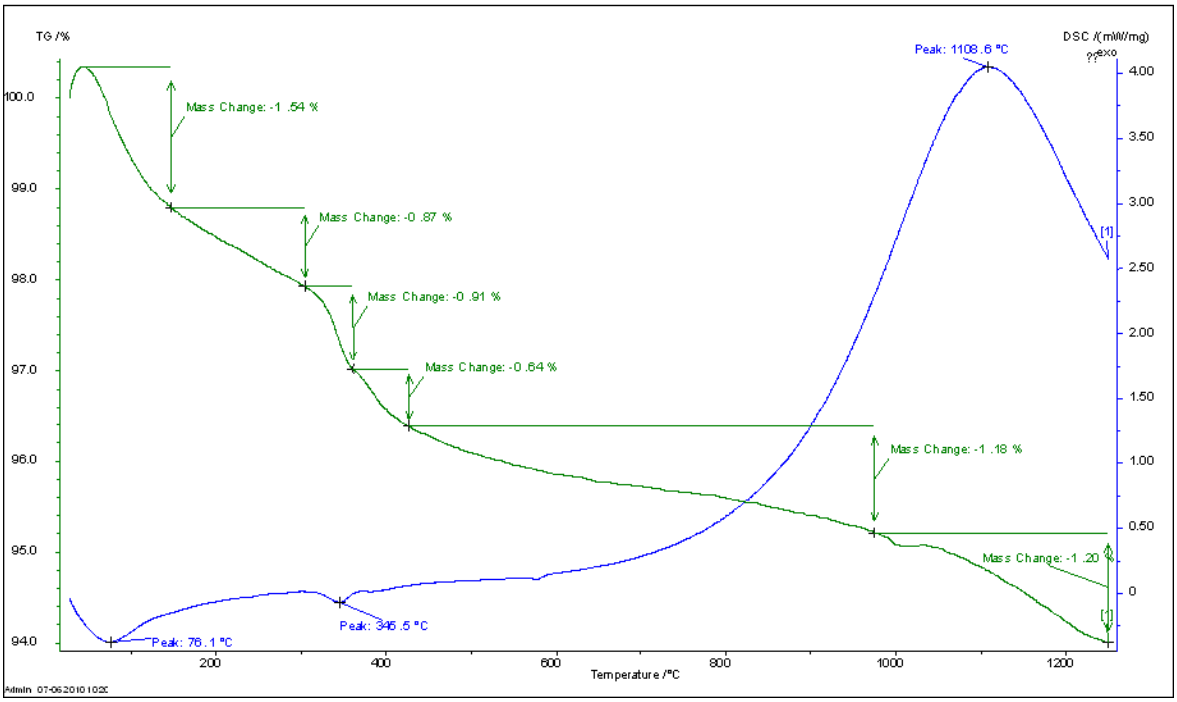

Fig.3.3: TGA-DSC of cordierite samples prepared from sol-gel method

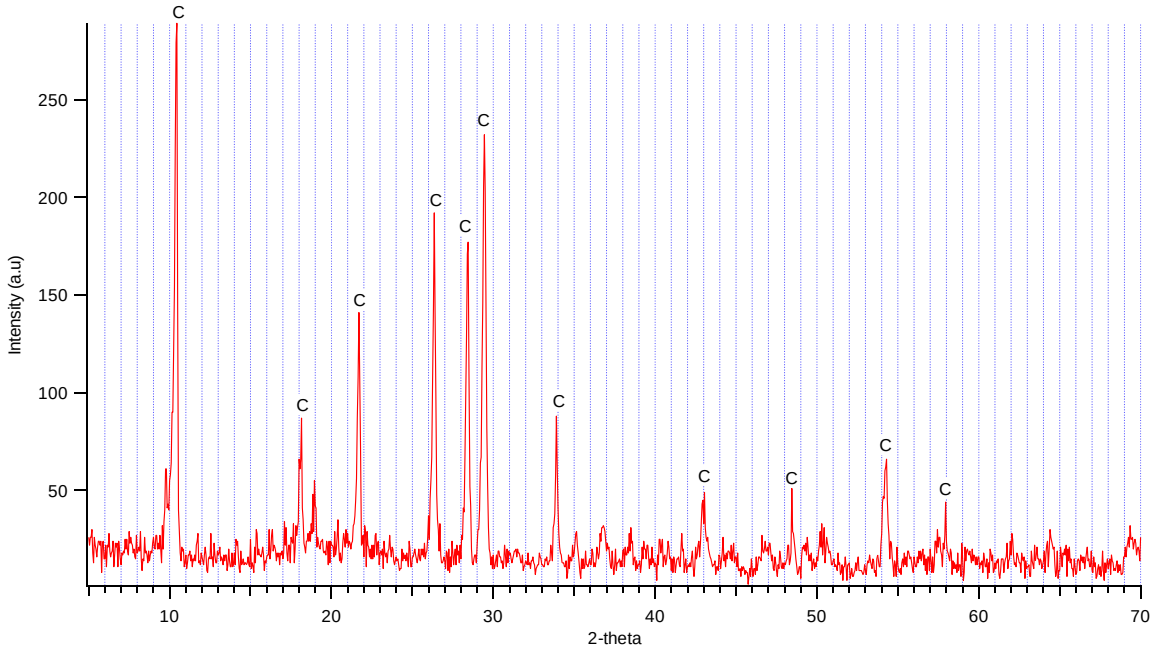

Fig. 3.4: XRD pattern of cordierite sample prepared by conventional sintering calcined at 1400^{o}C

3.1.2 The influence of burnable additives on the synthesis of Cordierite

As seen from the previous section, cordierite possesses very low surface area and porosity, leading to the difficulity for futher deposition of support and active phase. In order to improve the surface and porosity of cordierite samples, the additive as activated carbon and cellulose were added to the precursor. Both activated carbon and cellulose contain carbon and hydro mostly, therefore, during the thermal treatment, these substances would burn completely and wouldn't effect to the composition of the product. Besides, the

porosity of cordierite samples were also supposed to increase after activated carbon and cellulose are burnt out.

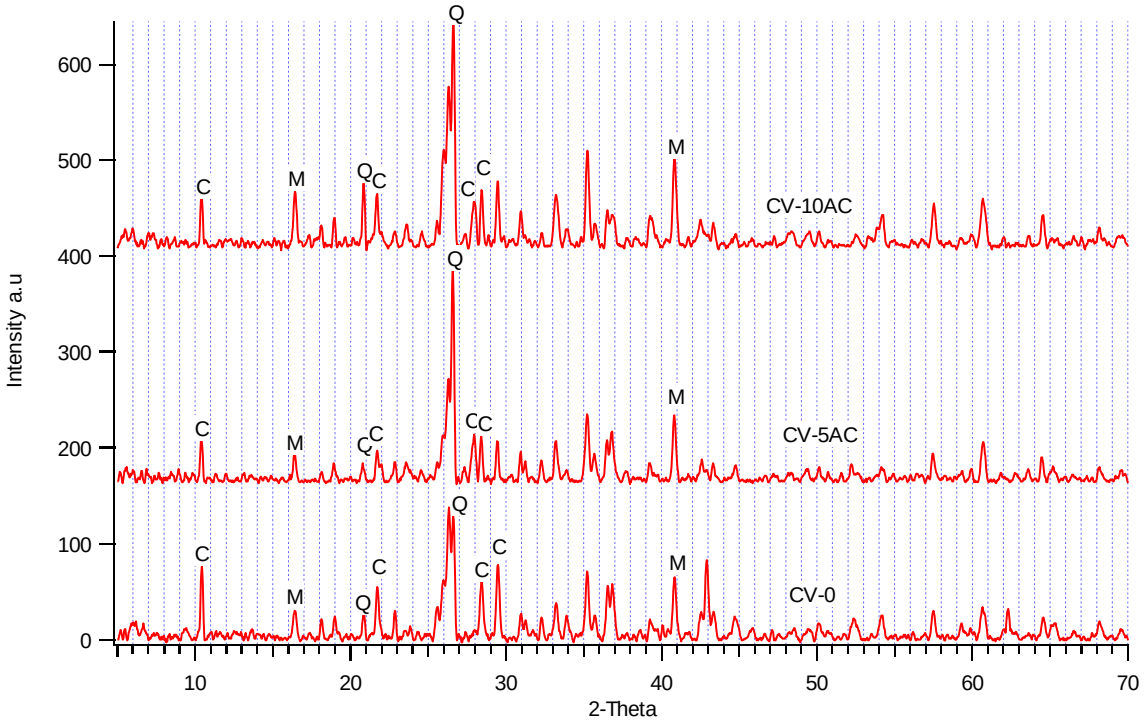

Fig3.5: XRD patterns of Cordierite prepared by conventional sintering with different addition of activated carbon

C: Cordierite Q: Quartz M: Mulite

Fig. 3.5 shows the XRD pattern of Cordierite samples produced from kaolin with different addition of activated carbon. As can be seen from the reflections in the different XRD spectra, a decrease in cordierite content going from 28.67 wt% to 13.21 wt% and 14.76 wt% is observed for the sample added with activated carbon (table 3.2). The reason for this is the oxidation of carbon at high temperature causing the blank inside the sample and leading to a decrease of crystallization. The same decrease of cordierite content in the samples with the addition of activated carbon prepared by sol-gel synthesis has also been observed as seen in fig. 3.6 and table 3.2, however, the content of cordierite in sample prepared by sol-gel with addition of activated carbon didn't decrease significantly since the mixing of precursor components in sol-gel synthesis is in atomic scale, therefore the addition of activated carbon after the framework of cordierite's precursor has been formed was not able to influence the crystallization of the desired cordierite phase.

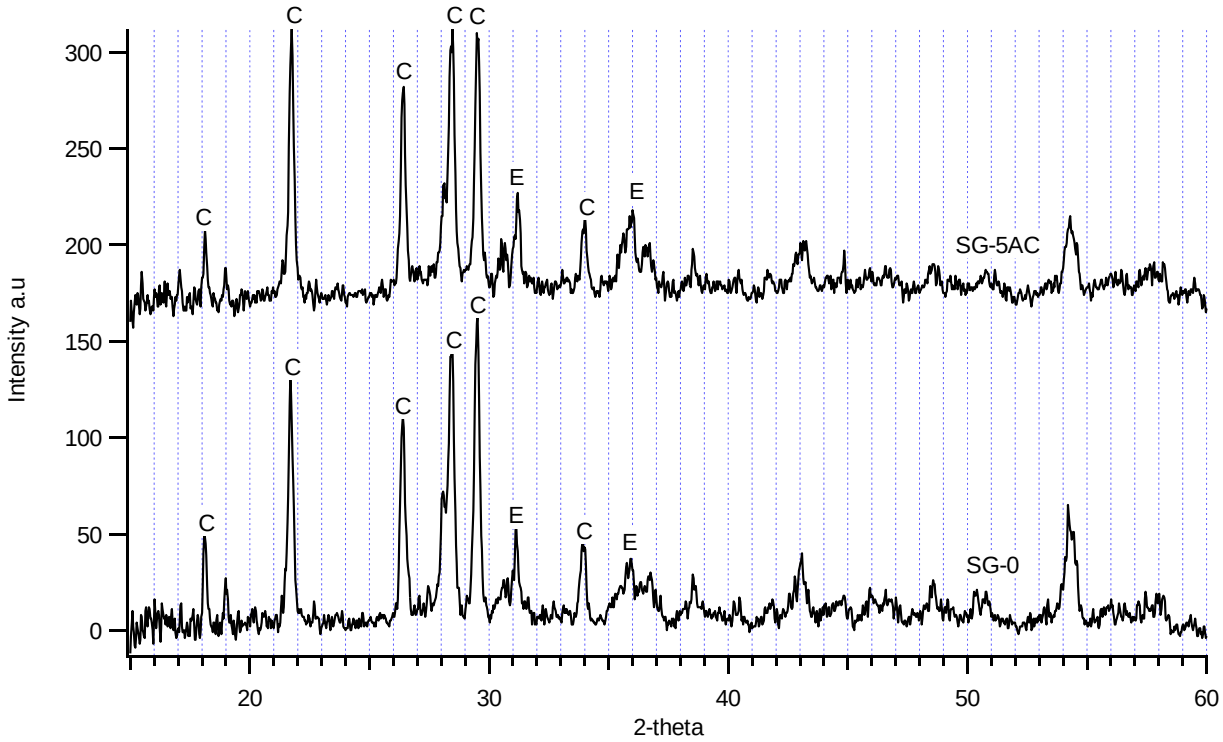

Fig.3.6: XRD patterns of Cordierite prepared by sol-gel with different addition of activated carbon

C: Cordierite ($2MgO.\ 3Al_2O_3.\ 5SiO_2$) E: Enstalite ($MgSiO_3$)

As can be seen in table 3.2, the mechanical strength of cordierite samples decreased when increasing the content of activated carbon. In the case of samples prepared by conventional sintering, the product contained activated carbon 10 wt%, the mechanical strength reduced from 556 to 305 (kN/cm^2). The similar results were observed in the case of samples prepared by sol-gel method.

Table 3.2: Properties of synthesized Cordierite using additives

No	Samples	Content of Cordierite (wt%) (*)	S_{BET} (m^2/g)	Minimum force to crack (10^4 N)	Mechanical strength limit (kN/cm^2)
1	CV-0	28.67	0.26	25	556
2	CV-5AC	13.21	0.35	20	442
3	CV-10AC	14.76	0.3	13	305
4	SG-0	75.23	0.57	20	916
5	SG-5AC	57.88	0.6	16	769

The SEM images (Fig.3.7) show that the two Cordierite samples, produced from kaolin with and without addition of activated carbon, have an average particle size of 5 - 10 µm. No significant change in porosity could be observed. A sintering effect was seen in the samples with activated carbon addition.

In the sol-gel method, the Cordierite samples which had the addition of activated carbon had the greater porosity, smaller particles (particle's size was about 5 µm) than that of one synthesized without this addition (particle's size was about 10 µm) (Fig.3.8). This happened due to the burning of carbon during the calcinations process. However, this phenomenon reduced significantly the mechanical strength of material as seen from table 3.2.

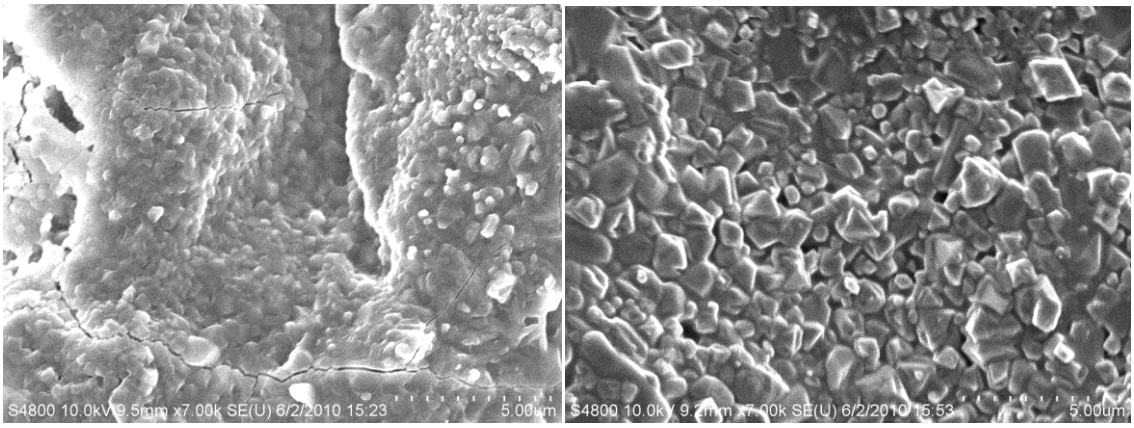

(a) *(b)*

Fig.3.7: SEM image of Cordierite produced from kaolin without - CV-0 *(a) and with* - CV-5AC *(b) the addition of activated carbon to the preform*s

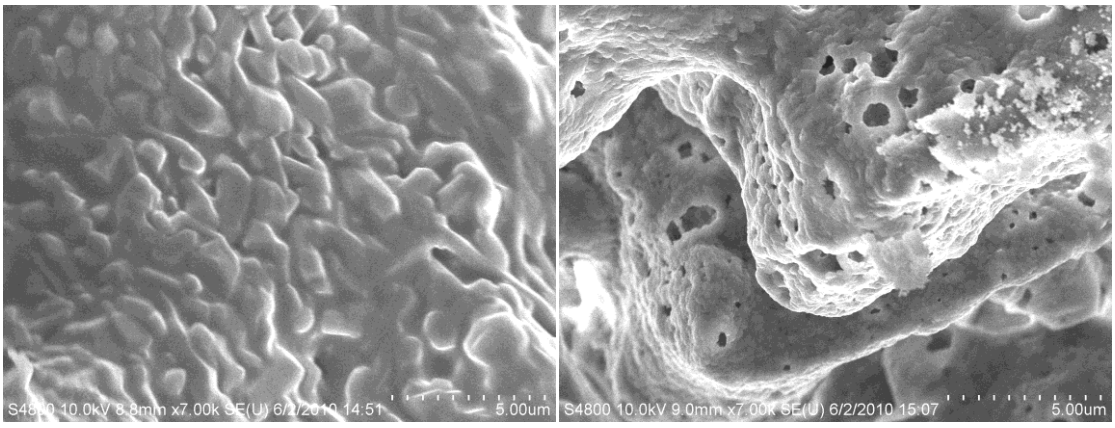

(a) *(b)*

Fig.3.8: SEM image of Cordierite produced by sol-gel processing without - SG-0 (a) and with - SG-5AC (b) the addition of activated carbon to the preforms

The addition of additives in the cordierite precursors aimed to improve the porosity and surface area of the cordierite. However, the surface areas of cordierite samples added activated carbon shown in table 3.2 do not increase significantly. The same remark could be seen with the addition of other additive as cellulose (table 3.3). Thus, the addition of the burnable additives (activated carbon and cellulose) didn't have influence on the BET surface area of the Cordierite pellets. The reason may be due to the high calcinations temperature of the synthesis, making a strong sintering, which leads to the collapses of holes previously formed by the presences of burnable additive and thus, prevents the improvement of the porosity of synthesized cordierite. Thus, the use of burnable additives did not improve surface area of cordierite as desire, therefore, burnable additives won't be used further.

Table 3.3: The BET surface areas of the Cordierite prepared by conventional sintering from kaolin with different addition of cellulose before sintering

Cellulose Content (%)	BET surface area (m^2/g)
0	0.3
5	0.61
10	0.57
15	0.59

3.1.3 The influence of dolomite on synthesis of Cordierite

Dolomite is a natural source of MgO, industrial $Al(OH)_3$ is a cheap source of Al_2O_3. Therefore the addition of dolomite and industrial $Al(OH)_3$ in the preparation of cordierite from kaolin aimed to reduce the cost of cordierite. However, dolomite also contains a large amount of CaO and industrial $Al(OH)_3$ contains Fe_2O_3 impurities (the composition of precursors is listed in table 3.4, content of impurities and cordierite phase in the product synthesized with different addition of dolomite are listed in table 3.5). Thus, the amount of dolomite and industrial $Al(OH)_3$ should be optimized to form the product with desired cordierite properties.

Table 3.4: Compositions of precursors to prepare cordierite

Samples	Kaolin Yên Bái	Dolomite	$Mg(OH)_2$	Industrial $Al(OH)_3$ from Tân Bình plant
SiO_2 (wt.%)	50.52			
Al_2O_3 (wt.%)	30.2	0.32		68.04
MgO(wt.%)	1.05	21.6	68.5	
CaO(wt.%)		31.42		
Fe_2O_3 (wt.%)	0.6	0.05		

Table 3.5: Content of cordierite phase in the product and impurities in the precursor

Content of dolomite in precursors (wt.%)	Samples	Content (wt.%)		
		Fe_2O_3	CaO	Cordierite
0	TX1	0,62		21,4
8.69	TD1	0,6	3,68	56,7
16.27	TD2	0,61	7,32	45,4

Figure 3.9 shows the XRD patterns of samples synthesized using 0 wt.%, 8.69 wt.% and 16.27 wt.% of dolomite (TX1, TD1 and TD2, respectively). It is obvious to prove the formation of cordierite with many typical peaks at angle 2-theta of 18.1, 21.8, 26.3, 28.3, 29.5, 34.9, 54.2 for all samples. However, there were still some small peak of impurities as fosterite (2-theta of 35.7 and 36.55), MgO (2-theta of 42.95) and quart (2-theta of 27.1) . The content of cordierite in samples TX1, TD1 and TD2 were calculated as 21.4, 56,7 and 45,4 wt.% respectively. Thus, adding dolomite in the precursor resulted in positive effect on the formation of cordierite. It maybe due to the precence of impurities in dolomite play a role as catalyst for the formation of cordierite phase. However, the added dolomite content should not be too high since it will then decrease the cordierite content (TD2).

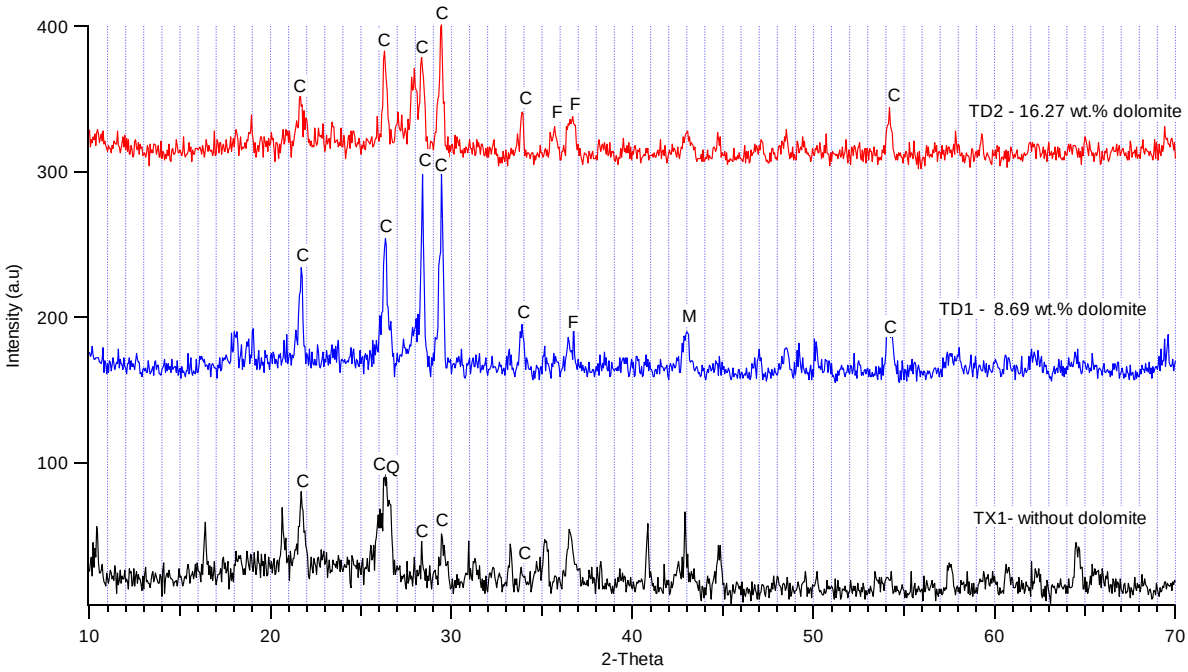

Fig.3.9: XRD patterns of cordierite samples prepared with different dolomite content (TX1, TD.1 and TD.2)

(C: cordierite, Q: Quart, F: Fosterite, M: MgO)

3.1.4 Influence of acid treatment on surface area of Cordierite

Since surface area and porosity of synthesized cordierite were very low, leading difficulties when impregnating support and catalysts on the cordierite substrate surface, acid treatment of the cordierite surface was studied with the aim to increase the surface area and porosity of the cordierite substrate for further impregnating processes. Surface areas of cordierite (CV-0) treated by hydrochloric acid for different periods of time were examined as shown in fig. 10. It is noticeable that the greatest value of specific area was 21.03 m^2/g after 8 hours of immersing cordierite pellets in the HCl acid solution. However, at the later periods of treatment, for example at 10 hours, there was a decrease of surface area of cordierite samples to 13.98 m^2/g, and no more increase at 12 hours or 14 hours.

Cordierite was also treated by oxalic acid 40% for different periods of time but the surface area wasn't improved as well as by HCl. For example, after 8 hour of oxalic acit treatment, the surface are of cordierite increased to 7 m^2/g, while the surface area of cordierite treated by HCl acid went up to 21.03 m^2/g. Therefore, the samples were not treated in oxalic acid any longer period.

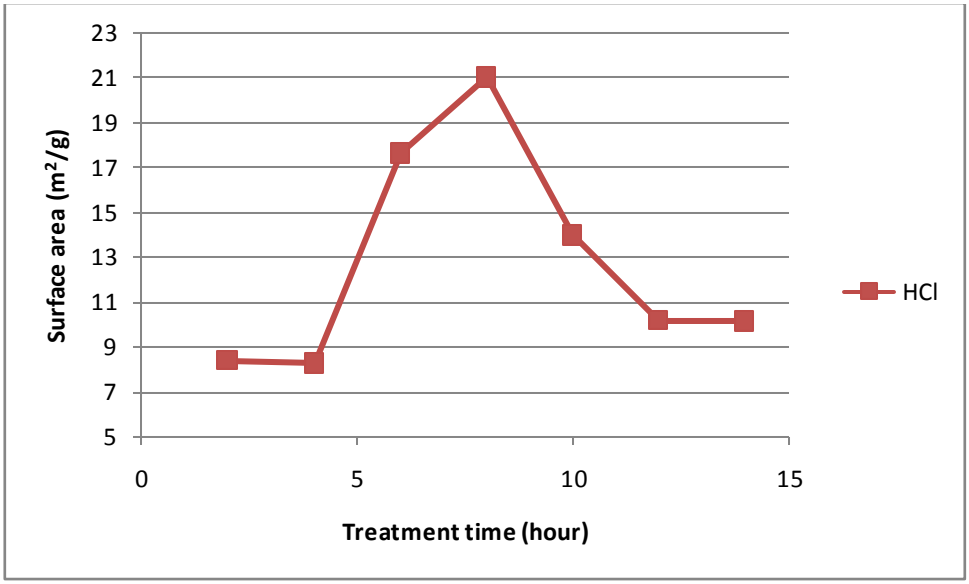

Fig. 3.10: BET surface area of HCl treated Cordierite pellets (CV-0) at different periods of time

The increase of the BET surface area of cordierite after acid treatment can be explained by the wet chemical attacks based on the selective leaching of the magnesium and aluminum cations. Migration of aluminum out of the tetrahedral structures organized in a six member ring configuration is the driving force for the rearrangement of the remaining silicon atoms in the structure, introducing a new amorphous phase responsible for the gain of BET surface area and porosity. The increase in surface area was accompanied by creation of micropores and mesopores centered between 20 and 30 Å diameter, whereas the original cordierite contained predominantly macropores. After long treatment times, the fractions of micropore volume and area decreased, and the pore size distribution shifted to the mesopore. Treatment for long times leads to lower surface area owing to the formation of larger mesopores. The mesopores may be formed by partial destruction of the silicate structure of the cordierite [83].

Fig. 3.11 shows the morphology differences between the sample Cordierite (CV-0) before and after acid treatment. It is obvious that the surface of treated Cordierite pellets was much rougher than the untreated ones. The SEM images of CV-0-HCl8 and CV-0-HCl12 are in an accordance with the decreasing the BET surface area. The rough surface with the high porosity was present on the substrates after acid treatment for 8 hour. However, after next 4 hour, the deep attack of acid on the porous surface of sample created the big holes. Thus, the small pores were replaced by the bigger pores leading to the drop of BET's value.

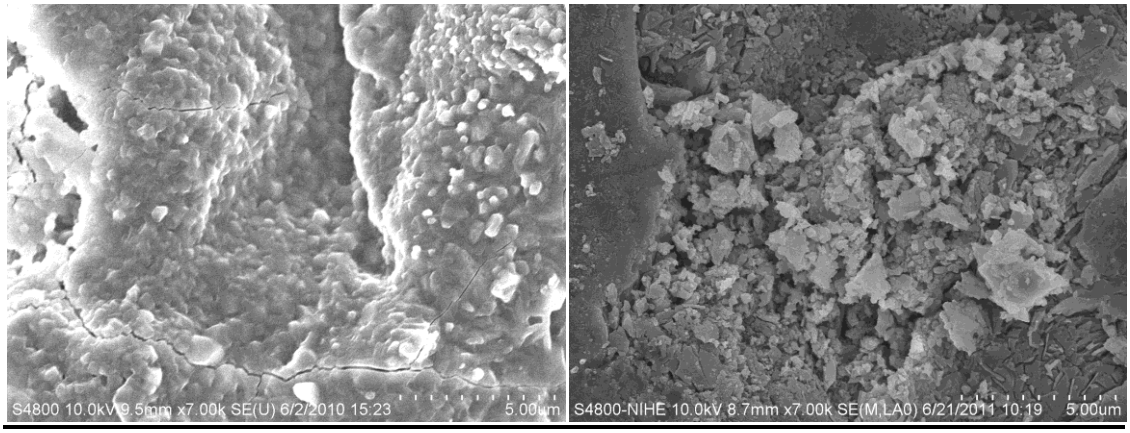

(a) CV-0 *(b)* CV-0-HCl 8

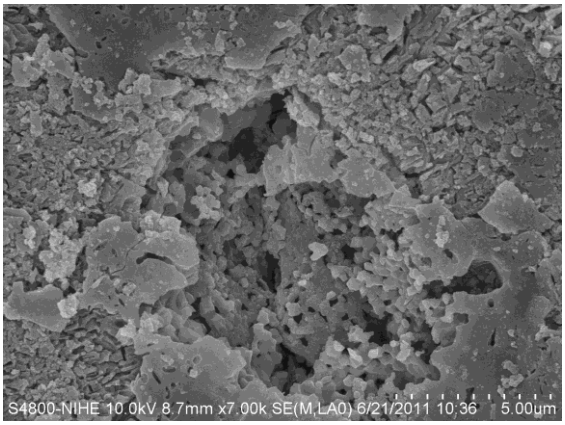

(c) CV-0-HCl 12

Fig.3.11: SEM images of substrates before and after hydrochloric acid treatment for 8h, 12h

As shown in fig.3.12 of the untreated and treated substrates by hydrochloric acid, there was gradually decreases of Cordierite peak's intensity at the angle 2-theta of 29.5 from the CV-0 to CV-0-HCl 12. It is due to the attack of strong inorganic acid, which leads to the leaching of Mg and Al ions from the structure of Cordierite. The change of cordierite content in the product on the time of treatment is indicated in fig. 3.13.

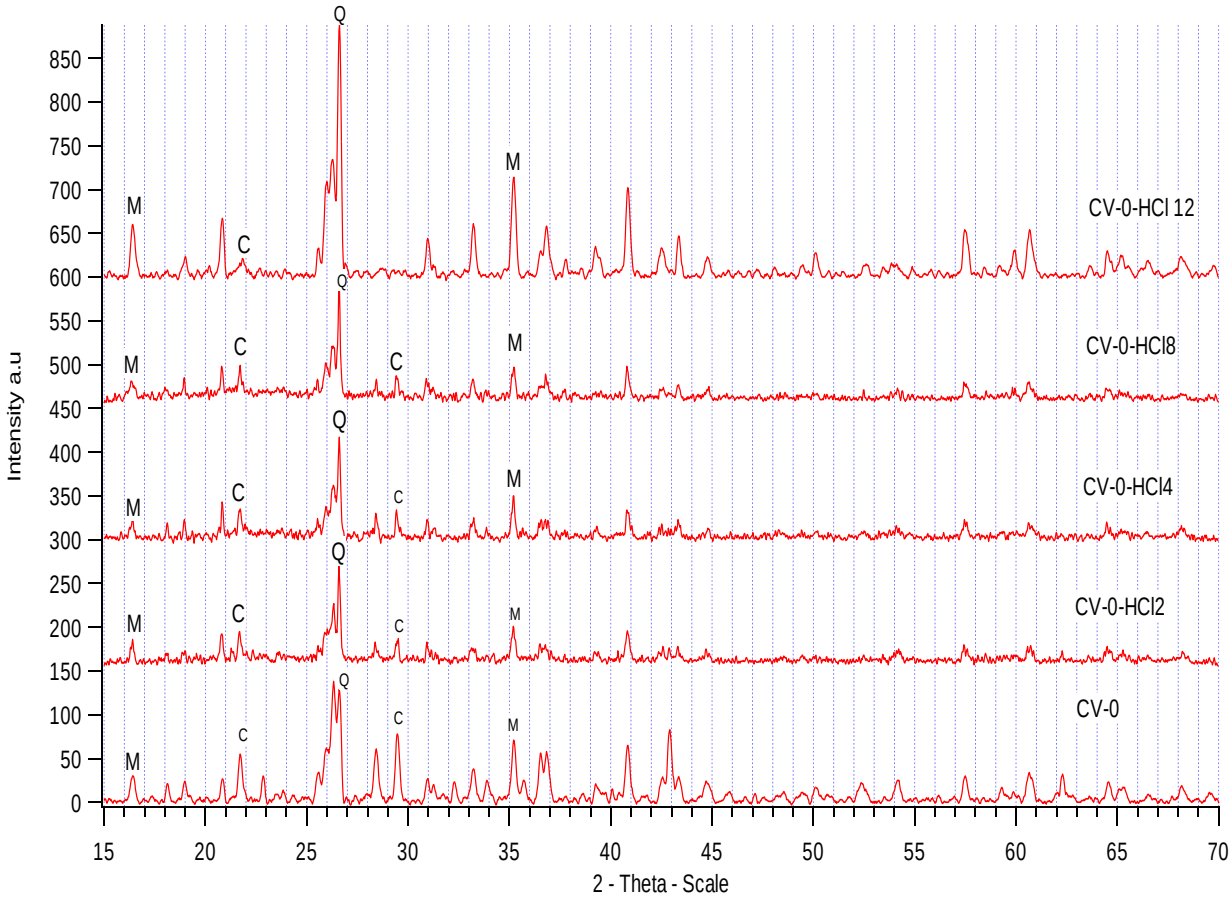

Fig.3.12: XRD patterns of samples treated Cordierite by hydrochloric acid.

C: Cordierite Q: Quartz M: Mulite

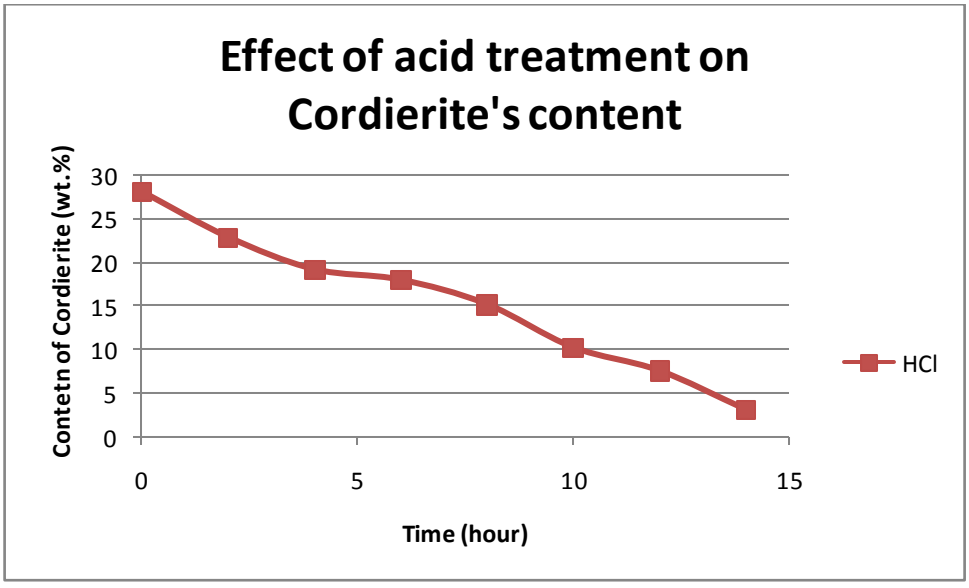

Fig. 3.13: Effect of acid treatment on Cordierite's content

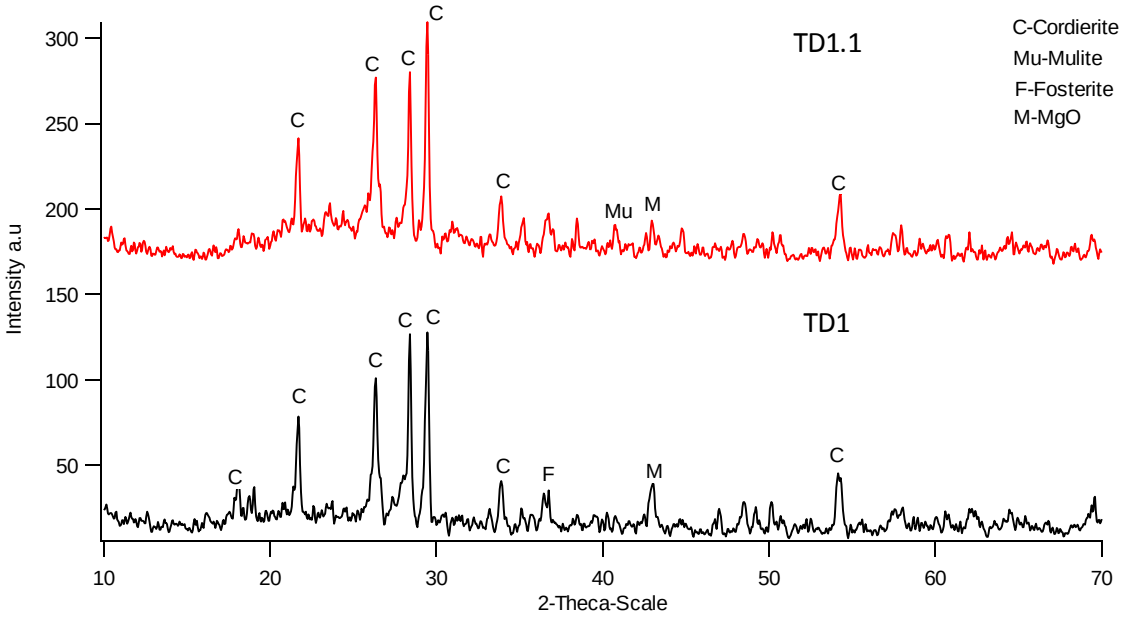

Fig. 3.14: XRD patterns of samples with 8.69 wt.% of dolomite before (TD1) and after HCl treatment (TD1.1)

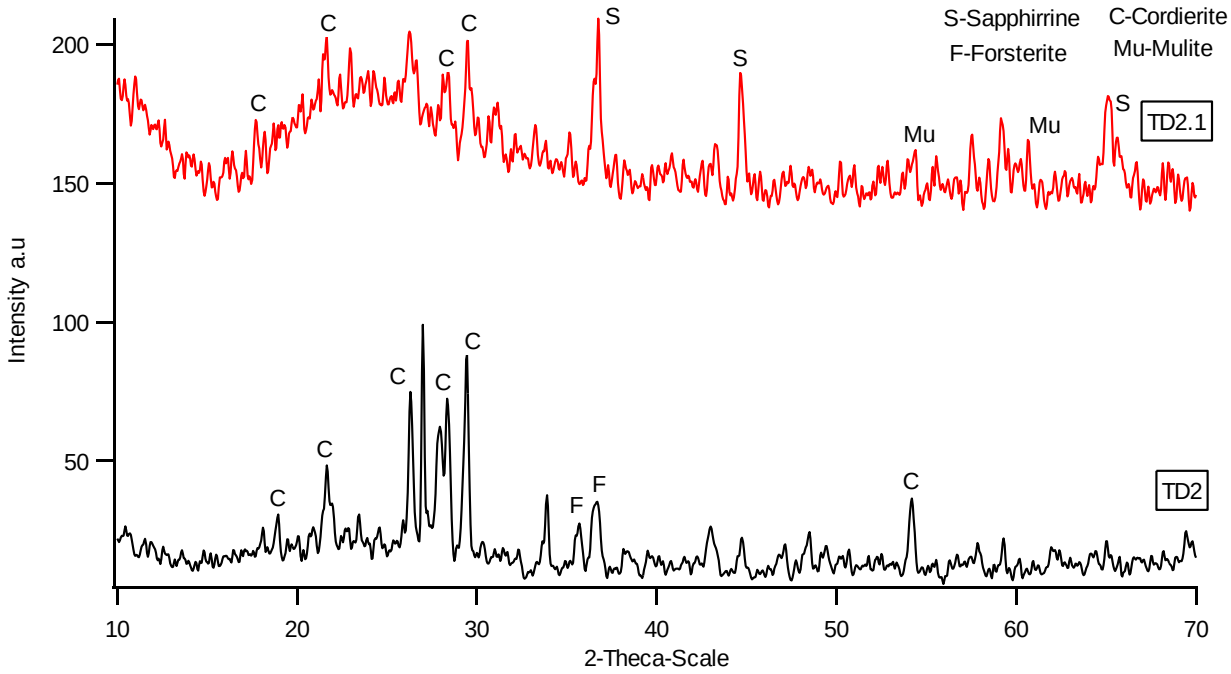

Fig. 3.15: XRD patterns of cordierite samples with 16.27 wt.% of dolomite before (TD2) and after HCl treatment (TD2.1)

The XRD patterns of the cordierite sample synthesized with the addition of dolomite TD1, TD2 and TD1.1, TD2.1 (samples TD1 and TD2 treated by acid solution at 90^{o}C for 8 hour, respectively) were illustrated on figure 3.14 and 3.15. After treatment by acid solution, there were still typical peaks of cordierite at angle 2-theta of 18.1, 21.8, 26.3, 28.3, 29.5, 34.9, 54.2. In addition, the content of cordierite in samples TD1.1 was 60.8 % approximately as the same as TD1 (fig. 3.16). It may be due to the impurities was removed during the process of acid treatment leading the increase of cordierite's content. However, the content of cordierite in sample TD2 after acid treatment decreased remarkably, from 45.4 % to 30 %. Although the typical peaks of cordierite in sample

TD2.1 still appeared at 2-theta of 18.1, 21.8, 26.3, 28.3, 29.5, but the intensities were lower than TD2, and the base line was higher (fig.3.15), that means the structure of cordierite was affected deeply during acid treatment. The sample TD2 contains 16.27 wt.% dolomite, twice as high as amount of dolomite in TD1. As a results, the impurities was removed much more than TD1, therefore the structure of formed cordierite maybe effected leading to the decrease of cordierite content.

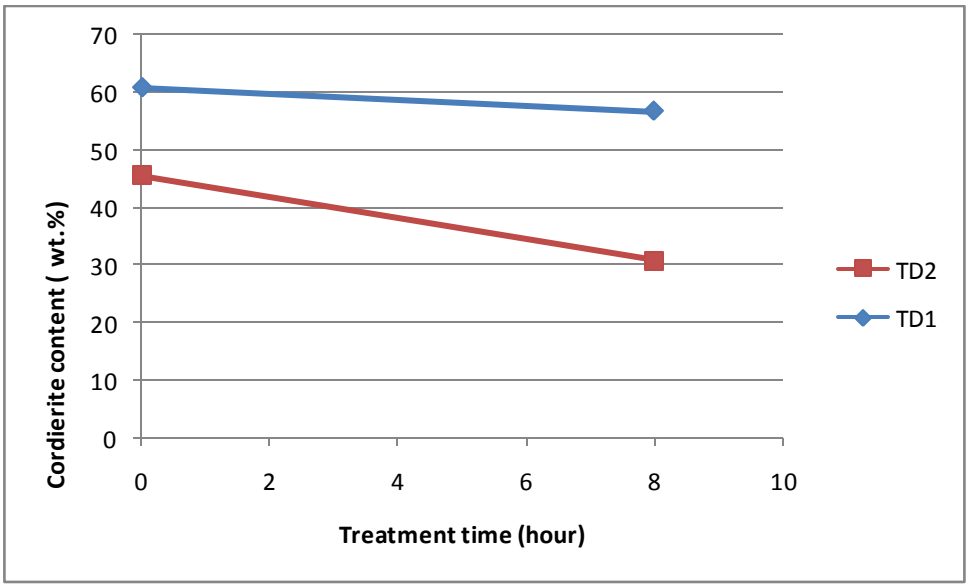

a,

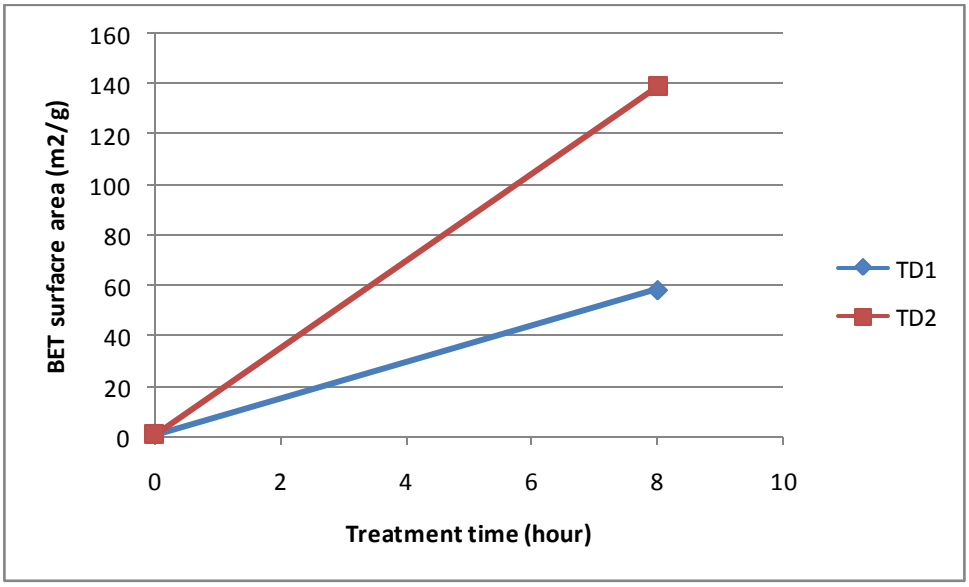

b,

Fig. 3.16: Properties of acid treated cordierite samples with addition of dolomite (8.69wt.% - TD1, 16.27 wt.% - TD2):

As can be seen from the fig. 3.16b, the untreated surface area of samples was very low, but after acid treatment, the BET surface area increased remarkably. The specific surface of samples TD1.1 and TD2.1 was 58.34 and 138.7 m^2/g, respectively. The reason is the removal of impurities in the sample during acid treatment, ions Ca, Fe which occupied large proportion was eliminated, inducing increase of pores in the sample, resulting in high BET surface area.

Dolomite was added to samples with the aim to improve the specific surface area by removing the high content of free ion (Ca^{2+}, Fe^{3+}) during process of acid treatment. The BET surface of sample TD1.1 and TD2.1 were 58,34 and 138,7 m^2/g. Thus, it is reasonable to add the suitable content of dolomite to improve the properties of cordierite without effect on the mechanical strength.

In conclusion, the preparation of cordierite was prepared successfully from the popular sources of material as kaolin, industrial MgO, and Al_2O_3 by conventional sintering. The products had high content of cordierite, and high mechanical strength, but still low BET surface area. Thus, some additives (activated carbon, cellulose and dolomite) were mixed with the precursors in order to improve the porosity of the substrates, to increase the adhesion between the supports with cordierite. Among the additives, the dolomite is the best choice because it increased the BET surface area to 138 m^2/g (with 16.27 wt.% dolomite added to the precursors). The treatment of cordierite by acid solution, especially HCl, dissolved some cations out of cordierite samples, leading to the increase of surface area.

3.2 Preparation of FeCr metal substrate

The metal substrates have high thermal shock resistance, high melting and softening points and facilitate the development of high cell densities with very low-pressure losses. Therefore, it has been used widely in the application of three-ways catalyst. However the adhesion of catalysis active phase on this material was a big problem. Thus, it is necessary to treat the metal samples before using it as the substrate of three-ways catalyst to increase the adhesion ability.

The aim of the treatment is to remove surface impurity and to form layer on the surface, leading to the increase of wet ability. The effect of the treatment can be evaluated by the decrease of wetness contact angle. The contact angle is a measure of the ability of a liquid to spread on a surface. The method consists to measure the angle between the outline tangent of a drop deposited on a solid and the surface of this solid. The contact angle is linked to the surface energy and so one can discriminate the polar and apolar interactions.

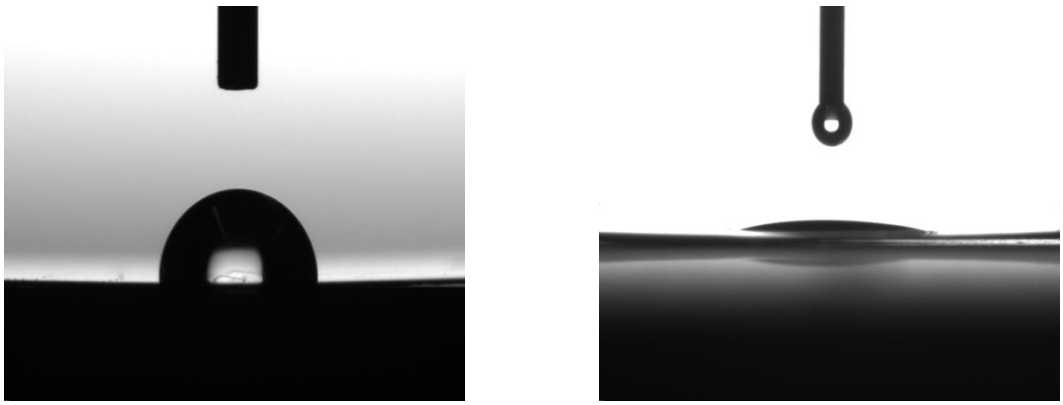

Fig.3.17:The determination of contact angle of untreated and treated metal substrates

An example about contact angle of the metal substrate is present in fig. 3.17. Contact angle of several metal sample treated by different method shown in table 3.6. It is obvious that the origin FeCr alloy possesses very high contact angle, thus, the wetting

ability is worst. After the thermal treatment, the angle decrease significantly but it is still high. It has been reported that a wetness contact angle below 10^o is suitable for a good wetting ability [84]. Therefore FeCr alloys were both thermal treated and chemical etching. In general, the samples were thermal treated before chemical etching (B samples) showed a lower contact angle than the samples treated oppositely (A samples) since thermal treatment may burn impurities such as grease … at the surface of the sample, leading to an easier treatment afterward by chemical etching.

For the A samples (the chemical etching before thermal treatment), among the different solutions for chemical etching, the combination between NaOH 10 wt.% and solution of H_2O_2 1 wt.%, oxalic acid 1.5 wt.% showed the best effect with the lowest wetness contact angle as 8.37^o after 15 mins. For the B samples (thermal treatment before chemical etching), even though all the solutions showed good effect on reducing the wetness contact angle, the samples treated withNaOH with 10 and 20 wt.% solution show the lowest wetness contact angle was 6.7 and 6, respectively (B2, B3). Therefore the treatment procedure including thermal treatment at 800^oC for 3 hour, then chemical etching in solution NaOH 10 wt.% (B3 sample) was applied to treated FeCr substrates.

Table 3.6: Contact angle of FeCr metal substrates

Samples	FeCr	A1	A2	A3	A4	A5	B0	B1	B2	B3	B4	B5	B6
Contact angle	76.2	14.1	16.1	13.3	8.37	17.2	20.12	16.1	6.7	6.0	8.05	12.4	9.2

3.3 Synthesis of supports

3.3.1 Synthesis of boehmite and γ-Al2O3

γ-Al_2O_3 has been used extensively in the application of automibile exhaust catalys because of its normal inexpensiveness, workability, long life criteria, are those allowing the greatest activity of the active catalytic agent, namely high specific surface and adequate porosity on one hand, and on the other hand that of the highest structural stability. γ-Al_2O_3 was synthesized from boehmite which was successfully prepared by many authors [14, 85-87], thus, in this work, γ-Al_2O_3 was prepared according to successful investigation [14].

Figure 3.18 shows the XRD pattern of synthesized boehmite. There is an appearance of typical peak of beohmite at angle 2-theta: $14,1^o$; $28,2^o$; $38,5^o$ và $49,4^o$, however, there are still aluminum hydroxide's peaks, this can affect the specific surface area of product.

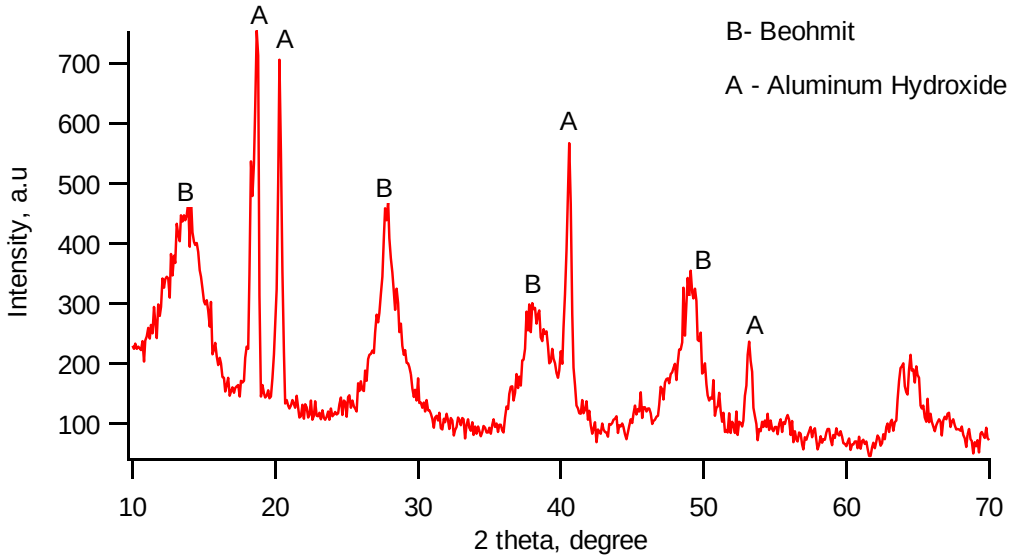

Fig.3.18: XRD pattern of boehmite

XRD pattern of boehmite calcined at 550°C is shown in fig.3.19, which indicated the presence of γ-Al_2O_3.

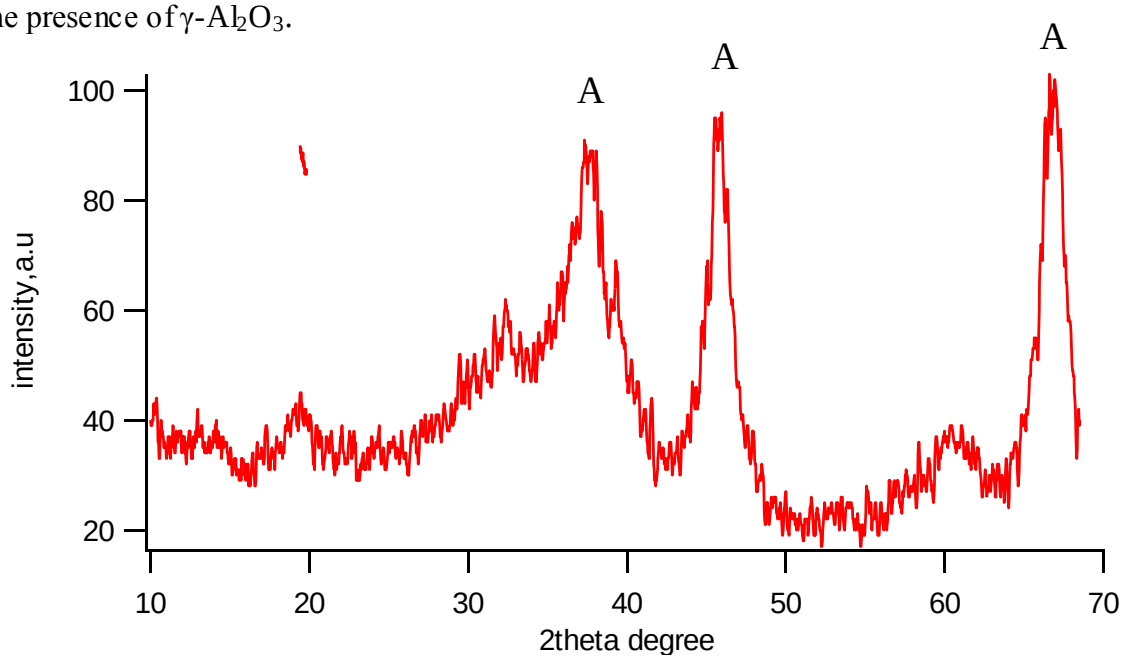

Fig.3.19: XRD pattern of γ-Al_2O_3

The specific surface area of beohmite and γ-Al_2O_3 are shown in table 3.7. Isotherm of the samples are presented in and fig.3.20. After calcinations, the surface area of γ-Al_2O_3 decreased from 359.45 to 207.7 m^2/g, and its pores were larger than that of boehmite due to removal of OH group. The adsorption isotherm of boehmite and γ-Al_2O_3 was type III. Since possessing high surface area, the synthesized materials were suitable to be used as support in the application of preparation three-ways catalyst for treatment of exhaust gases.

Table 3.7: Charaterization of boehmite and γ-Al_2O_3

No	Samples	**BET Surface area** (m^2/g)	**Pore size** (nm)	**Pore volume** (cm^3/g)
1	Beomite	359.45	10.8	0.54
2	Gamma – Al_2O_3	207.7304	12.3	0.92

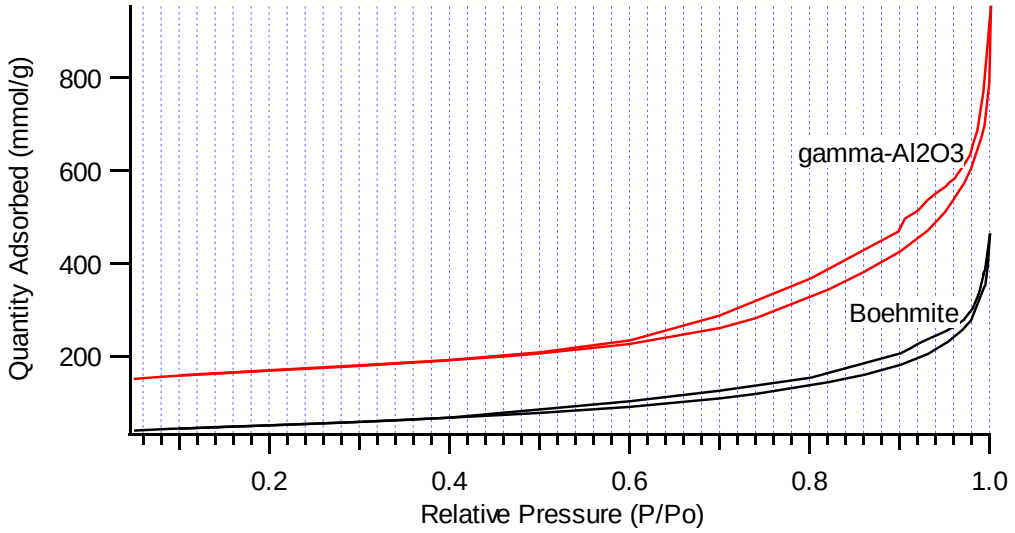

Fig.3.20: Isotherm adsorption of boehmite and γ-Al_2O_3

3.3.2 Synthesis of $Ce_{0.2}Zr_{0.8}O_2$ mixed oxide

More recently, Di Monte et al. reported that the nanostructured $Ce_{0.2}Zr_{0.8}O_2$ (CZ28) mixed oxides supported on γ-Al_2O_3 maintained high OSC even after calcination at 1100oC [88]. Afterward, Rui Si et al. proved the thermal stability of $Ce_{0.2}Zr_{0.8}O_2$ after calcinations at 1000^{o}C, but it still remains its tetragonal phase and homogenous structure. Besides, they also reported the high catalytic activity in CO oxidation [89]. That's the reason why more attentions was focused on investigation of this material to apply in three-ways catalysts from 2010 until now [90, 91, 92]. In this work, $Ce_{0.2}Zr_{0.8}O_2$ was prepared for the use as support for the catalyst unit.

XRD patterns of $Ce_{0.2}Zr_{0.8}O_2$ mixed oxide prepared with and without using template (CZ28-CTAB and CZ28-non template) are present in fig.3.21. It shows that there were only tetragonal $Ce_{0.2}Zr_{0.8}O_2$ phase in the samples due to the only appearance of characteristic peaks at 2-theta of 29.9, 34.65, 49.8 and 59.4.

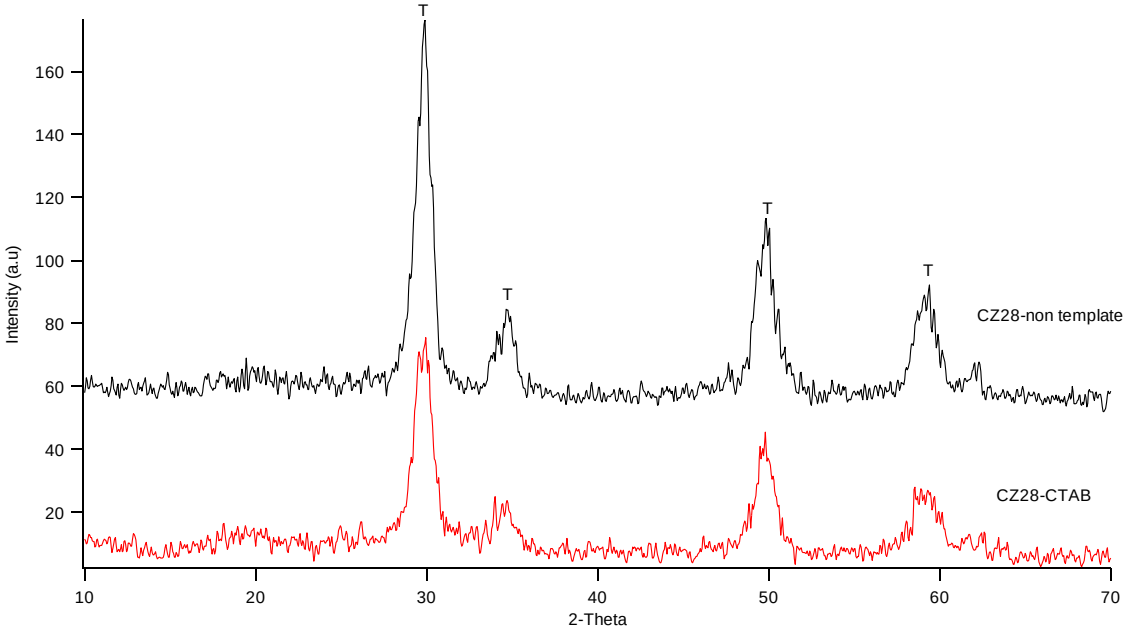

Fig. 3.21: XRD pattern of CZ28-CTAB and CZ28-non template (T: tetragonal $Ce_{0.2}Zr_{0.8}O_2$)

Nitrogen adsorption–desorption isotherms of the as prepared and calcined CZ28 samples are shown in Fig.3.22. All the isotherms can be attributed to type IV, characteristic of capillary condensation taking place in meso-pores. According to IUPAC classification of hysteresis loops, the hysteresis of CZ28-non template can be attributed to type II – resulted from so call "bottleneck" or "inkbottle" pores. In pores of this shape, emptying of the wide portion will be delayed during desorption until the narrow neck can evaporate. Therefore, the desorption curve exhibits a small slope at high relative pressures and a large slope where the wide part of the pores evaporates. The hysteresis of the remained CZ28 samples can be attribute to type H4-hysteresis is associated with slit-shaped pores or the spaces between parallel plates [84]. Moreover, the hysteresis loops of uncalcined samples was lasted longer range of relative pressure than that of calcined samples, due to change in pore during calcinations. The pores in calcined samples were more order than as-prepared samples, leading the hysteresis loops was at higher and shorter range of P/Po.

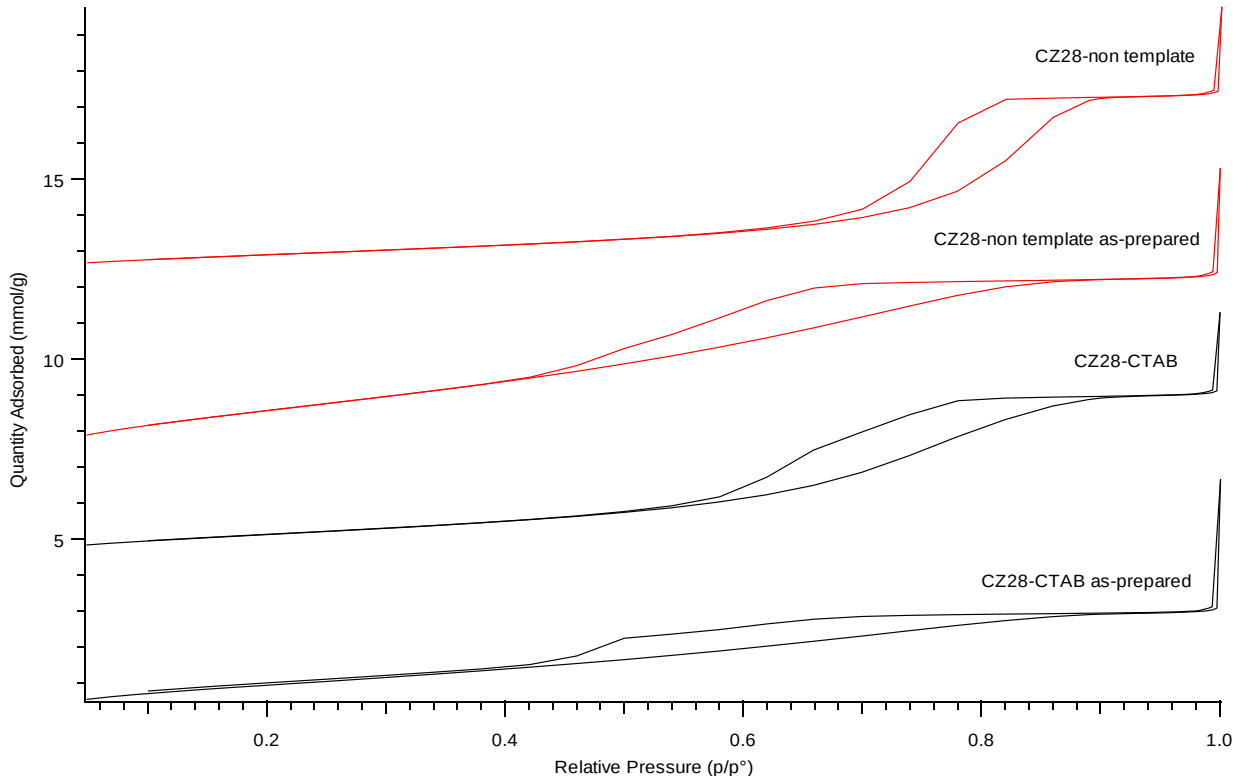

Fig.3.22: N_2 adsorption–desorption isotherm of samples with and without CTAB, and uncalcined and calcined (CZ28-CTAB, CZ28-CTAB as-prepared, CZ28-non template and CZ28-non template as-prepared)

The surface areas and BJH pore sizes and volumes of the CZ28 samples are summarized in table 3.8. The surface area values of the CZ28 samples are between 71 and 207 m^2/g. In case of no use the surfactant, the surface areas of the calcined samples fell from 207 to 71 m^2/g at 500°C. Interestingly, contrary to the loss of the surface area of the sample CZ28-non template, both the surface and pore size of CZ28-CTAB were higher than that of as-prepared sample, due to the removal of the templates by high-temperature calcination. After calcinations, the surface area of the sample prepared using template was higher than that of sample prepared without template, thus proved the positive effect of using template on the increase of surface area. In both cases of with and without template, the pore size of as-prepared samples was lower than the calcined samples. However, there

was contrary in change of pore volume after calcinations. The pore volume of CZ28 non-template reduced from 0.2196 to 0.1881 cm^3/g due to effect of sintering, while pore volume of CZ28-CTAB increased from 0.0951 to 0.1770 cm^3/g, this is due to CTAB in the pores of samples was burnt out leading to increase of pore volume.

Table 3.8: BET specific surface areas, pore sizes, pore volumes of the CZ samples

No	Samples	**BET Surface area** (m^2/g)	**Pore size** (nm)	**Pore volume** (cm^3/g)
1	CZ28 non-template	71.95	8.4	0.1881
2	CZ28 non-template as-prepared	207.73	3.9	0.2196
3	CZ28-CTAB	90.92	6.05	0.1770
4	CZ28-CTAB as prepared	85.57	4	0.0951

Generally, highly ordered mesostructure is derived from diverse templating methods. In most cases, the regular pore structure after the removal of the templates by high-temperature calcination and a short-range ordered or disordered pore structure is finally produced. It is interesting that the mesoporous CZ28 materials with a short-range ordered pore network could be prepared without the use of any templates followed by high temperature calcination. However, the decrease of surface area after calcinations indicated the low thermal stability of samples without template. In addition, the textural properties of CZ28-CTAB was suitable for application as the support of three-ways catalyst, thus this procedure would be used for further investigation.

3.3.3 $AlCe_{0.2}Zr_{0.05}O_2$ mixed oxides

As a new kind of support material, Al_2O_3-CeO_2-ZrO_2 (ACZ) can both combine the advantages of high specific surface area of Al_2O_3 and excellent oxygen storage capacity of the CeO_2-ZrO_2 soild solution. Therefore investigations of these materials are significant to enhance the performance of TWC. Several influenced fators were studied for the preparation of ACZ material.

The influence of precipitant:

KOH, NH_4OH and NH_4HCO_3 were chosen to be precipitant in the solution of Al^{3+}, Ce^{3+} and Zr^{4+}. The XRD patterns of the three samples prepared using these different precipitants (ACZ08, ACZ09, ACZ10) are shown in the figure 3.23. There were only the characteristic peaks of single fluorite CeO_2 observed at 2-theta angle of 28.9, 33.3, 47.92 56.58, and no Al_2O_3 diffraction pattern was detected due to the homogeneity of Al_2O_3 to the CeO_2 lattice. The peaks of the ACZ samples are symmetrical, which suggests that the samples are homogenous. However, the broadest peaks of ACZ10 implied that the crystallites were small size, and the sharper peaks observed for ACZ08, ACZ09 indicates that the crystallites are larger than ACZ10's crystallite.

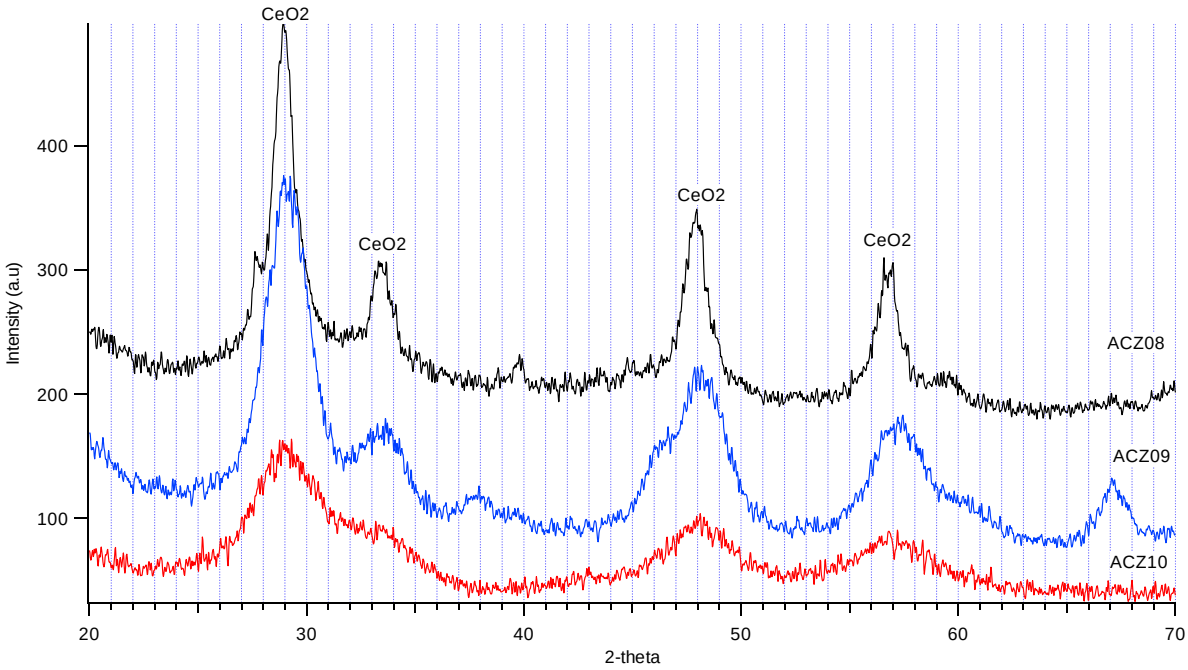

Fig. 3.23: XRD spectra of samples prepared using these different precipitants calcined at 550°C (ACZ08, ACZ09, ACZ10)

All the isotherms of three samples, which are illustrated in fig.3.24, can be attributed to type IV, characteristic of capillary condensation taking place in meso-pores. The hysteresis loops in the P /Po range of 0.4–0.9 associated with this isotherm were classified to type H2, quite typical of porous materials with the pore could be formed in the shape of "neckbottle". The differences between the desorption curve of ACZ9 and ACZ8, ACZ10 may caused from the dissimilarity of the pores of each samples. In sample ACZ8, ACZ10, the relative pressure P/Po of desorption curve decreased sharply with high absorbed quantity (approximately 100 cm^3/g STTP) indicated the large pores, however, in the case of ACZ9, the P/Po remained constantly from 0.9 to 0.6 with low absorbed quantity (60 cm^3/g STTP) maybe because of small pores in the samples.

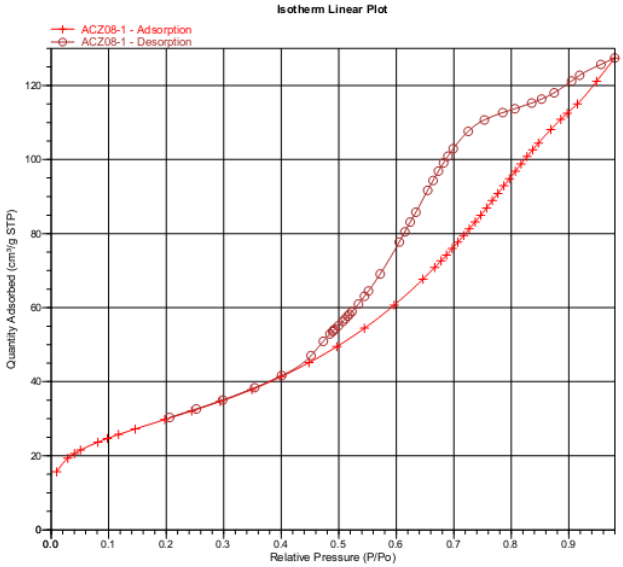

a,

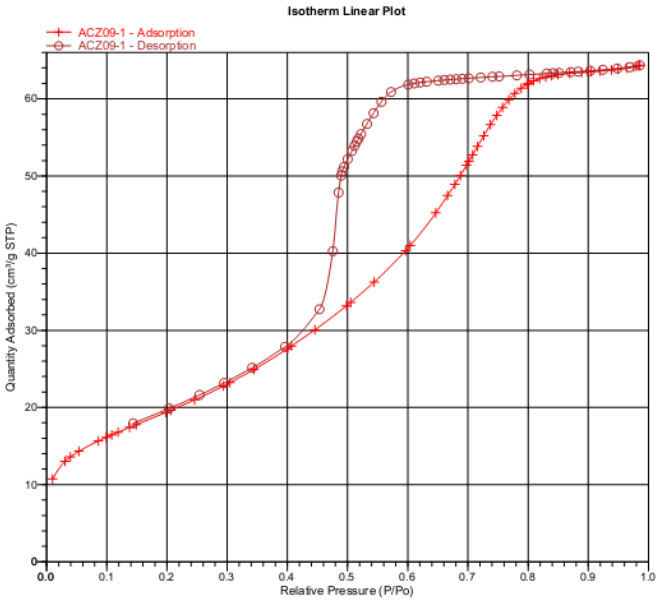

b,

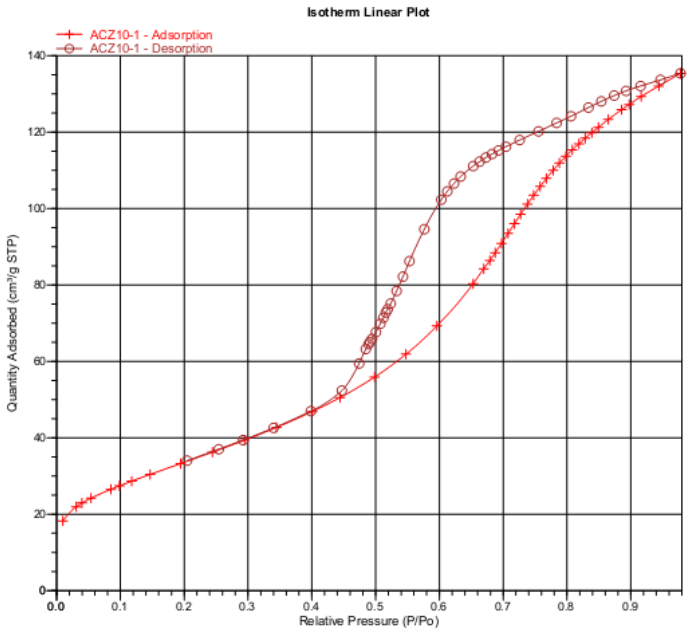

c,

Fig.3.24: Isotherm plots of samples prepared using these different precipitants: (a) ACZ08, (b) ACZ09, (c) ACZ10 calcined at 550°C

All three samples had the surface area over 100 m^2/g but the ACZ10 had the highest value while the ACZ08 had the lowest one (table 3.9). The pore of ACZ09 was smallest in the comparison with the others, which was in agreement with above discussion. It is clear that the different precipitants lead to the different properties of products. The KOH has the highest rate of yielding OH-, thus it resulted the highest surface area. The sample ACZ09 has the lower surface area, also lower pore diameter and pore volume than ACZ10. That means the low rate of producing -OH of NH_4OH makes the material to be dense, not as porous as ACZ10. However, the sample ACZ08 had the biggest pore size and volume though NH4HCO3 had the slow rate of yielding –OH. That can explain that during

the formation of crystallite, there was not only appearance of $Ce(OH)_3$, but also hexagonal $Ce(CO_3)_2OH$ crystal. This $Ce(CO_3)_2OH$ decomposed according to the followed reaction:

$$Ce(CO_3)_2OH \rightarrow CeO_2 + CO_2 + H_2O$$

It decomposed until 750°C to form CeO_2 creating the larger pore than the others. After calcinations at 800oC, the BET surface area of sample ACZ09 reduced 50%, ACZ10 reduced 30%, and the ACZ08 reduced 20%. That means the sample synthesized by NH_4HCO_3 as the precipitant exhibited the higher thermal stability than the others.

Table 3.9: BET surface area of ACZ samples synthesized using different precipitants.

Samples	Precipitates	BET surface area (m^2/g)		Pore diameter (A^o)		Pore volume (cm^3/g)	
		550°C	800°C	550°C	800°C	550°C	800°C
ACZ08	NH_4HCO_3	108.21	80.213	256.22	317.17	0.7096	0.6525
ACZ09	NH_4OH	148.83	73.25	44.71	76.15	0.1851	0.1503
ACZ10	KOH	183.96	127.95	105.88	135.39	0.5030	0.4433

Figure 3.25 shows the SEM images of the ACZ samples synthesized using different precipitants. It is evident to observe the agglomeration in the sample prepared with NH_4OH (ACZ09) and KOH (ACZ10). While the sample ACZ08 had the porous surface, the particles of the others agglomerated to form big clusters. That's the reason why after calcinations at 800°C, the sintering accelerated the combination of atom in the cluster, to increase the particles size, while decrease sharply the surface area, which was agreed with the BET results.

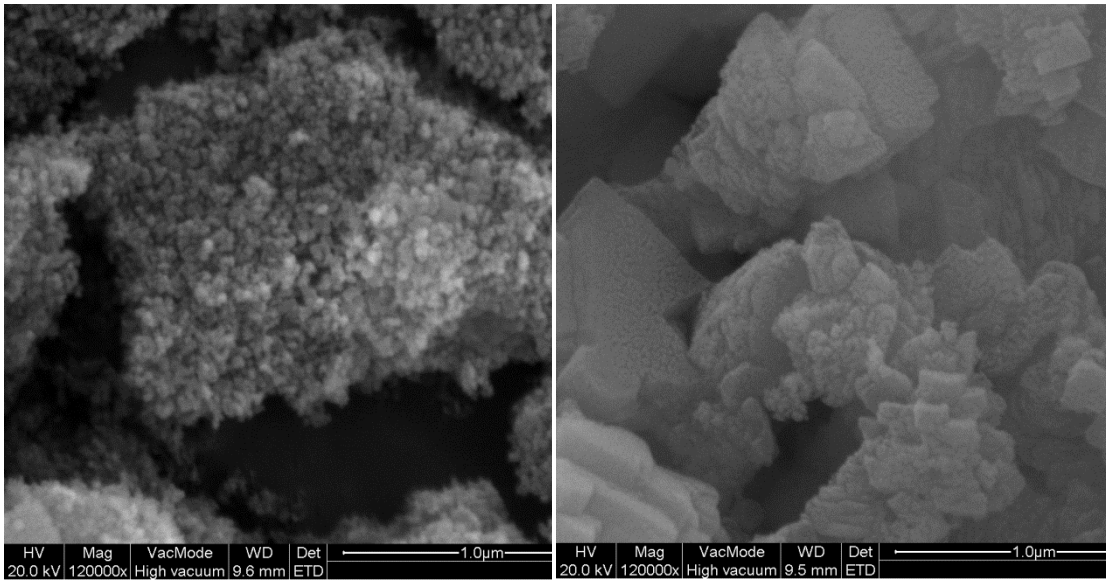

ACZ08 ACZ09

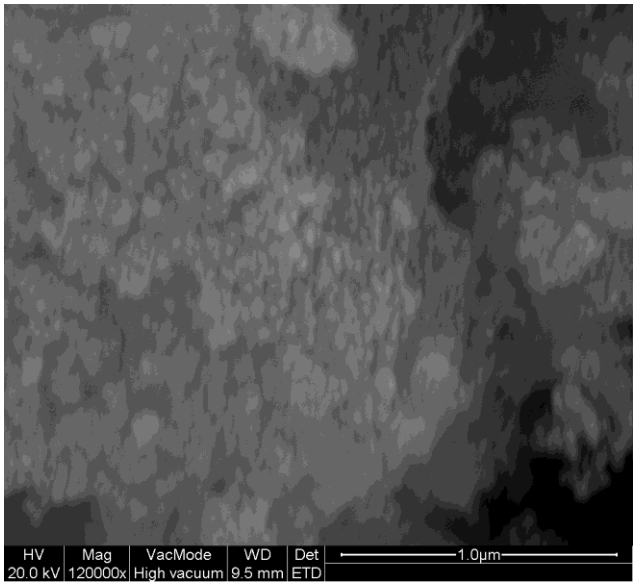

ACZ10

Fig.3.25 : SEM images of samples using with different precipitants calcined at 550°C

Due to the advantage of porous surface and high thermal stability of the sample prepared by NH_4HCO_3, NH_4HCO_3 would be used for further investigation.

The influence of ageing (hydrothermal treatment):

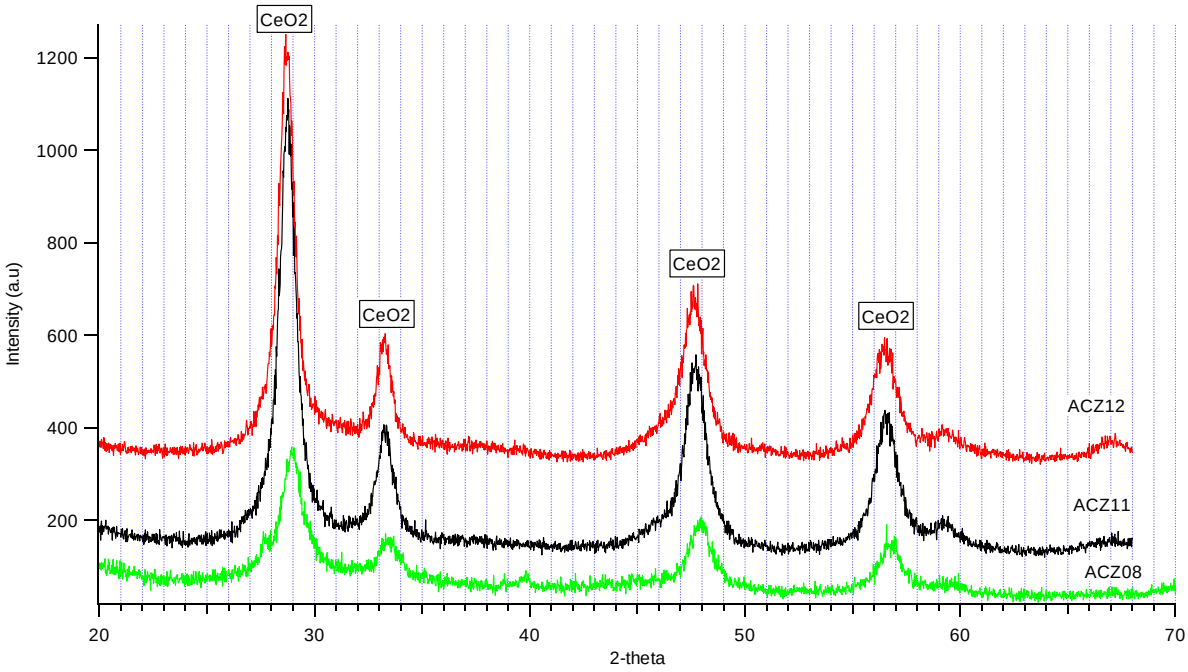

Fig.3.26 : XRD patterns of ACZ samples with different aging conditions calcined at 550°C (ACZ08, ACZ11, ACZ12)

ACZ08, ACZ11 and ACZ12 were the samples prepared with the same procedure using NH_4HCO_3 but different ageing time. As can be seen from their XRD patterns (figure 3.26), the typical peaks of CeO_2 were observed at 2-theta angle of 28.9, 33.3, 47.92 56.58. However, the aging treatment definitely affected to the formation of crystal. The aged samples (ACZ11 and ACZ12) had the higher and sharper peaks than that of the sample without aging (ACZ08), indicating the better crystallite levels due to aging's effect.

From the table 3.10, it can be seen that the ACZ12 has the highest value of specific surface area, and the ACZ08 has the lowest one. After aging at 90°C and 160°C, both the

pore volume and the pore size are smaller than the sample without aging. After the reaction happening, the ACZ08 was continuously stirred for next 5 hour, then filtering. While other sample ACZ11 and ACZ12 was put in static condition with high temperature and high pressure, the crystal and the lattice under these strict conditions would arranged more order than the ACZ08.

During the aging at 90°C and 160°C for 20h, the structure of as-prepared samples was rearranged. The high temperature created the elevated pressure which effect on the structure of material. Hydrothermal synthesis implements, therefore, a first step of crackdown of possibly present "macromolecular" units by chemical reaction, existing e.g. as colloidal solution, as precipitated colloidal solution (crystalline, partially crystalline (e.g. gel), glassy and amorphous) or solid state precursor materials of the same kind, because bigger units exceeding the size present in true solutions are not stable under high pressure hydrothermal conditions. The formation of a true solution is therefore assumed in which the smallest possible structural building units as well as cations with their respective hydration spheres are transported. The ACZ12 was aged at highest temperature, therefore, the pore structure was best formed, leading to the highest surface area. Thus, aging at 160°C for 20 hour would be used in further experiments.

Table 3.10: The BET surface area of samples synthesized with and without aging

Samples	Aging	BET surface area (m^2/g)		Pore diameter (A^o)		Pore volume (cm^3/g)	
		550°C	800°C	550°C	800°C	550°C	800°C
ACZ08	non	108.21	80.213	256.22	317.17	0.7096	0.6525
ACZ11	90°C	156.46	81.49	140.25	198.41	0.6088	0.4287
ACZ12	160°C	198.64	70.73	70.82	125.55	0.4009	0.2780

The influence of surfactant:

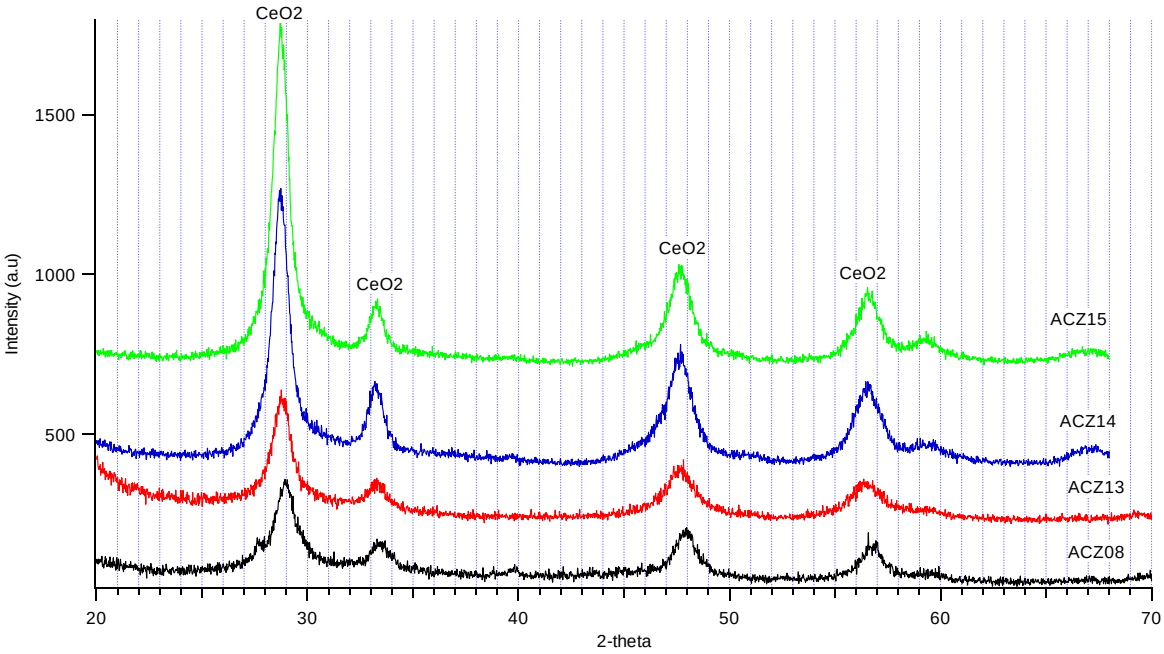

Fig.3.27 : XRD patterns of ACZ samples prepared using different surfactants calcined at 500°C (ACZ08, ACZ13, ACZ14, ACZ15)

Figure 3.27 show the XRD patterns of samples prepared with different surfactants. Similarly, the XRD patterns of these samples also had the characteristic peaks of CeO_2. Compared with sample prepared with CTAB (ACZ14) and PEG (ACZ15), the sample using SDS (ACZ13) exhibited the lower peaks, meaning the smaller crystal's size, resulting in the higher surface area. As can be seen in table 4, the highest surface area as 397.03 m^2/g was obtained for the sample ACZ13 which used SDS as surfactant, while the other samples prepared with CTAB or PEG had much lower BET surface area. That is because the differences in interaction between surfactant with metallic ion. As a kind of anionic surfactant, the formation of micelle SDS combined with Al, Ce and Zr would lead to the oriented arrangement of mixed oxides.

SDS dissolved completely into distilled water following reactions in the solution:

$C_{12}H_{25}SO_4Na \rightarrow (C_{12}H_{25}SO_4)^- + Na^+$

$n(C_{12}H_{25}SO_4)^- \rightarrow (C_{12}H_{25}SO_4)_{-n}$

Dissociated $(C_{12}H_{25}SO_4)^-$ molecules aggregated together to form supramolecular micelles $(C_{12}H_{25}SO_4)_{-n}$ composed of ordered external directing polar hydrophilic group ($-SO_3^-$) and inner directing nonpolar hydrophobic alkyl chain ($C_{12}H_{25}$-). Meanwhile, numberous $Ce(H_2O)_x(OH)_y^{(3-y)}$ and $Zr(H_2O)_x(OH)_y^{(4-y)+}$ and $Al(H_2O)_x(OH)_y^{(3-y)}$ ion existed in the solution due to hydrolysis of Ce, Zr and Al ions.

These $Ce(H_2O)_x(OH)_y^{(3-y)}$ and $Zr(H_2O)_x(OH)_y^{(4-y)+}$ and $Al(H_2O)_x(OH)_y^{(3-y)}$ species combined with the group $(-OSO_3)^-$ in $(C_{12}H_{25}SO_4)^-$ by electrostatic interaction so as to be embed into the supermolecular group $(C_{12}H_{25}SO_4)_{-n}$ generating the inorganic – organic complex precursor with spherical structure. With the addition of OH-, the pH value of the solution increased, causing the free $Ce(H_2O)_x(OH)_y^{(3-y)}$ and $Zr(H_2O)_x(OH)_y^{(4-y)+}$ and $Al(H_2O)_x(OH)_y^{(3-y)}$ ions in the solution and the ion embedded in the supermolecular group to be linked together through oxygen brigde between Al, Ce and Zr atoms, and hence forming mono dispersed solid solution precursor [93].

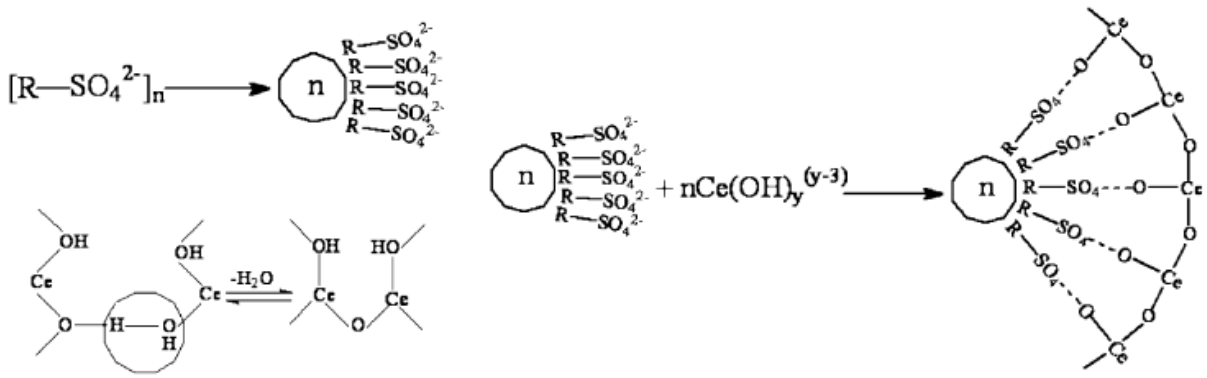

Fig.3.28 : Mechanism of forming micelles of SDS

Differently, CTAB is a cationic surfactant, therefore after adding the CTAB to the solution of Al^{3+}, Ce^{3+}, Zr^{4+}, the alkyltrimethylammonium cations exchange into the structure of the hydrous aluminum (III) oxide, hydrous cerium (III) oxide as well as hydrous zirconium(iv) oxide. This mechanism is more like scaffolding, rather than templating [95]. In case of PEG – a non polar surfactant, the formation of the mesostructure is attributed to the interaction between precursors and PEG20000. This interaction is achieved by hydrogen bonding between PEG20000 and precursors [96]. The weak bonding formed in these two mechanisms made the process took long time to form

the crystallite, leading agglomeration and then low surface area. That explains the differences in BET surface area between the samples using different surfactants.

Table 3.11: The BET results of mixed oxides with different surfactants.

Surfactant	Samples	BET surface area (m^2/g)		Pore diameter (A^o)		Pore volume (cm^3/g)	
		550°C	800°C	550°C	800°C	550°C	800°C
Non	ACZ08	108.21	80.213	256.22	317.17	0.7096	0.6525
SDS	ACZ13	397.03	68.52	48.29	111.76	0.5537	0.2232
CTAB	ACZ14	115.11	96.66	107.06	144.68	0.3223	0.3605
PEG	ACZ15	115.37	91.01	130.48	143.26	0.3828	0.3346

Surface area of samples prepared using different surfactants are indicated in table 3.11. Amongst investigated samples, sample synthesized SDS (ACZ13) had the highest surface area, but its pore size was the smallest. After calcination at 800°C, its surface area and pore volume reduced remarkably (68.52 m2/g and 0.2232 cm3/g), while the pore size increased twice. Oppositely, the samples using CTAB or PEG didn't change a lot during calcinations process.

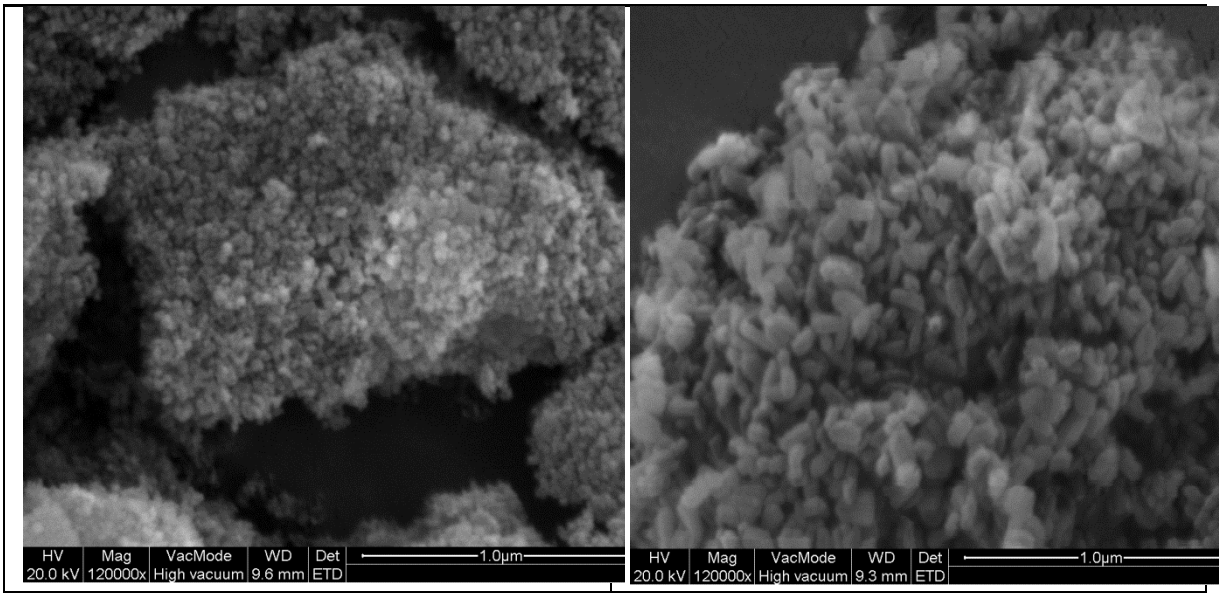

ACZ08	ACZ13

Fig. 3.29: SEM images of mixed oxides without (ACZ08) and with surfactant SDS (ACZ13)calined at 500°C

From SEM images of fig.3.29, it is obvious to see the change of surface when using the surfactant in the synthesis of materials. The SEM image of ACZ13 shows that the surface of this sample is shown less agglomeration than that of the ACZ08. The crystal of ACZ13 has the shape like the worm. The surface of this material is definitely good when used as a support. The particles of active phase can be hosted in the pore of the support.

In conclusion, for the ACZ samples possessing highest surface area is the sample prepared using NH_4HCO_3 as the precipitant, SDS as the surfactant. The precipitation was aged at 160°C for 20 hours. This sample will be used further to prepare the complete catalyst.

3.4 Deposition of support on substrates

Consistent with the appearance of the substrate, the deposition has been investigated widely. There are many methods to load the support on the substrates, but depending on the properties materials, the methods should be adapted. A sol–gel method allows penetrating the porosity, whereas the use of the suspension technology resulted in pore blocking in the case of ceramic monolith coating. To avoid the penetration of the oxide precursor in the porosity, a hybrid method between suspension and sol–gel is preferred than sol–gel alone. Hybrid indeed combines the advantages of the sol (precise control and tuning of the catalyst microstructure) and that of the suspension (ease of deposition). Therefore, we investigate all three chemical preparations for deposit support on ceramic, while we use dip-coating for metallic substrate because these chemical methods depend on "anchoring" on the surface of the substrate, while the metal substrate lacks of porosity.

3.4.1 Preparation of $Ce_{0.2}Zr_{0.8}O_2$ on cordierite

3.4.1.1 Influence of deposition methods on surface areas

Different deposition methods were performed to deposit $Ce_{0.8}Zr_{0.2}O_2$ support on cordierite substrate.

The influence of deposition methods on surface areas of $Ce_{0.2}Zr_{0.8}O_2$/cordierite samples is indicated in Table 3.12. It can be seen that although the loading contents of $Ce_{0.2}Zr_{0.8}O_2$ is highest with direct combustion method, this method even decrease surface area of the samples, especially when the combustion temperature is high (420^{o}C). It may be due to the fact that surface area of ceria-zirconia mixed oxide synthesized using this method is low (surface area of the powder form is around 50 m^2/g) since there was not enough time for a porous structure of ceria-zirconia to be formed at such immediate evaporation of solution at high temperature. When this low surface area was covered on cordierite substrates, the surface area decreased more due to the closer arrangement of particles in a continuous layer on the surface of cordierite.

Table 3.12. Surface area of $Ce_{0.2}Zr_{0.8}O_2$/cordierite samples prepared by different deposition methods

Samples	Deposition method	BET surface area (m^2/g)		wt% loading of $Ce_{0.2}Zr_{0.8}O_2$ on cordierite
		Coated pellets	$Ce_{0.2}Zr_{0.8}O_2$ powder obtained under the same preparation procedure	
CordxH8	No deposition	20	-	-
SC-120	Direct combustion, oven temperature 120^{o}C	18	50.12	3.84
SC-420	Direct combustion, oven temperature 420^{o}C	14	45.59	10.09
HD	Hydid deposition	18.09	32.87	0.98
Seed	Secondary growth on $Ce_{0.2}Zr_{0.8}O_2$	7.6	45.59	9.49

	seeds		(seeding) 117.16 (hydrothermal)	
Su	Suspension, 1 ml Brij56, mixing time 24h, deposite 5 time	23.76	73.89	3.5
DD	Second deposition of double deposition method	24.84	56.24	4.39

With the aim to obtain high loading contents of ceria – zirconia layer on cordierite substrate, hydrid deposition was applied since it was expected that the sol of $Ce(NO_3)_3$ and $ZrOCl_2$ can act as a binder to attach $Ce_{0.2}Zr_{0.8}O_2$ powder on cordierite surface. However, $Ce_{0.2}Zr_{0.8}O_2$ loading contents of the sample prepared by hydrid deposition method was lowest compared to other methods (only 0.98%). $Ce_{0.2}Zr_{0.8}O_2$ powder obtained under the same preparation procedure also possess much lower surface area (32.87 m^2/g) compared to uncalcined as-prepared $Ce_{0.2}Zr_{0.8}O_2$ powder (117 m^2/g), indicating that the hydrid preparation and the calcinations procedure decrease significantly surface area of as-prepared $Ce_{0.2}Zr_{0.8}O_2$ powder, thus, when it was covered on cordierite substrates, the surface area decreased more (18.09 m^2/g) due to the closer arrangement of particles in a continuous layer on the surface of cordierite.

$Ce_{0.2}Zr_{0.8}O_2$ powder prepared by hydrothermal method usually exhibited high surface area. However, due to tough surface of cordierite and the differences in the crystal structure between the cordierite and ceria – zirconia mixed oxides, it is very difficult for the $Ce_{0.2}Zr_{0.8}O_2$ growing on the cordierite surface. Therefore, the method which was called secondary growth on $Ce_{0.2}Zr_{0.8}O_2$ seeds was performed with the aim to form a layer of $Ce_{0.2}Zr_{0.8}O_2$ seeds on cordierite surface by direct combustion method prior to use for hydrothermal method. $Ce_{0.2}Zr_{0.8}O_2$ seeds were expected to act as nuclei to grow the continuous layer of $Ce_{0.2}Zr_{0.8}O_2$ formed afterwards by hydrothermal synthesis. However, the BET surface area of the sample obtained from secondary growth is even lower than that of the sample prepared by solid combustion method. The first growth $Ce_{0.2}Zr_{0.8}O_2$ layer was formed using the direct combustion method, which has an advantage of high loading content, but a disadvantage of loose adhesion of $Ce_{0.2}Zr_{0.8}O_2$ layer on cordierite surface. Thus, during the second growth by hydrothermal synthesis, the cluster of $Ce_{0.2}Zr_{0.8}O_2$ can be detached from the surface due to the presence of hydrothermal solution. In the mean times, it seems that no $Ce_{0.2}Zr_{0.8}O_2$ particles formed during the hydrothermal step could be deposited on the first layer previously prepared direct combustion. Consequently, the aim of seeding for the secondary growth was failed; therefore, the BET surface area as well as $Ce_{0.2}Zr_{0.8}O_2$ loading content of the final sample was not as high as those of the sample obtained after the first growth.

The dispersion of solid particles on a hard surface as cordierite ceramic is rather difficult. One of the most efficient ways to deposit is using powder slurry. The viscosity of the slurry plays an important role to the efficiency to attach solid particles on the surface of a substrate. In this work, brij-56 was used as a binder to make suitable viscosity of the slurry for the coating process. In order to determine the optimal procedure, quantity of brij56 binder (0.5-1ml in a total 5mml of the suspension) and mixing time (24-48h) of the

slurry were altered. However, only minor influence of Brij56 quantity and mixing time on surface area was observed, thus, the quantity of brij56 was finally chosen as 0.5 ml and the mixing time was chosen as 24h. When the deposition time increases, surface area tends to increase. After 5 time of deposition, surface area of the sample prepared by suspension method was about 24 m^2/g, which is higher than those obtained by other methods. The loading content of $Ce_{0.2}Zr_{0.8}O_2$ obtained by suspension method (3.5%) was lower than that obtained by direct combustion method but not too low. However, a lot of cracks have been observed on the surface of $Ce_{0.2}Zr_{0.8}O_2$ layer (section 3.4.1.2).

With the aim to remove the cracks on the $Ce_{0.2}Zr_{0.8}O_2$ layer deposited by suspension, the treated cordierite substrates were deposited twice by the method called double depositions combining of wet impregnation and suspension. Using this method, a smooth layer of $Ce_{0.2}Zr_{0.8}O_2$ had been formed prior to the deposition of $Ce_{0.2}Zr_{0.8}O_2$ by suspension method, thus created the better condition for the adhesion of the second $Ce_{0.2}Zr_{0.8}O_2$ layer. The BET surface area of the sample prepared by that method was almost as the same as that of the sample prepared by suspension method since both methods use the same $Ce_{0.2}Zr_{0.8}O_2$ slurry and the synthesis procedures were not significantly different. However, less cracks have been observed on the surface of the sample prepared by double deposition method (section 3.4.1.2). The double deposition method also has an advantage of higher loading content of $Ce_{0.2}Zr_{0.8}O_2$ compared to that obtained by suspension method.

3.4.1.2 Influence of deposition methods on morphology

Surface of $Ce_{0.2}Zr_{0.8}O_2$/cordierite samples prepared by different methods observed under a microscope are presented in fig. 3.30. It can be seen that surface of the samples prepared by direct combustion at 120°C (SC-120), hydrid deposition (HD), seed are not very different from that of the unimpregnated cordierite (CV-OHCl8), proving that these methods were not able to impregnate a recognized amount of $Ce_{0.2}Zr_{0.8}O_2$ on the surface of cordierite. Meanwhile, images of $Ce_{0.2}Zr_{0.8}O_2$ layers may be seen on the surfaces of other impregnated samples. Thus, direct combustion at 120°C, hydrid deposition and seed are not effective method. However, the morphologies of $Ce_{0.2}Zr_{0.8}O_2$ layers on samples prepared by effective methods (solid combustion at 420°C, suspension and double deposition) are also different. The double deposition method resulted in the most smooth surface of $Ce_{0.2}Zr_{0.8}O_2$ layers while inhomogeneous surface was seen on the sample prepared by solid combustion at 420°C and many cracks were obtained on the surface of the sample prepared by suspension method. The adhesion between of $Ce_{0.2}Zr_{0.8}O_2$ layers with the cordierite substrate was extremely loose in the sample prepared by direct combustion at 420°C. The $Ce_{0.2}Zr_{0.8}O_2$ agglomerates on the cordierite surface can be easily detached since the evaporation of water during the deposition process at high temperature was too rapid. Although the use of binder in suspension method was able to produce the more viscous slurry to result in higher $Ce_{0.2}Zr_{0.8}O_2$ loading content compared to other methods, the burning of the polymer binder remained in the $Ce_{0.2}Zr_{0.8}O_2$ layer on the substrate during the calcinations may be the reason for the presence of cracks on the surface of the sample. Meanwhile, the presence of the previous formed $Ce_{0.2}Zr_{0.8}O_2$ layer

prior to the deposition of the other $Ce_{0.2}Zr_{0.8}O_2$ layer by suspension method may prevent the growth of cracks on the surface of the final samples prepared by double deposition method. Thus, on vision, the sample prepared by double deposition seems to be the best sample.

CV-0-HCl8

SC – 120

SC – 420

HD

Su

Seed

DD-CZ

Fig.3.30. Images of $Ce_{0.2}Zr_{0.8}O_2$/cordierite samples prepared by different deposition methods (magnification 40 times)

Morphologies of the samples which possessed a thick enough layer of $Ce_{0.2}Zr_{0.8}O_2$ (the samples prepared by suspension and double deposition method) may be seen clearer from SEM images (fig. 3.31a, b). In comparison with morphology of unimpregnated cordierite (fig. 3.31c), it is clearly seen that in these samples, a layer of $Ce_{0.2}Zr_{0.8}O_2$ with completely different morphology have been covered all surface of the cordierite substrate. However, the morphology of $Ce_{0.2}Zr_{0.8}O_2$ layer prepared by suspension method was also different from that prepared by double deposition method. $Ce_{0.2}Zr_{0.8}O_2$ layer on the sample prepared by suspension method possessed much finer particles than the $Ce_{0.2}Zr_{0.8}O_2$ layer on the sample prepared by double deposition method. It may be due to the fact that the double deposition method includes two calcination steps of two continuous $Ce_{0.2}Zr_{0.8}O_2$ layers, thus, making more sintering of particles which resulted in larger particle sizes. Nevertheless, two time deposition may result in more close $Ce_{0.2}Zr_{0.8}O_2$ particles, making

more homogeneous layer of $Ce_{0.2}Zr_{0.8}O_2$ without any cracks in the sample prepared by double deposition method.

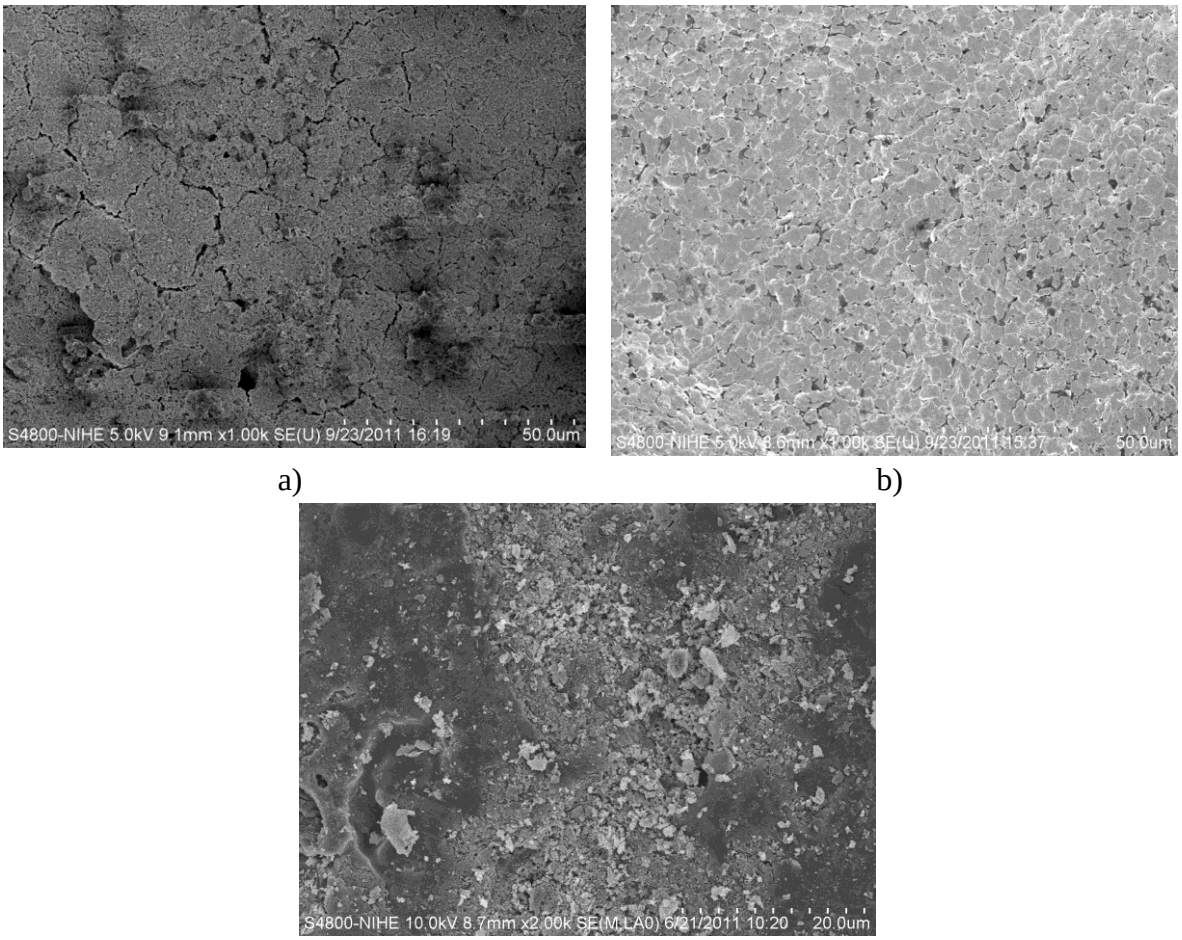

a) b)

c)

Fig. 3.31. SEM images of $Ce_{0.2}Zr_{0.8}O_2$/cordierite samples prepared by suspension method-Su (a), double deposition method – DD (b), and acid treated cordierite – CV-0-HCl8 (c)

3.4.1.3 Phase composition of $Ce_{0.2}Zr_{0.8}O_2$/cordierite

Since the impregnation of $Ce_{0.2}Zr_{0.8}O_2$ on cordierite substrate using double deposition method resulted in the most homogeneous and stable layer of $Ce_{0.2}Zr_{0.8}O_2$ on cordierite, the samples prepared by this method was selected to continue to deposit the catalytic active phase on. XRD pattern of the $Ce_{0.2}Zr_{0.8}O_2$/cordierite sample (DD) is presented in fig. 3.32. In the figure, characteristics of $Ce_{0.2}Zr_{0.8}O_2$ were seen at peaks with 2theta of 30, 35, 49 and 59^o, characteristics of cordierite were seen at peaks with 2theta of 26.5, 29.5, 34, 43, 47^o. Peaks belonged to mullite and quartz were also found since they existed together with cordierite sample synthesized from kaolin.

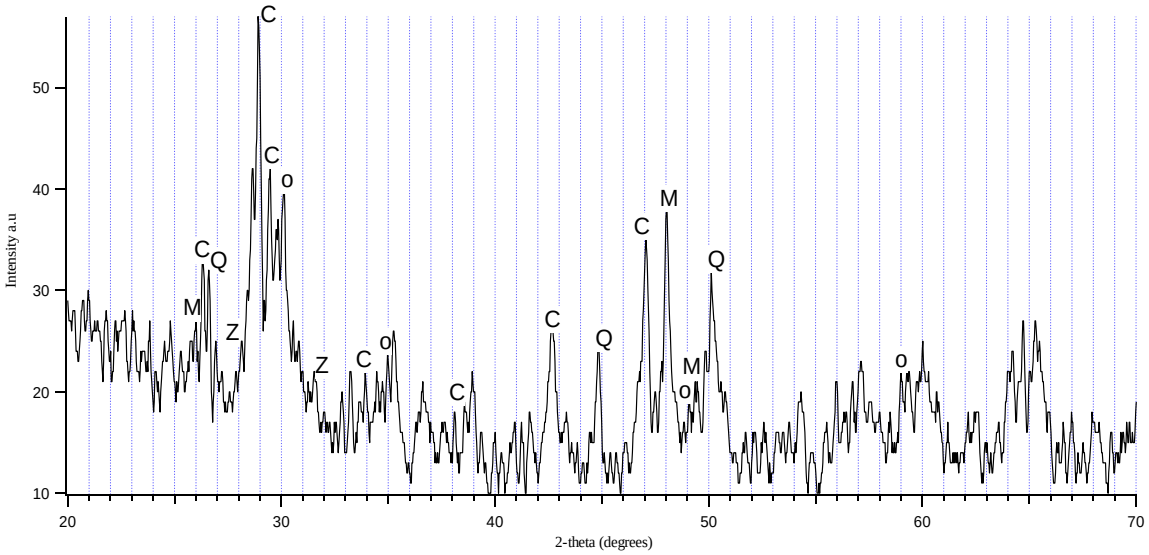

Fig. 3.32. XRD pattern of the $Ce_{0.2}Zr_{0.8}O_2$/cordierite sample (DD) (C: cordierite, Q: quartz, M: mullite, Z: monoclinic zirconium oxide, 0: $Ce_{0.2}Zr_{0.8}O_2$)

3.4.4 Preparation of γ-Al_2O_3 support on cordierite substrate

The γ-Al_2O_3 was a very popular support in three-ways catalyst because of its high surface area, and high ability in dispersion of active phase, especially noble metal in the application of catalysis. Moreover, γ-Al_2O_3 has been investigated to prepare successfully from boehmite, therefore, in this work, γ-Al_2O_3 was also deposited on cordierite substrate by using boehmite in suspension method. Besides, sol-gel and double depositions methods were utilized to load γ-Al_2O_3 on cordierite substrate.

The characterization of γ-Al_2O_3 on cordierite was shown in table 3.13 and fig.3.33.

Table 3.13: Characterization of γ-Al_2O_3 support on cordierite substrate

Samples	Content of loading γ-Al_2O_3 (wt.%)		BET surface area (m^2/g)	
	On untreated cordierite	On treated cordierite	γ-Al_2O_3 /untreated cordierite	γ-Al_2O_3 /treated cordierite
Cordierite	0	0	0.60	5.90
SG-A	5.80	8.59	6.13	4.96
Su-A	6.58	**16.67**	**12.25**	**11.52**
DD-A	-	**6**	-	**13.17**

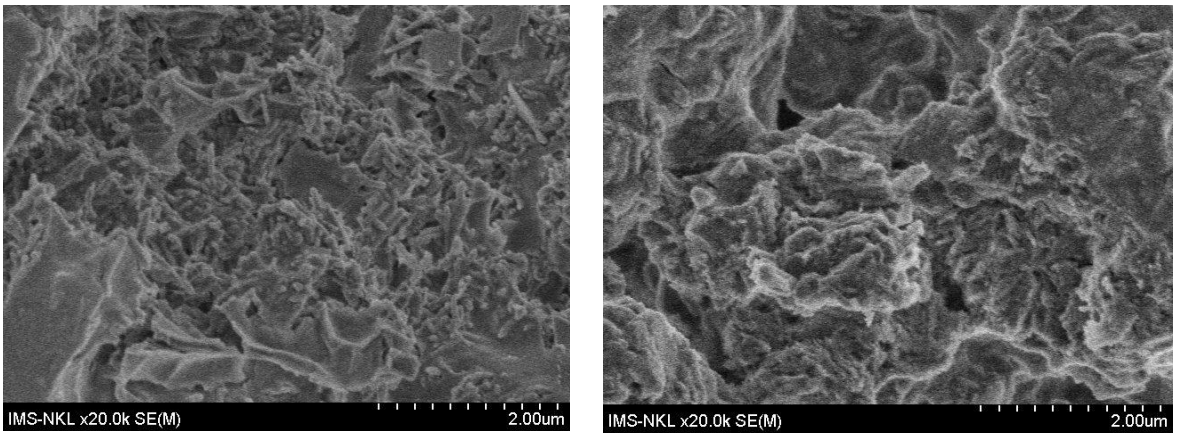

a) *b)*

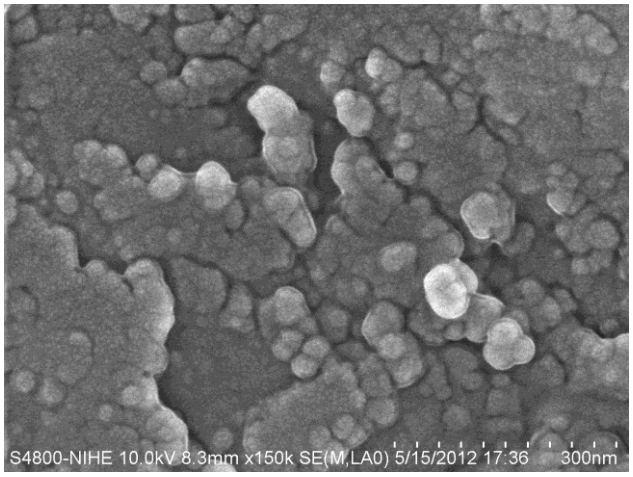

c,

Fig. 3.33. SEM images of a) SG-A; b) Su-A; c) DD-A

As can be seen in table 3.13, the loaded content of γ-Al_2O_3 on untreated cordierite and HCl treated cordierite was so different. The loaded γ-Al_2O_3 on untreated cordierite was about 6 wt.%, while the loaded Al_2O_3 on HCl treated substrate was 85 wt.% by sol-gel, and 16.67% by suspension. Thus, the acid treatment played an important role in improving the adhesion between the Al_2O_3 and the substrate. However, the BET surface area of coated cordierite was not changed a lot compared with treated cordierite. This might be due to the incomplete covering of support on substrate's surface, leading the low BET surface area of total support-substrates system. Moreover the BET surface area of γ-Al_2O_3 prepared from sol-gel was lower than that from boemite, thus sol-gel method didn't result in high surface area and Al_2O_3. SEM images of Al_2O_3 on cordierite samples were demonstrated on fig.3.33. The changes in morphology of surface proved the cover of support on substrate. From the results, it is obvious that the suspension and double depositions expressed the better efficiency than sol-gel.

However, compared with the sol-gel and suspension, the sample prepared by double deposition had smoother layer. This smooth layer formed by the close particles as can be seen in high magnification.

3.4.5 Preparation of $AlCe_{0.2}Zr_{0.05}O_2$ support on cordierite substrate

$AlCe_{0.2}Zr_{0.05}O_2$ support was deposited on cordierite substrate by double deposition method since the advantages of this method has been observed in coating $Ce_{0.2}Zr_{0.8}O_2$ and γ-Al_2O_3 support on cordierite substrates. The morphology of $AlCe_{0.2}Zr_{0.05}O_2$/ cordierite was illustrated on fig.3.35. The sample shows some crack of $AlCe_{0.2}Zr_{0.05}O_2$ layer on the surface. Thus, the deposition of $AlCe_{0.2}Zr_{0.05}O_2$ on cordierite is more difficult than the deposition of $Ce_{0.2}Zr_{0.8}O_2$, which resulted in worse surface. However, in a small area of the surface, the fine particle (10 nm) arranged homogeneously, it can be seen that particles of $AlCe_{0.2}Zr_{0.05}O_2$ coverd completely this small surface. Surface area of the sample is 20.16 m^2/g, which is much smaller than that of the original $AlCe_{0.2}Zr_{0.05}O_2$ prepared by hyfrothermal synthesis. That is because the agglomeration of fine particles on the support layer.

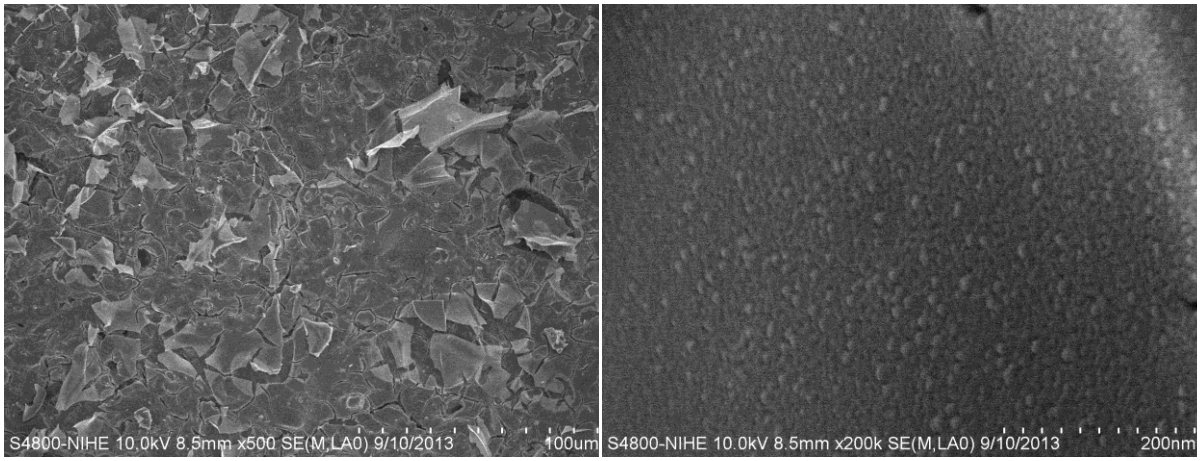

Fig.3.35: SEM images of DD-ACZ

In summary, due to the multi layers formed by impregnation and suspension, the surface of substrate was guaranteed to cover completely. Therefore, double depositions method was used for further investigation.

3.5 Characterization of complete catalysts

In another parallel study, it has been found that unsupported mixed metal oxides MnO_2 – NiO – Co_3O_4 and MnO_2 – Co_3O_4 – CeO_2 exhibited outstanding catalytic activity for the simultaneously treatment of HC, CO and NO_x. Therefore, in this study, these active phases were selected to deposit on support-substrate.

3.5.1 MnO_2 – NiO – Co_3O_4 /$Ce_{0.2}Zr_{0.8}O_2$/ cordierite

To deposit on $Ce_{0.2}Zr_{0.8}O_2$/cordierite, MnO_2 – NiO – Co_3O_4 was used instead of MnO_2 – Co_3O_4 – CeO_2 because Ce component was already existed in the support. The wet impregnation procedure resulted in 5 wt.% MnO_2 – NiO – Co_3O_4 on the support-substrate (Ca.3) and 6 wt.% MnO_2 – NiO – Co_3O_4 on the cordierite (Ca.2). XRD pattern of Ca.3 sample is shown on fig. 3.36. When MnO_2 – NiO – Co_3O_4 active phase was impregnated on the $Ce_{0.2}Zr_{0.8}O_2$/cordierite sample (Ca. 3 sample), $NiCo_2O_4$ phase was found together with $Ce_{0.2}Zr_{0.8}O_2$. However, the rough and high baseline indicated that other active components (MnO_2, NiO, Co_3O_4) may exist as amorphous phase. This may also be the reason for hiding peaks belonged to cordierite, quartz or mullite from the substrate.

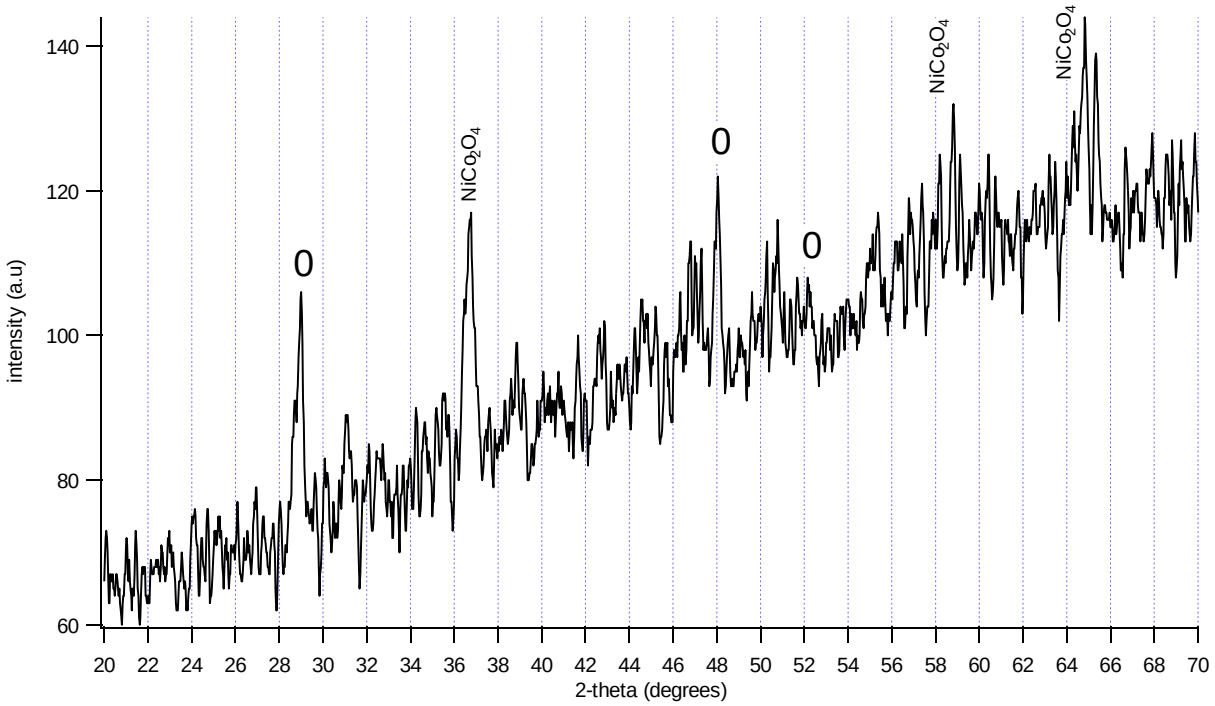

Fig. 3.36. XRD pattern of the complete catalyst with MnO_2 – NiO – Co_3O_4 / $Ce_{0.2}Zr_{0.8}O_2$/cordierite (Ca. 3)

The presences of element components of the final catalysts were also detected using EDX analysis as shown in table 3.14. The results show that the presences of O, Mn, Co, Ni were found with reasonable equal ratios in both catalysts (with and without $Ce_{0.2}Zr_{0.8}O_2$ support layer). The presences of Si, Al, Mg, the compositions of cordierite substrate and Ce, Zr, the compositions of $Ce_{0.2}Zr_{0.8}O_2$ support were not found in both catalysts. Thus, the active layers of MnO_2 – NiO – Co_3O_4 were supposed to be deposited thick enough to cover completely the substrate and support layer, therefore, X-ray beam was not able to reach to underneath $Ce_{0.2}Zr_{0.8}O_2$ and cordierite surface. The presence of $Ce_{0.2}Zr_{0.8}O_2$ will be proved by the technique XPS as shown latter. The EDX detected ratios of NiO – Co_3O_4 were reasonable fitted with theoretical ratios calculated from contents of starting chemicals, however the ratios of MnO_2 were lower than calculated.

Table 3.14. Atomic compositions (%) of components in Ca.2 and Ca.3 catalysts

Elements	Ca. 2 (MnO_2 – NiO – Co_3O_4 /cordierite)	Ca. 3 (MnO_2 – NiO – Co_3O_4/ $Ce_{0.2}Zr_{0.8}O_2$/cordierite
O	50.26	52.75
Mn	3.30	2.21
Co	33.32	30.03
Ni	13.12	15.00

SEM images of the final catalysts are presented in Fig. 3.37. The images show that at low magnification, the morphology of the catalyst with a $Ce_{0.2}Zr_{0.8}O_2$ support layer (Ca. 3) looked different from that of the catalyst without a $Ce_{0.2}Zr_{0.8}O_2$ support layer (Ca. 2), The catalyst with a $Ce_{0.2}Zr_{0.8}O_2$ support layer revealed two different parts. Part 1 seemed to lay underneath incompletely covered part 2 (Fig. 3.37a). However, the portion of part 1 was much smaller than that of part 2 over the whole catalyst. Part 1 may be assigned for the $Ce_{0.2}Zr_{0.8}O_2$ support layer while part 2 is later deposited MnO_2 – NiO – Co_3O_4 active

layer. At higher magnification (Fig. 3.37 c, d), two catalyst showed more similar morphology with sphere particles of about 100nm. It proves that the $MnO_2 – NiO – Co_3O_4$ active layer remained their specific morphology even if it was deposited on bare cordierite substrate (Ca. 2) or $Ce_{0.2}Zr_{0.8}O_2$ support on cordierite sample (Ca. 3).

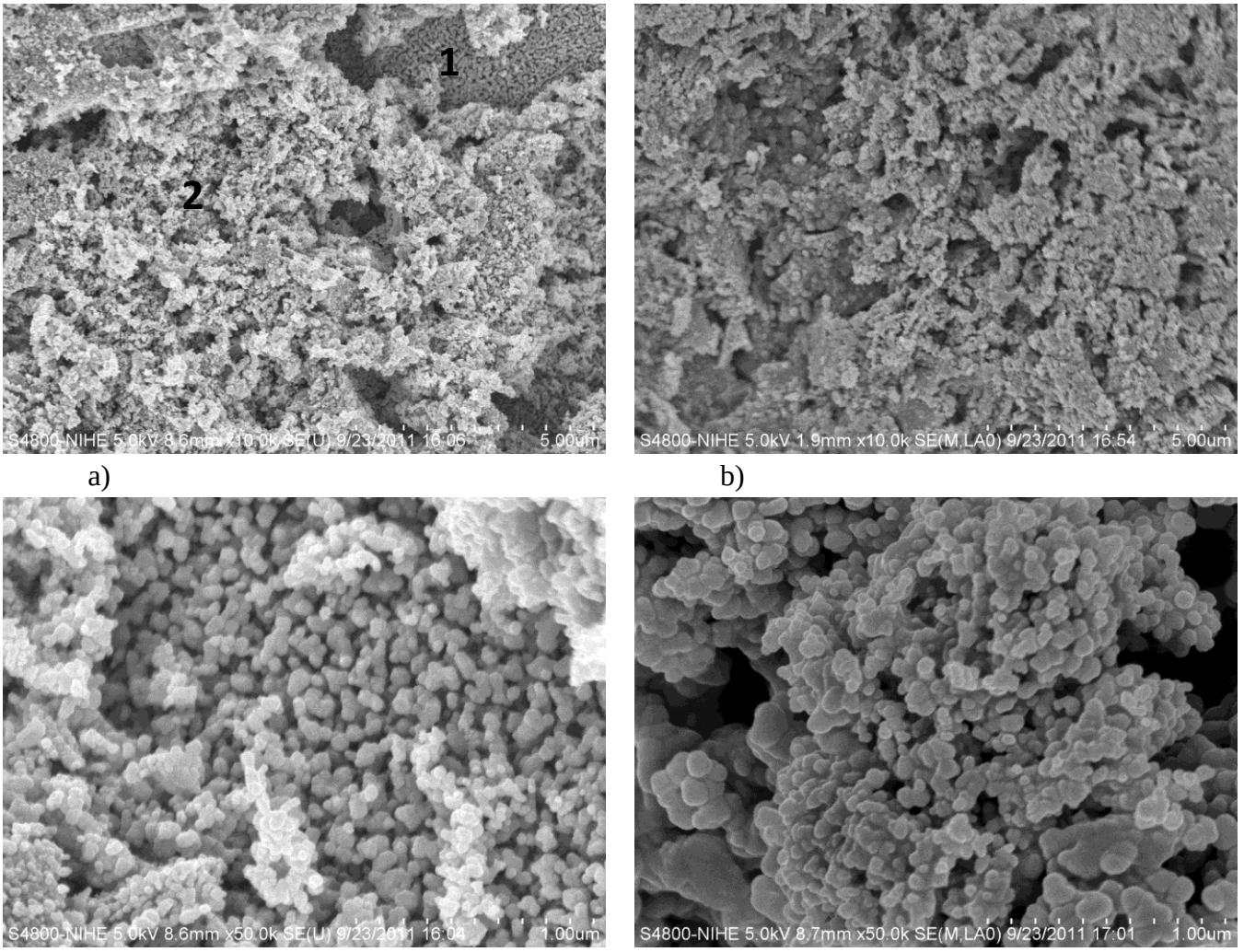

Fig. 3.37. SEM images of final catalysts: Ca. 2 ($MnO_2 – NiO – Co_3O_4$ /cordierite) and Ca. 3 ($MnO_2 – NiO – Co_3O_4$ / $Ce_{0.2}Zr_{0.8}O_2$/cordierite: a) Ca. 3 at magnification 10000 time, b) Ca. 2 at magnification 1000 time, c) Ca. 3 at magnification 50000 time, b) Ca. 2 at magnification 50000 time,

More information about the composition of these as-prepared samples was obtained from XPS measurements, which exposed the presences of all expected components of the catalysts (Mn, Ni, Co) on the surface (Fig. 3.38, Table 3.15). The components of the underneath $Ce_{0.2}Zr_{0.8}O_2$ layer and the substrate cordierite (Si) are also seen in XPS spectra of Ca.3 sample. The thickness of the catalyst layer on Ca. 2 sample was assumed to be thicker than that of the Ca. 3 sample since the peak belong to Si, the composition of the cordierite substrate, was almost unseen. Moreover, the peak concentrations of the components of the active phase (Mn, Ni, Co) in Ca. 3 sample are smaller than those from Ca. 2 sample.

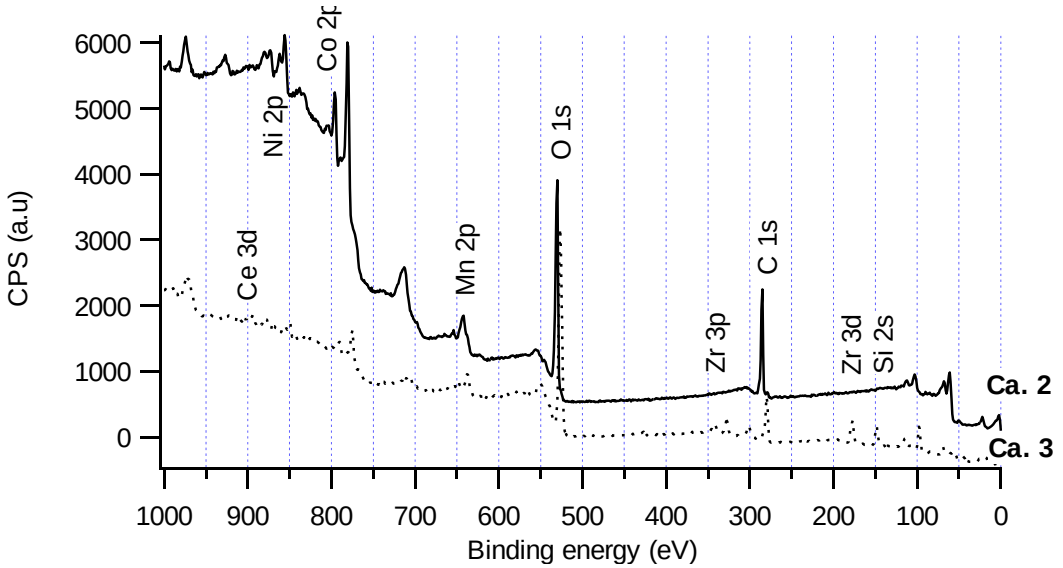

Fig. 3.38: XPS Survey of the as-prepared sample Ca. 2 (MnO_2 – NiO – Co_3O_4 /cordierite) and Ca. 3 (MnO_2 – NiO – Co_3O_4/ $Ce_{0.2}Zr_{0.8}O_2$/cordierite)

Table 3.15. Atomic compositions (%) of components in Ca.2 and Ca.3 catalysts by XPS

Elements	Ca. 2 (MnO_2 – NiO – Co_3O_4 /cordierite)	Ca. 3 (MnO_2 – NiO – Co_3O_4/ $Ce_{0.2}Zr_{0.8}O_2$/cordierite
Si	0	78.8
Mn	18.5	3.5
Co	54.3	7
Ni	27.2	2.3
Ce	0	0.6
Zr	0	7.7

3.5.2 MnO_2-Co_3O_4-CeO_2 /$AlCe_{0.2}Zr_{0.05}O_2$/ cordierite

Mixed metal oxides MnO_2-Co_3O_4-CeO_2 has also been proved to be the most active catalyst phase for the simultaneously treatment of HC, CO and NOx. Therefore, this active phase was also chosen to deposit on support-substrate. Since Ce has been a component of active phase, the support without CeO_2 (γ-Al_2O_3) or less CeO_2 ($AlCe_{0.2}Zr_{0.05}O_2$) was chosen instead of $Ce_{0.2}Zr_{0.8}O_2$ support. Moreover, these support are more economic, exhibits high surface area than that of $Ce_{0.2}Zr_{0.8}O_2$ support due to the presence of Al component. Besides, $Ce_{0.2}Zr_{0.8}O_2$ support was still be used for comparison. In this section, characterization of MnO_2-Co_3O_4-CeO_2/$AlCe_{0.2}Zr_{0.05}O_2$/ cordierite was present.

XRD patterns of MnO_2-Co_3O_4-CeO_2 /$AlCe_{0.2}Zr_{0.05}O_2$/ cordierite (Ca.7) and MnO_2-Co_3O_4-CeO_2 /cordierite (Ca.4) are shown in figures 3.39 and 3.40. Only peak of MnO_2, Co_3O_4 were detected. That means the coating of active phase not only covering entire the substrates, but also so thick enough to hide the existence of substrates' peaks. Moreover, the base lines in all XRD patterns were high, that means the deposited phases exhibited high amorphous nature.

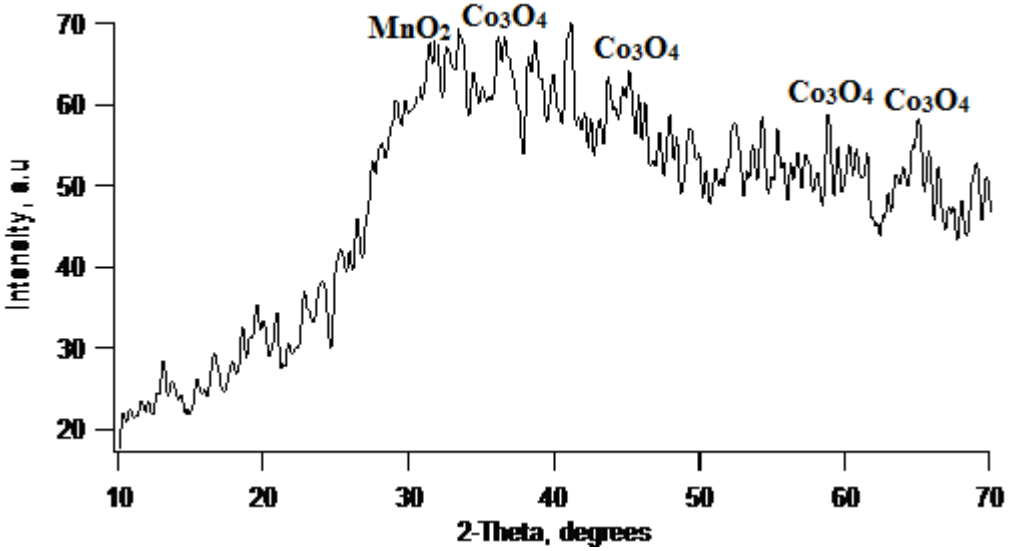

Fig. 3.39 : XRD pattern of MnO_2-Co_3O_4-CeO_2 /$AlCe_{0.2}Zr_{0.05}O_2$/ cordierite (Ca.7)

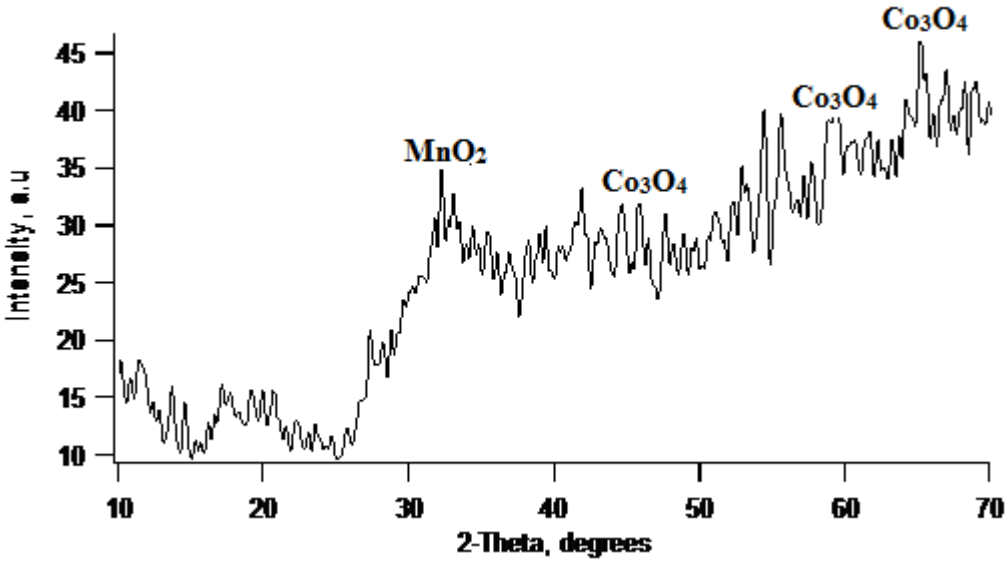

Fig. 3.40 : XRD pattern of MnO_2-Co_3O_4-CeO_2 /cordierite (Ca.4)

The surface area of some MnO_2-Co_3O_4-CeO_2 catalysts on cordierite were listed in the table 3.16. After deposition the active phase on support/substrates, the BET surface area of catalysts decreased compared with the treated cordierite by acid solution. This is maybe due to the active phase's coverage on pores of substrate. The difference of surface area of catalysts between deposited on different support and directly on substrate is not significant. Thus, the surface area of the complete catalysts was contributed mostly by MnO_2-Co_3O_4-CeO_2 active phase as the top layer. Although surface area of support and cordierite substrate maybe high, after deposition of support on substrate and the deposition of MnO_2-Co_3O_4-CeO_2 active phase, surface area of the complete catalyst was just about surface area of close arranged MnO_2-Co_3O_4-CeO_2 because the whole surface has been covered by this layer.

Table 3.16: Results of BET surface area of catalysts

samples	Composition	BET surface area (m^2/g)	Loading of active phase (wt.%)
CV-0-HCl8	cordierite	20.5	0
Ca.4	MnO_2-Co_3O_4-CeO_2/cordierite	13.11	5
Ca.5	MnO_2-Co_3O_4-CeO_2/Al_2O_3/cordierite	9.68	6.1
Ca.6	MnO_2-Co_3O_4-CeO_2/$Ce_{0.2}Zr_{0.8}O_2$ /cordierite	8.8	7.3
Ca.7	MnO_2-Co_3O_4-CeO_2/ $AlCe_{0.2}Zr_{0.05}O_2$/cordierite	10.45	5.6

The SEM images of catalysts with MnO_2-Co_3O_4-CeO_2 loading on cordierite were shown on figure 3.41 and 3.42. At low magnification, the distribution of active phase on substrates was observed. Both catalysts MnO_2-Co_3O_4-CeO_2 /$AlCe_{0.2}Zr_{0.05}O_2$/ cordierite (Ca.7) and MnO_2-Co_3O_4-CeO_2 /cordierite (Ca.4) had the substrates covered completely by active phase. Because the mixed oxides were loaded on cordierite from homogeneous solution of Mn, Co and Ce, the surface of catalysts were very porous with many pores. However, the differences between with and without supports of two catalysts was noticed at high magnification. When the active phase was impregnated on cordierite directly from solution, there was formation of clusters which had a size of approximately 50 – 200 nm (fig.3.41b). It is difficult to estimate the size of particle which formed cluster when capturing the cluster's surface, but when observing the edge of a cluster, particles of about 30 nm gathering to yield cluster (fig. 3.41c). But the particles forming cluster in catalyst using support $AlCe_{0.2}Zr_{0.05}O_2$ was smaller than 30 nm, may be just a few nm (fig. 3.42 b and c). The active phase was distributed uniformly on the surface of DD-ACZ ($AlCe_{0.2}Zr_{0.05}O_2$/ cordierite), in addition, the cluster with smaller particles and more porous which made an advantage in increasing contact's area between catalyst and exhausted gases. Therefore, the catalyst deposited on $AlCe_{0.2}Zr_{0.05}O_2$/cordierite will be studied further.

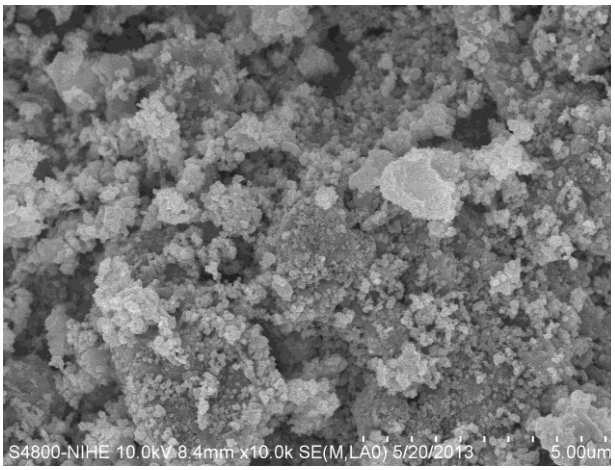

a

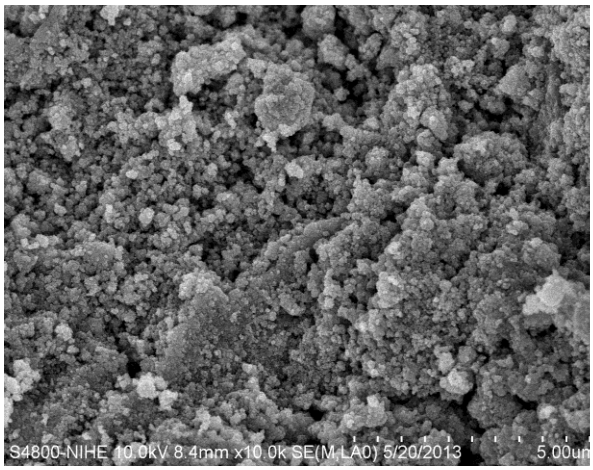

a

b

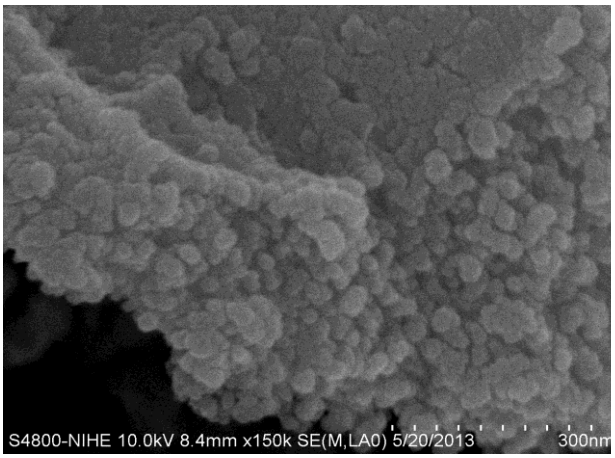

c

Fig 3.41 : SEM images of MnO_2-Co_3O_4-CeO_2 /cordierite (Ca.4)

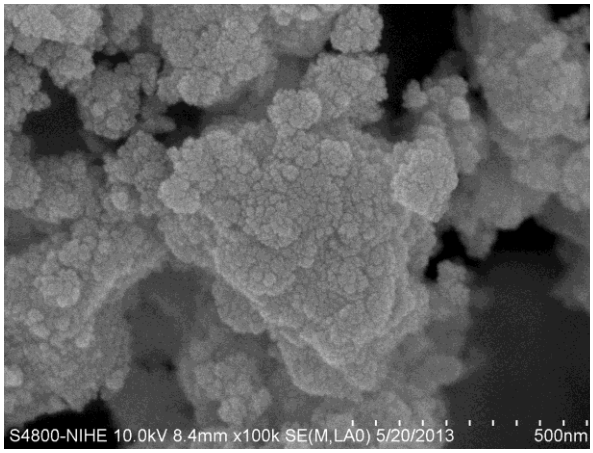

b

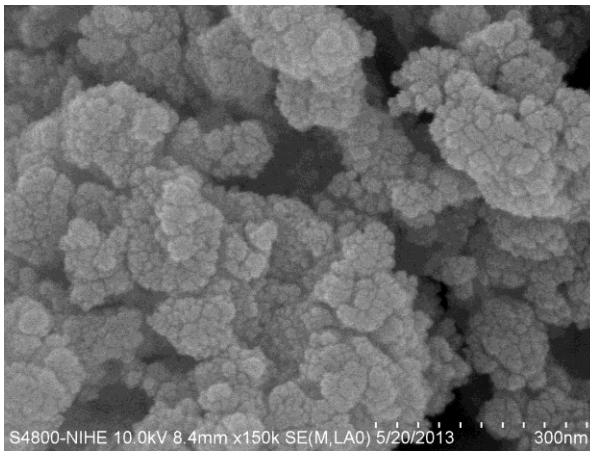

c

Fig 3.42 : SEM images of MnO_2-Co_3O_4-CeO_2 /$AlCe_{0.2}Zr_{0.05}O_2$/ cordierite (Ca.7)

3.5.3 MnO_2-Co_3O_4-CeO_2 /support/ FeCr alloys

MnO_2-Co_3O_4-CeO_2 was also deposited on FeCr substrate. This section present the characterization of these catalyst. XRD patterns of MnO_2-Co_3O_4-CeO_2 deposited on metallic substrates were shown on fig. 3.43 and 3.44. The high amorphous nature of MnO_2-Co_3O_4-CeO_2 active phase again presented here. It proves that MnO_2-Co_3O_4-CeO_2 was deposited successfully on the FeCr substrates.

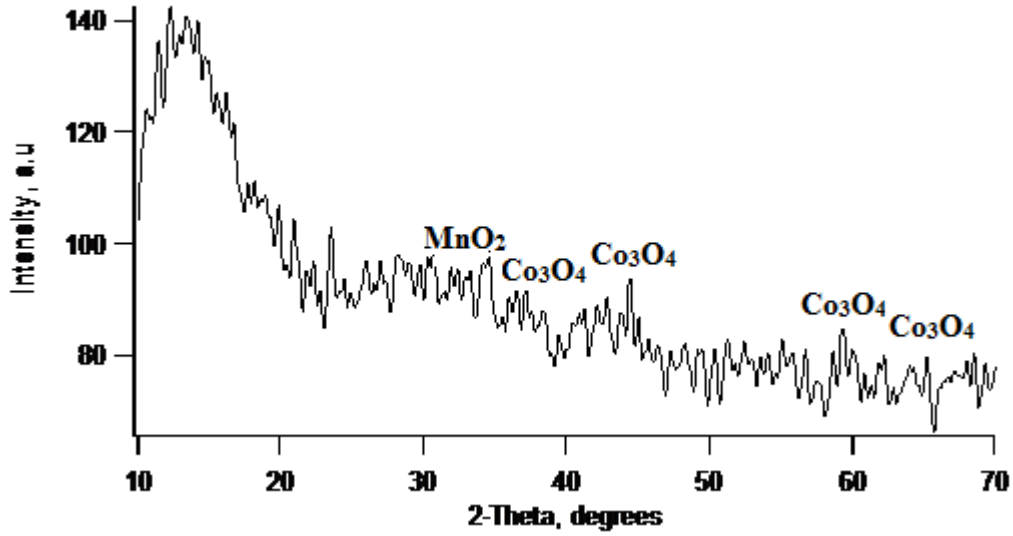

Fig.3.43 : XRD pattern of MnO_2-Co_3O_4-CeO_2 /$AlCe_{0.2}Zr_{0.05}O_2$/FeCr alloy (Ca.10)

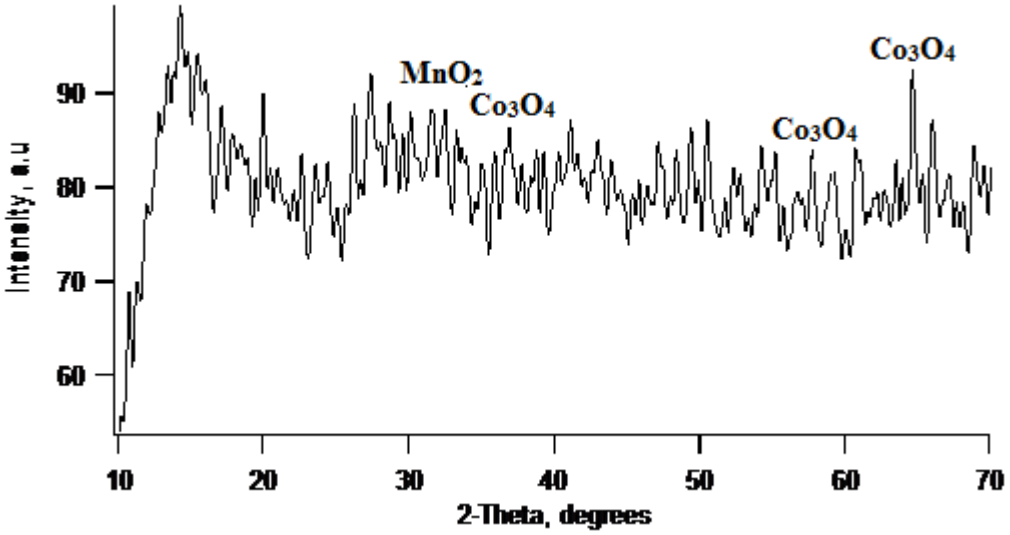

Fig.3.44 : XRD pattern of MnO_2-Co_3O_4-CeO_2 / FeCr alloy (Ca.8)

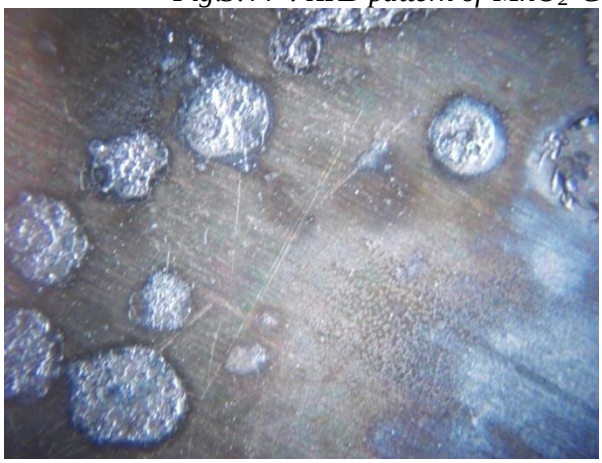

MnO_2-Co_3O_4-CeO_2 / FeCr alloy (Ca.8)

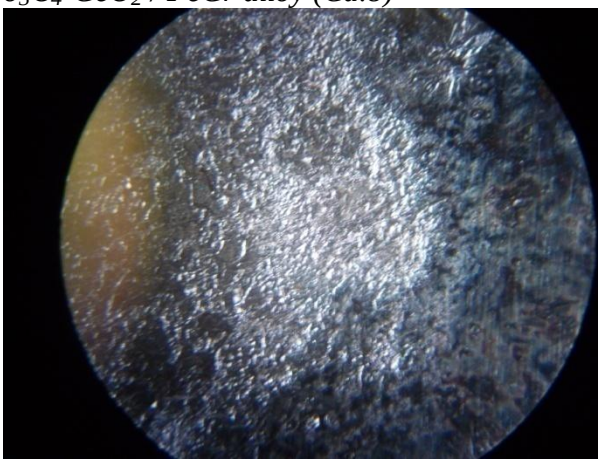

MnO_2-Co_3O_4-CeO_2 / γ-Al_2O_3 /FeCr alloy (Ca.9)

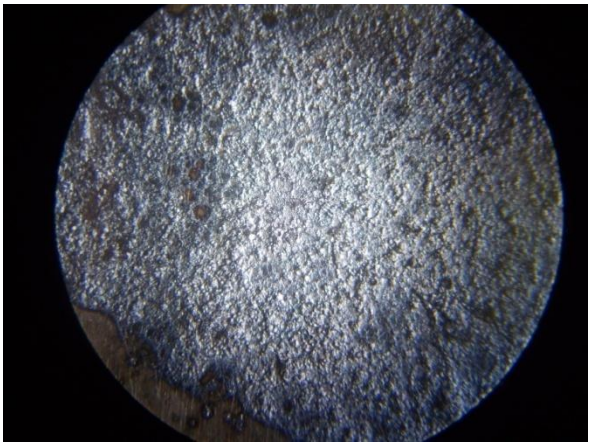

MnO_2-Co_3O_4-CeO_2 /$AlCe_{0.2}Zr_{0.05}O_2$/FeCr alloy (Ca.10)

Fig.3.45: Images of MnO_2-Co_3O_4-CeO_2 deposited on FeCr substrates with and without support

Fig.3.45 present images of catalysts under microscope. This observation shows that the MnO_2-Co_3O_4-CeO_2 layer on the substrates is deposited stably on the substrates.

Figure 3.46 present the SEM images of active phase MnO_2 – Co_3O_4 – CeO_2 on FeCr substrate. The surface of mixed oxides on metal foil without support (Ca.8) was uniform and smooth on the entire foil, at the first look at low magnification (fig. 3.46a). There were some small accumulations at some points on surface; they would be seen at high magnification to estimate the particles' size of mixed oxide. Nevertheless the catalysts with supports γ-Al_2O_3 and $AlCe_{0.2}Zr_{0.05}O_2$ (Ca.9 and Ca.10) had the porous layer of active phase (fig.3.46 c and e). In addition, there was cluster with the shape of bar with many sizes. No observation of different morphology was captured, that means the active phase was covered completely on support/ FeCr substrate. At high magnification (50 000 times), SEM images of catalyst present the layer of mixed oxides having even particles distribution on the whole surface of substrate in both cases of with and without supports. But the particles' size of mixed oxides in the catalyst having support was smaller (30 nm) than the one without support (60 nm). Thus, the use of support help for dispersion the active phase, inhibition the agglomeration when coating.

Ca. 8

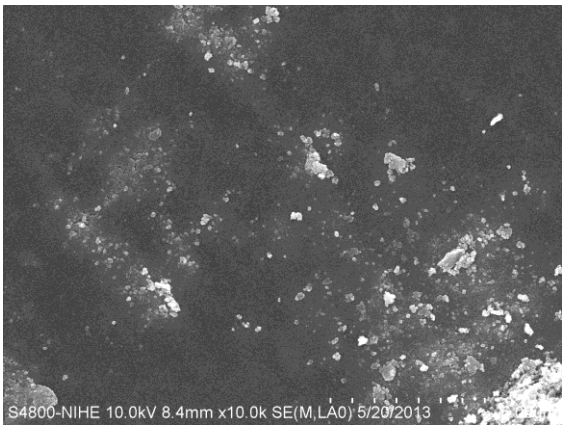

a – Magnigication of 10 000 times

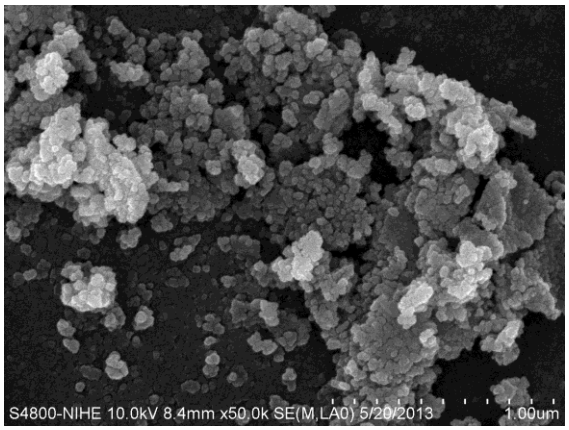

b - Magnigication of 50 000 times

Ca. 9

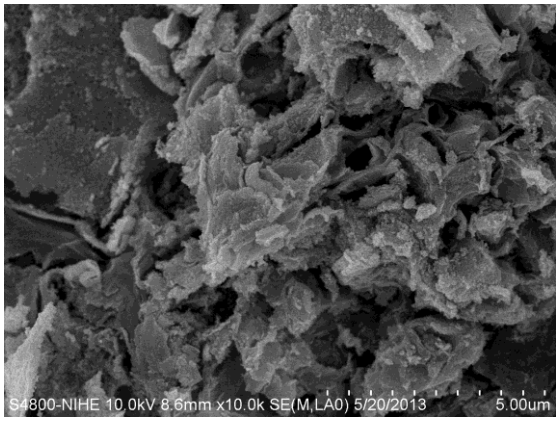

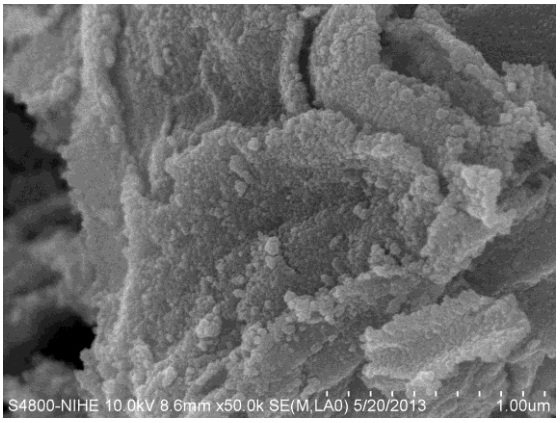

c - Magnigication of 10 000 times d - Magnigication of 50 000 times

Ca. 10

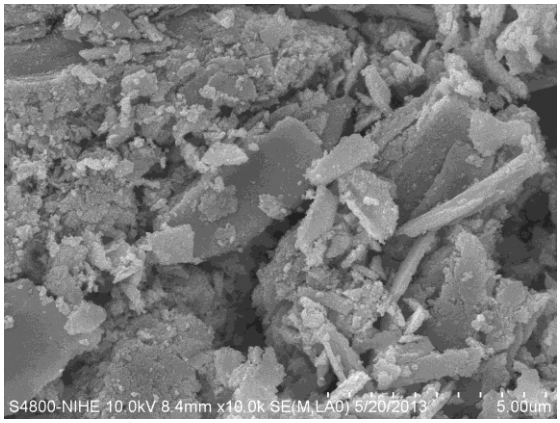

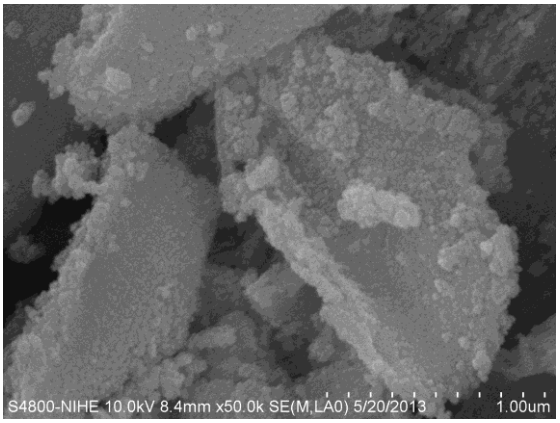

e - Magnigication of 10 000 times f - Magnigication of 50 000 times

Fig 3.46: SEM images of MnO_2-Co_3O_4-CeO_2 / FeCr alloy (Ca.8), MnO_2-Co_3O_4-CeO_2 / γ-Al_2O_3 /FeCr alloy (Ca.9), and MnO_2-Co_3O_4-CeO_2 /$AlCe_{0.2}Zr_{0.05}O_2$/FeCr alloy (Ca.10)

3.6 Catalytic activities of the complete catalysts

3.6.1 MnO_2 – NiO – Co_3O_4 /$Ce_{0.2}Zr_{0.8}O_2$/ cordierite

Catalytic activity of MnO_2 – NiO – Co_3O_4/ $Ce_{0.2}Zr_{0.8}O_2$/cordierite was performed under the following conditions of reactions: 0.42 g catalyst was used with a total gas flow of 184.7 ml/min at a pressure of 1 atm. The volume composition of the gas flow was 2.6% CO, 7.7% O_2, 1.5% C_3H_6, 1.9%NO and the reaction temperatures range from 150^0C to 550^0C.

The ability to treat toxic components in exhaust gases: NO, CO, C_3H_6 of the MnO_2 – NiO – Co_3O_4 /cordierite (Ca.2) and MnO_2 – NiO – Co_3O_4/ $Ce_{0.2}Zr_{0.8}O_2$/cordierite (Ca.3) catalysts are demonstrated in Fig. 3.47. It is clear that bare cordierite exhibited almost no activity to treat NO, CO and C_3H_6. At high temperature (500-550^{o}C), cordierite exhibited a small conversion of NO (10%) and a conversion of C_3H_6 up to 60%. However, C_3H_6 was converted to a large amount of CO, leading to the increase of CO concentration in the gas (conversion of CO became minus). When MnO_2 – NiO – Co_3O_4 was deposited on cordierite, the catalytic activity increase significantly. The Ca. 2 catalyst was able to convert 100% CO from low temperature (200^{o}C), 80-100% C_3H_6 at temperature from 400^{o}C, 40% NO from 450^{o}C. The sample including MnO_2 – NiO – Co_3O_4 active phase on $Ce_{0.2}Zr_{0.8}O_2$ support on cordierite – Ca. 3 –exhibited even higher activity since a conversion of 40% NO was reached from lower temperature (350^{o}C) and 80% conversion

of C_3H_6 was obtained from as low temperature as 250°C. Thus, the presence of $Ce_{0.2}Zr_{0.8}O_2$ support, indeed, improved catalytic activity of the catalytst although the $Ce_{0.2}Zr_{0.8}O_2$ support (DD-CZ), itself, didn't exhibit better activity than bare cordierite except for the activity for CO treatment (Fig. 3.48). The higher activity of the catalyst with $Ce_{0.2}Zr_{0.8}O_2$ support may be assigned for the high oxygen storage capacity of $Ce_{0.2}Zr_{0.8}O_2$ as known from literature [77], which may help to provide rapidly the used oxygen for the oxidation reaction. Here, the role of surface area may not be significantly influenced since both catalysts exhibited rather equal surface area (surface area of Ca. 2 and Ca. 3 catalysts are 29 m^2/g and 23 m^2/g, respectively).

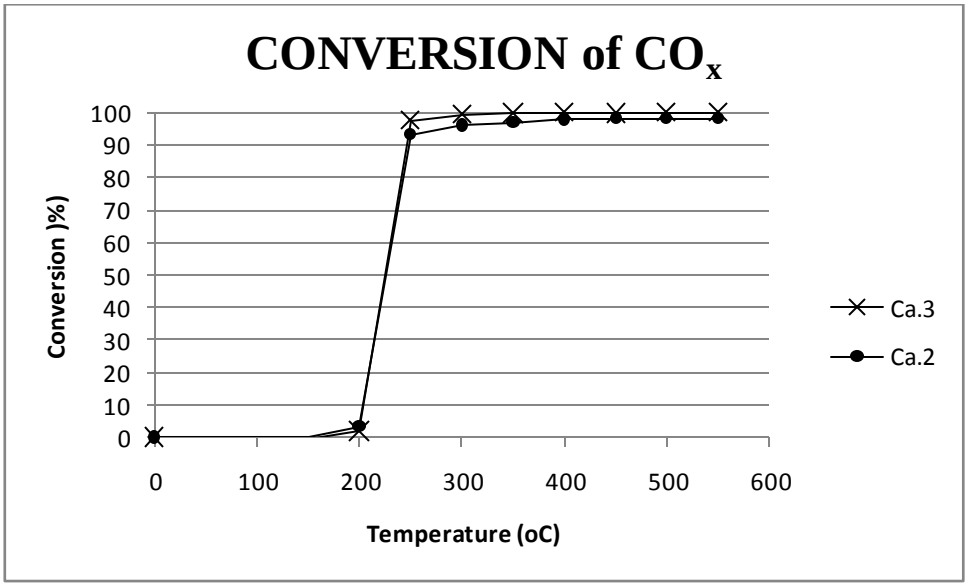

a)

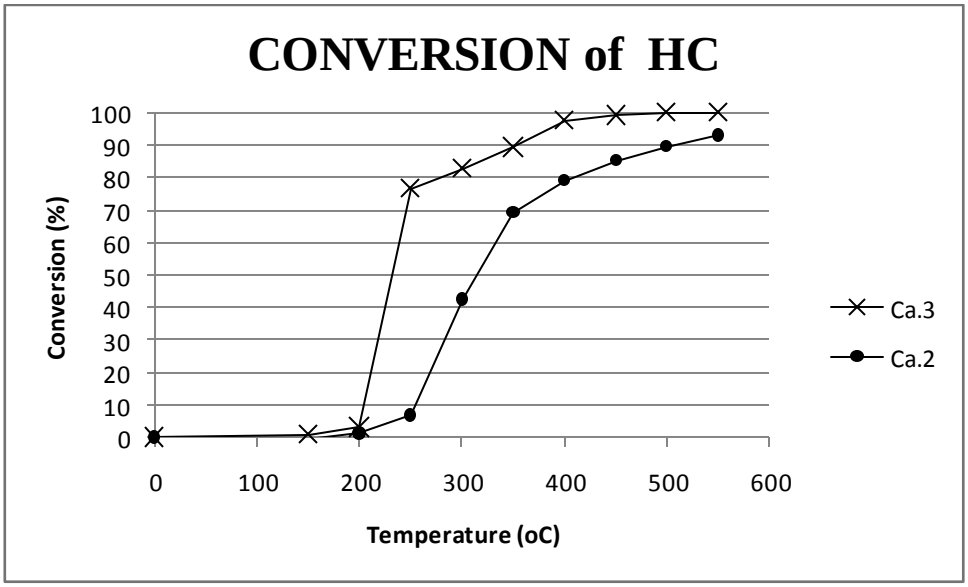

b)

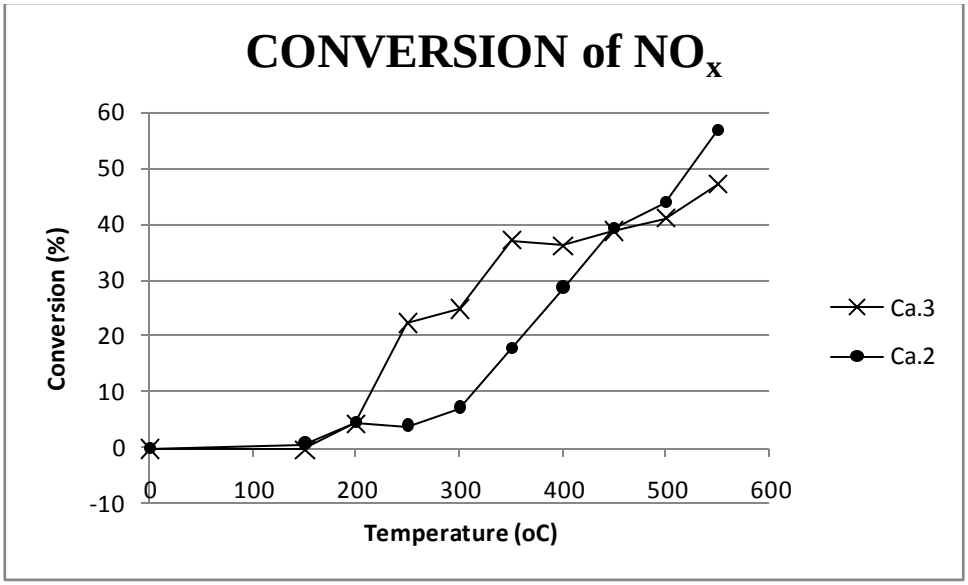

c)

Fig. 3.47. Catalytic activities for the treatment of CO (a), C_3H_6 (b), NO (c) of MnO_2 – NiO – Co_3O_4/cordierite (Ca. 2), MnO_2 – NiO – Co_3O_4/ $Ce_{0.2}Zr_{0.8}O_2$/cordierite (Ca. 3)

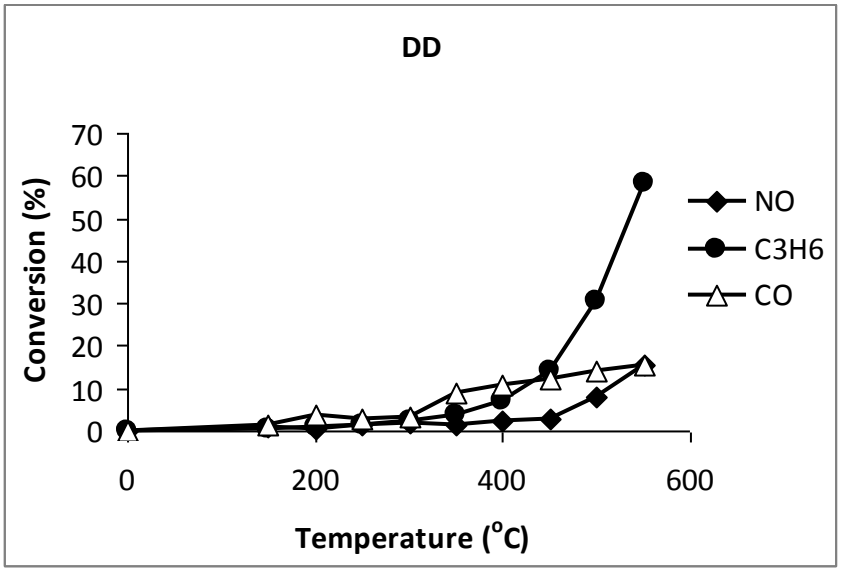

Fig. 3.48. Catalytic activity of $Ce_{0.2}Zr_{0.8}O_2$/cordierite (DD)

3.6.2 MnO_2-Co_3O_4-CeO_2 /supports/ cordierite

Catalytic activity of MnO_2-Co_3O_4-CeO_2 / supports /cordierite was performed under the following conditions of reactions: 0.42 g catalyst pellets (with the weight of active phase as 0.02g) was used with a total gas flow of 184.7 ml/min at a pressure of 1 atm. The volume composition of the gas flow was 4,34 % CO, 7.7% O_2, 1.14 % C_3H_6, 0.59%NO and the rest is N_2, the reaction temperatures range from 150^0C to 550^0C

Figure 3.49 demonstrated the catalytic activities of catalyst which had the same active phase, MnO_2-Co_3O_4-CeO_2 on different supports-cordierite, in the reaction of C_3H_6 and CO (with the presence of NO). In the C_3H_6 reaction, the catalyst having the $AlCe_{0.2}Zr_{0.05}O_2$ support (Ca.7) converted 40 % of propylene at 200^oC, while the others mostly haven't convert any propylene until 250^oC. Most of the catalysts present their good activities at 250^oC and treat about 80 % of C_3H_6, and then increased gradually to nearly 100% when

temperature reached 500°C. Although the catalyst having the support $Ce_{0.2}Zr_{0.8}O_2$ (Ca.6) started to catalyze for the reaction at highest temperature (300°C), however this one could convert 100 % of C_3H_6 when the temperature reached to 500°C. It may because $Ce_{0.2}Zr_{0.8}O_2$ only exhibits high oxygen storage capacity at high temperature.

In the CO oxidation, all the catalyst demonstrated their performance at 250°C. While the catalyst with $AlCe_{0.2}Zr_{0.05}O_2$ support (Ca.7) had the lowest conversion 80%, the catalyst with $Ce_{0.2}Zr_{0.8}O_2$ support (Ca.6) had the highest conversion as 97%. Afterward, the catalyst Ca.6 still remained it best catalytic activities, but the catalyst without support could not increase its performance, and only treated 90% of CO at 500°C. As the $Ce_{0.2}Zr_{0.8}O_2$ support is oxygen storage material, the catalyst contained this material was able to get the best conversion of both CO and C_3H_6, but it also began to take part in the reaction at the highest temperature compared with the others because $Ce_{0.2}Zr_{0.8}O_2$ support is Zr-rich solid solution, therefore, it cannot have as many oxygen vacancies as material in the Ce-rich region. The $AlCe_{0.2}Zr_{0.05}O_2$ support performed its advantage in treatment of C_3H_6 at the lowest temperature (200°C), but still had lower activities than catalyst having $Ce_{0.2}Zr_{0.8}O_2$ support. The catalytic activity of catalyst with γ-Al_2O_3 support was lower than the others.

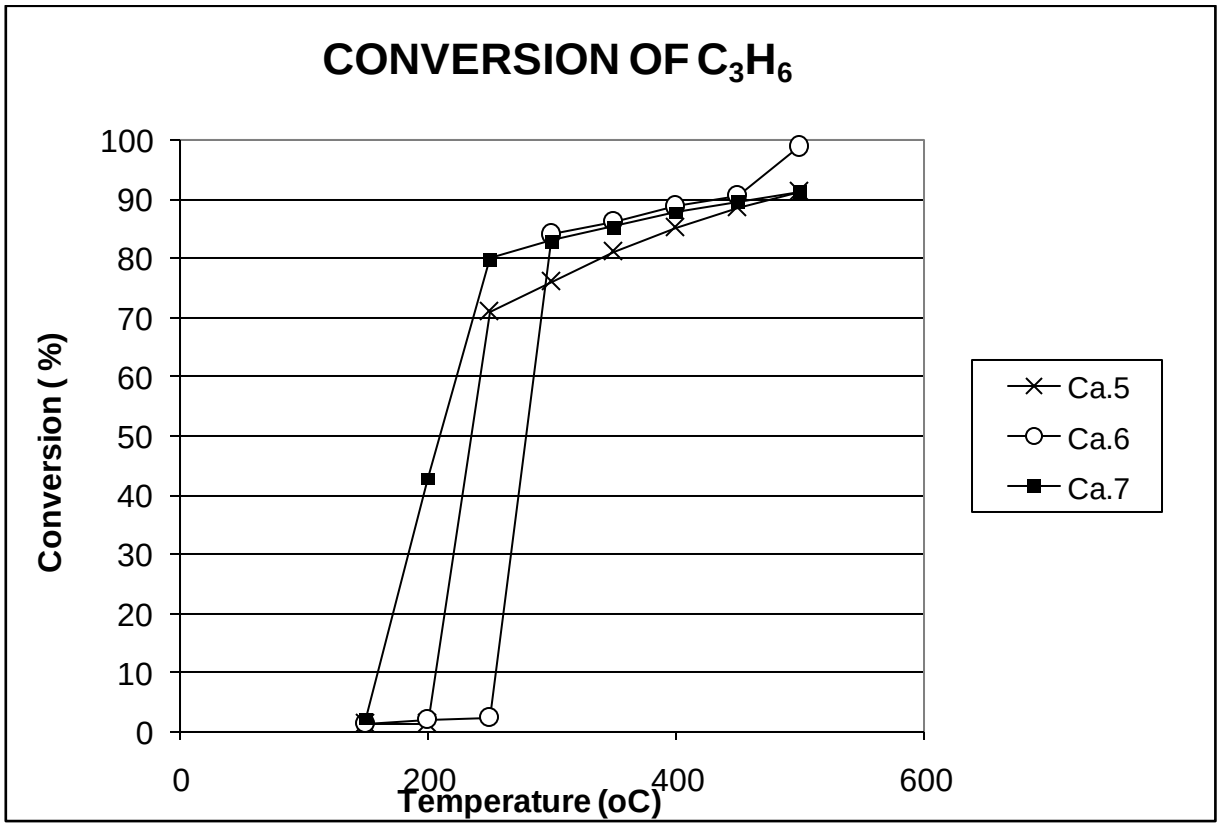

a,

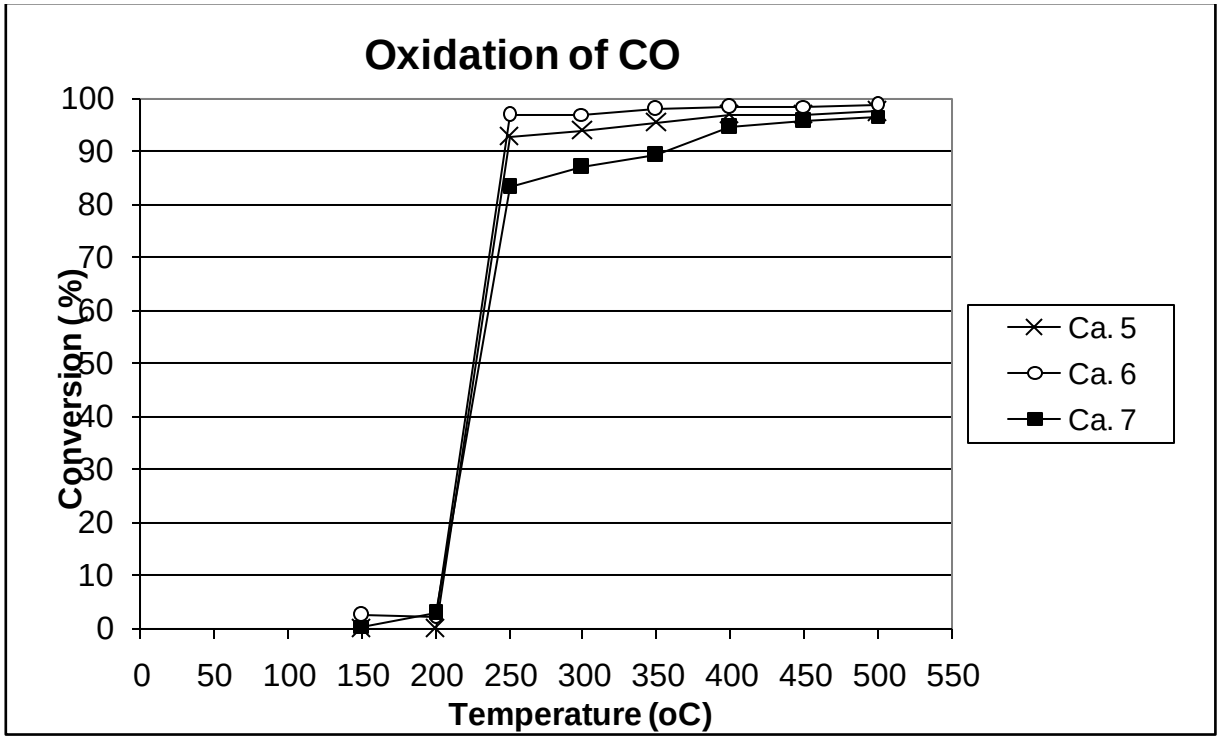

b,

Fig. 3.49: Catalytic activities for the treatment of (a) C_3H_6, (b) CO of $MnO_2 – Co_3O_4$-CeO_2/ γ-Al_2O_3 /cordierite (Ca.5), $MnO_2 – Co_3O_4$-CeO_2/ $Ce_{0.2}Zr_{0.8}O_2$/ cordierite (Ca.6), MnO_2–Co_3O_4-CeO_2/ $AlCe_{0.2}Zr_{0.05}O_2$/ cordierite (Ca.7)

In conclusion, the complete catalysts with active phase as MnO_2–Co_3O_4-CeO_2 over support/substrates present its good performance in reaction of CO and C_3H_6. All the catalyst started to catalyze at 250^{o}C and treated 90% of CO and C_3H_6 at 500^{o}C. Even though there were differences in catalytic activities of all catalyst with dissimilar supports and substrates, but the differences is negligible.

Amongst two investigated family of catalysts, the $MnO_2 – Co_3O_4$-NiO treated C_3H_6 completely at higher temperature than $MnO_2 – Co_3O_4$-CeO_2. In the CO oxidation, both actice phases exhibited same activity.

3.6.3 MnO_2-Co_3O_4-CeO_2 /support/ FeCr alloys

Catalytic activity of MnO_2-Co_3O_4-CeO_2 / supports /FeCr substrate was performed under the following conditions of reactions: 0.42 g catalyst pellets (with the weight of active phase as 0.02g) was used with a total gas flow of 184.7 ml/min at a pressure of 1 atm. The volume composition of the gas flow was 4,34 % CO, 7.7% O_2, 1.14 % C_3H_6, 0.59%NO and the rest is N2, the reaction temperatures range from 150^{0}C to 550^{0}C.

The catalytic activity of catalyst which the substrates were metallic substrates (Ca.9, Ca.10) was shown on figure 3.50. All catalyst began to take part in the reactions at 350^{o}C, just a few percentage of C_3H_6 and CO were converted. The catalysts exhibited conversion as 6 and 9 % for MnO_2-Co_3O_4-CeO_2/Al_2O_3/ FeCr foil (Ca.9) and MnO_2-Co_3O_4-CeO_2/Al-Ce-Zr/ FeCr foil (Ca.10), respectively. When the reaction temperature was 400^{o}C, the conversions increased significantly. At 500^{o}C, the maximum conversion were reached at nearly 80 % of C_3H_6 and 95 % of CO treated. Thus, the behavior of the catalyst deposited on different support was similar. Compared with MnO_2-Co_3O_4-CeO_2 /support/

cordierite catalysts, the activity of catalysts based on metal substrates occurred at much lower temperature, because of small content of active phase in the samples.

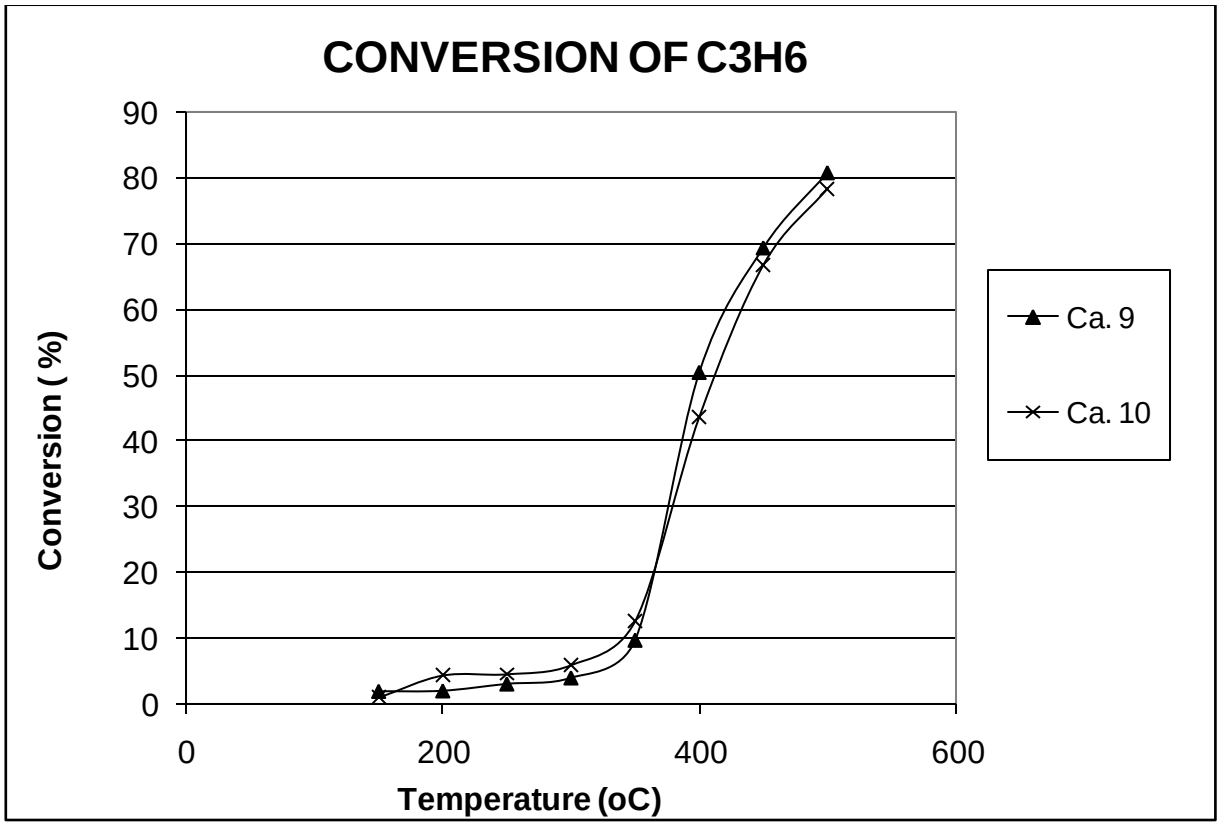

a,

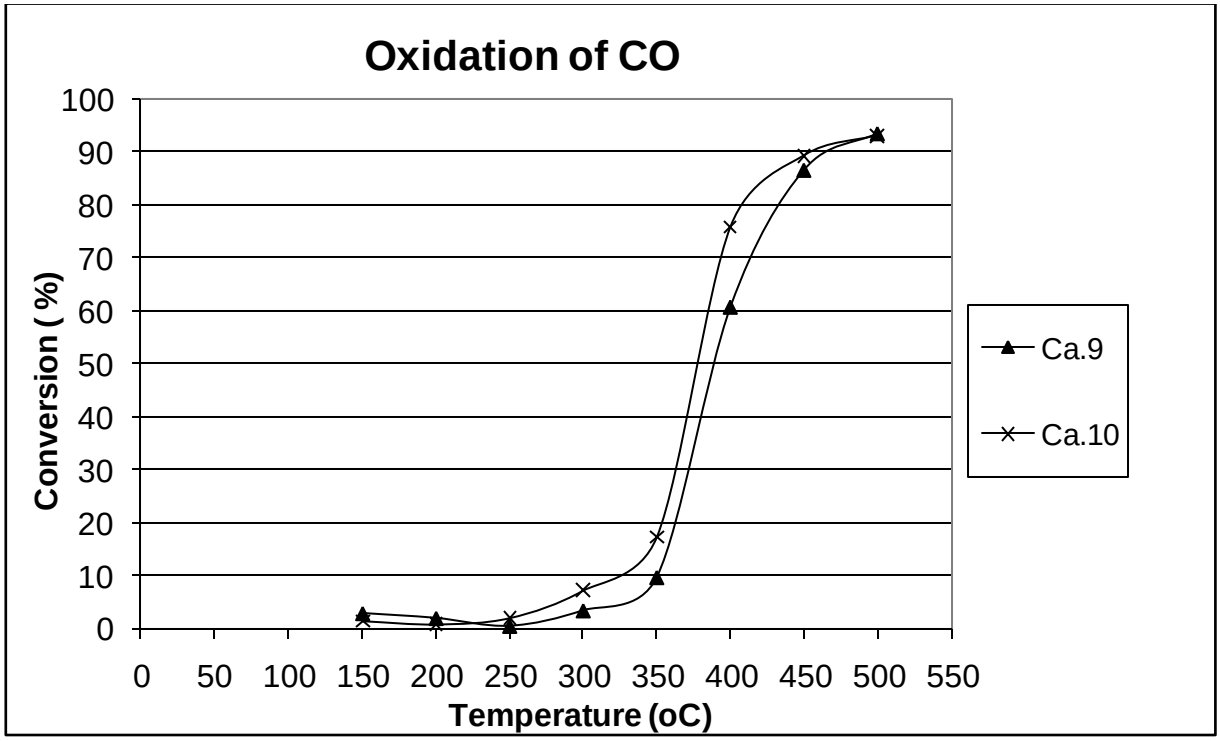

b,

Fig.3.50: Catalytic activities for the treatment of C_3H_6 (a),CO (b) of MnO_2 – Co_3O_4-CeO_2/Al_2O_3/ FeCr foil (Ca. 9), MnO_2 – Co_3O_4-CeO_2/Al-Ce-Zr-O/ FeCr foil

3.7 Commercial catalyst

In order to compare the prepared catalyst with the commercial one, a commercial catalyst (CAT-920, CatCo, USA) was also investigated. This commercial catalyst was made from noble metals on ceramic substrates. XRD pattern of the ground sample is presented in Fig. 3.51, which shows that only cordierite phase was detected. The fact that the composition of washcoat layer and catalyst phase was not detected indicates that the contents of washcoat and catalyst materials were minor compare to the substrate. The commercial cordierite substrate is almost pure cordierite phase. The commercial catalyst possesses a surface area of 33.28 m^2/g, which is not significantly different from the catalyst prepared in this work.

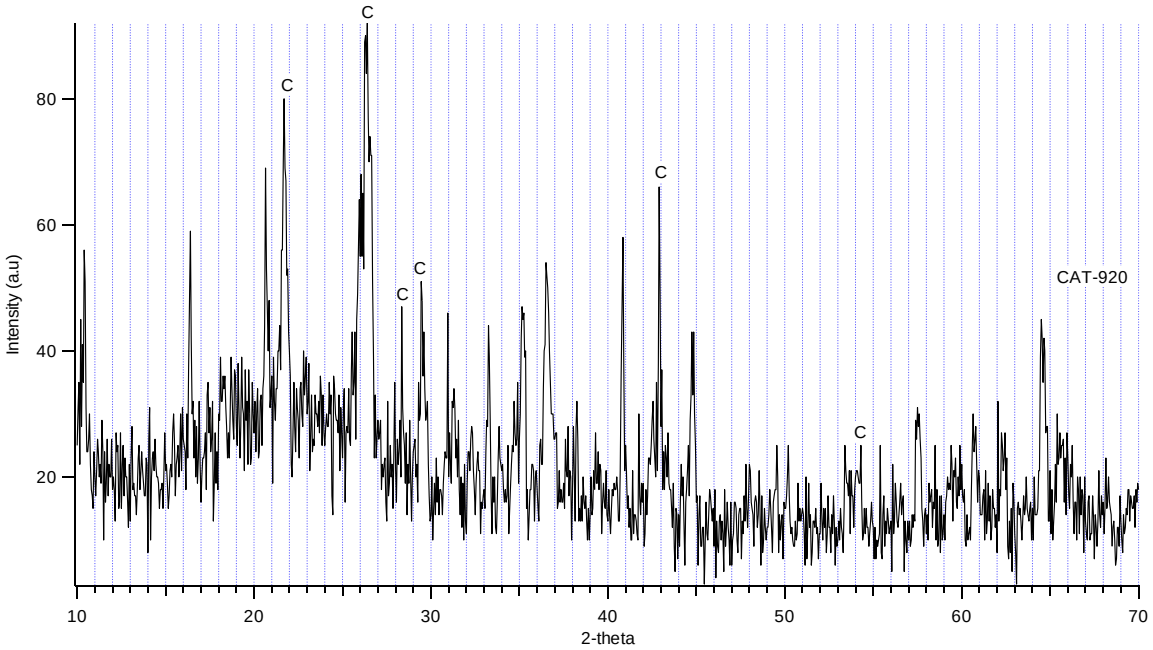

Fig. 3.51: XRD pattern of ground CAT-920, CatCo, USA (C – cordierite)

The SEM image of the commercial sample in Fig. 3.52a, b shows that in the first sight, the washcoat layer was deposited rather thick and homogeneous on the cordierite substrate (position 1). However, at higher magnification (Fig. 3.52c), it could be seen that the washcoat layer contains two different morphologies. Atomic compositions determined by EDX (Table 3.17) of these two different morphologies are, however, not significantly different. The composition of the catalyst reveals that it contains many elements. The composition of noble active phase (Pt, Pd, Rh) is rather high (about 2%). Ce, Zr and Al appeared with reasonable composition, which may be the composition of the support for the noble active phase. Thus, the support might be Al-Ce-Zr mixed oxide. Other elements (Ni, Co, Ni, Mn, Cu) existed with low content, which may be assigned for addition components of the active phase.

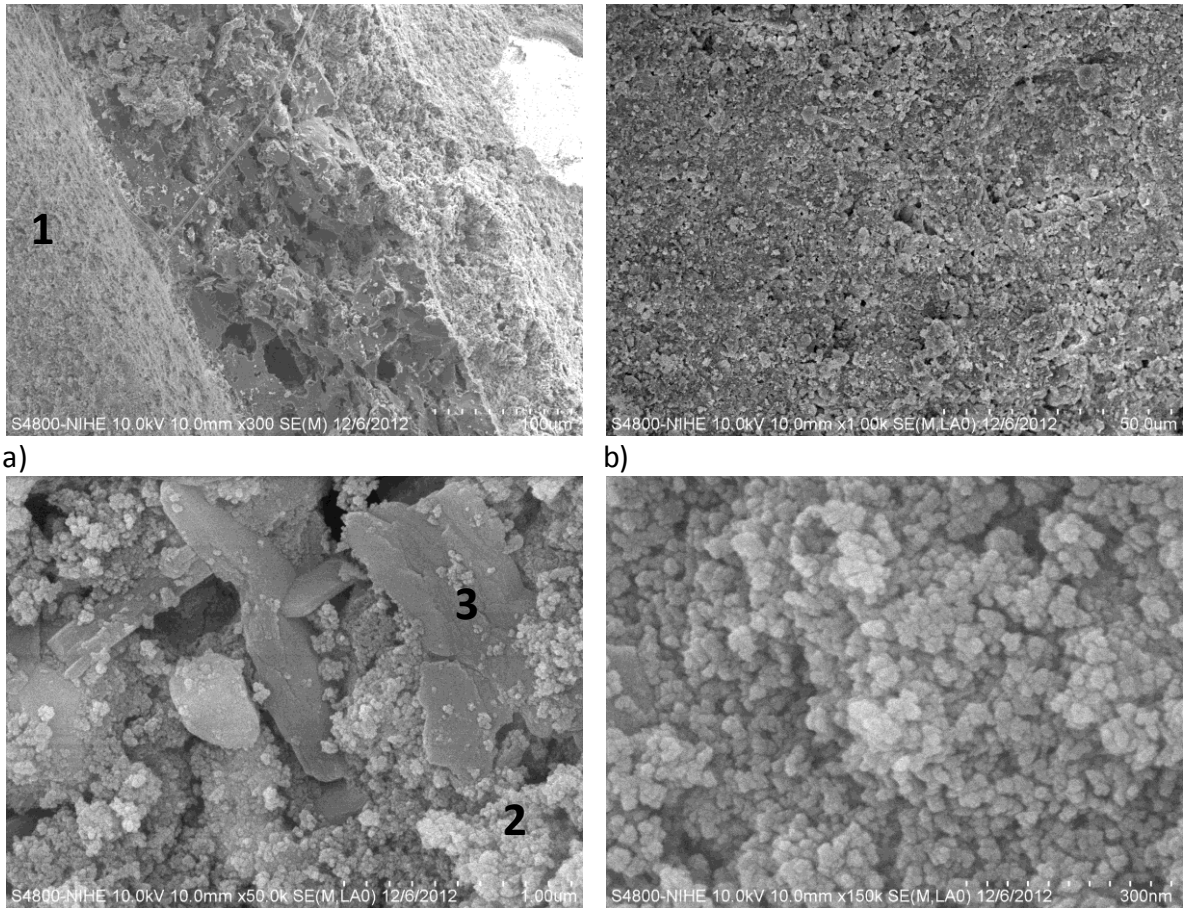

Fig. 3.52: SEM images of the hole – inside area of a CAT-920, CatCo, USA: a) the hole – inside area, b) enlarged photo of part 1 in a, c) higher manification of b, d) enlarged photo of part 2 in c.

Table 3.17. Atomic composition (%) of the commercial catalyst CAT-920 based on metal substrate

Atom	Position 1	Position 2	Position 3
O K	78.27	77.07	73.11
Mg K	0.08	0	0
Al K	8.70	12.37	13.10
Si K	0.18	0.21	0.46
Co K	0	0.06	0
Mn K	0.05	0	0.24
Ni K	0.73	0.28	0.18
Cu K	0.20	0.02	0.06
Br L	2.01	0	0
Zr L	4.48	3.67	4.41
Rh L	0.03	0	0
Pd L	0.62	0.61	0.83
Ce L	3.14	3.67	4.64
Pt M	1.51	2.05	2.97

The catalytic of commercial nobles catalyst on cordierite was shown on fig.3.53. The catalysts treated CO and C_3H_6 completely at 350^{o}C with the cordierite substrate. That is proving the excellence of noble metals for the treatment of exhausted gases. Compared with MnO_2-Co_3O_4-CeO_2 / supports/ cordierite prepared in this work, the commercial catalyst

could convert more completely HC and CO, however, prepared MnO_2-Co_3O_4-CeO_2 catalysts are able to treat CO, HC at lower temperature. This is the advantage of these catalysts.

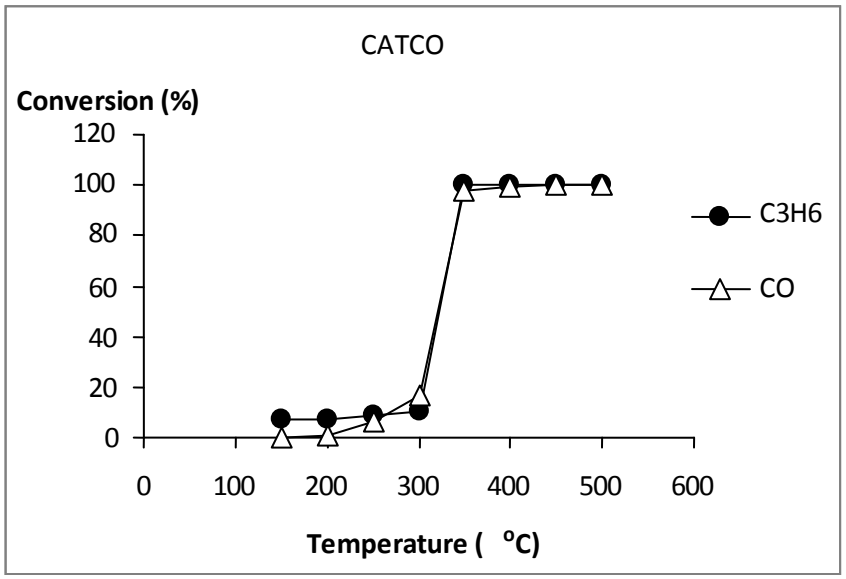

Fig. 5.53: Catalytic activity of commercial noble catalyst on cordierite (CATCO)

3.8 Catalytic activity of MnO_2-Co_3O_4-CeO_2/ cordierite monolith installed in motorbike

For the first approach of application of catalytic complex, the catalyst MnO_2-Co_3O_4-CeO_2/ cordierite monolith was prepared and installed into the exhaust pipe of a real motorbike.

The motorbike Vespa LX used Electro Fuel Injection (EFI) with the advantage of providing the suitable oxygen for complete combustion of fuel. The content of emission gases in two cases with and without catalyst was listed in table 3.18.

Table 3.18: The content of emission gases with and without catalytic complex (Ca.11 -MnO_2-Co_3O_4-CeO_2/$AlCe_{0.2}Zr_{0.05}O_2$/ cordierite monolith)

Time on stream (min)	CO(%)			CO_2(%)			HC(ppm)			O_2(%)		
	A	**B**	C	A	**B**	C	A	**B**	C	A	**B**	C
First start	3,83	0,59	0.5	5,6	15.2	15.2	164	55	45	10,74	0,65	0.63
t= 5	3,19	0,56	0.54	5,6	15	14.9	148	48	40	11,16	0,66	0.68
t= 10	2,55	0,55	0.52	6,2	15,1	14.7	97	44	38	10,16	0,67	0.69
t= 15	2,38	0,55	0.5	7,4	15	14.9	88	47	37	10,14	0,22	0.67
t= 20	2,12	0,54	0.52	7,8	15	15	79	48	37	9,76	0,22	0.62
t= 25	2,12	0,52	0.51	8,3	15	14.7	64	51	30	9,74	0,22	0.65
t= 30	2,12	0,53	0.52	8,4	15	14.9	61	45	34	9,74	0,22	0.62
t= 35	2,12	0,53	0.54	8,5	15.3	14.9	55	45	36	9,72	0,22	0.62
t= 40	2,12	0.53	0.52	8,5	15,2	14.9	55	45	34	9,71	0,22	0.63

A: without catalyt
B: with catalyst for the first use
C: with catalyst after running 110 km on the road

Table 3.18 shows that in the case of without catalyst, the content of CO, HC and O_2 was high, but the content of CO_2 was low in the initial period of engine, especially in the cold start. In the first beginning of operation, the low and unstable temperature of the engine cause the uncomplete combustion of fuel, leading the high content of polluted gases, the concentration of CO and HC was 3.8 % (according to the volume), 164 ppm, respectively . After 20 minute, the system operation and engine's reactant gases were stable resulting in the big decrease of polluted gases, the concentration of CO and HC reduced 44%, 66%, respectively. However, after installing the catalytic complex to the exhaust tube, the gases CO and HC reduced remarkably. The decrease of CO and HC was 87 % and 73 %, respectively. The concentration of CO and HC were under the standard of of emission published by Ministry of Transport in 2005 and met the Euro 3 standard. Therefore, it is evident to notice the great activity of catalytic complex at low temperature. In order to access the stability of the catalytic complex, the exhausted gases of motorbike installed the catalyst (Ca.11) was measured after operation for 110 km distance (table 3.18). The results show that the content of HC and CO was similar as the intinial period of installing the catalyst. Moreover, during the operation, there wasn't noise, or any effect to the operation system, indication the good thermal stability and high mechanical strength of the catalyst.

Table 3.19 : Emission of motorbike Vespa installed the commercial catalysts from Vespa based on metal substrates

Time (min)	CO(%)	CO_2(%)	HC(ppm)	O_2(%)
t=0	0,06	15.2	20	0,46
t= 5	0,02	12,8	2	0,24
t= 10	0,02	13,1	3	0,22
t = 15	0,02	15,4	4	0,22
t = 20	0,02	15,3	4	0,22
t =25	0,02	15,2	4	0,22
t = 30	0,02	15,2	4	0,22
t =35	0,02	15.3	4	0,22
t =40	0.02	15,2	4	0,22

Table 3.19 shows the results of treating CO, HC by commercial catalyst produced from Vespa. This catalyst had the rare elements (Pt, Rh) covering over metallic substrate. The catalytic activity of this Vespa catalyst treats much better than transition metal oxides over ceramic honeycomb. The concentration of CO and HC was reduced to 0.02 % and 4

ppm, respectively. These results were agreed with the reaction performance using micro-reactor setup.

4. CONCLUSION

1. The cordierite substrates were prepared successfully from the popular natural sources such as kaolin, industrial MgO and industrial Al_2O_3 by conventional sintering method. The products had high content of cordierite, and high mechanical strength, but very low BET surface area. The addition of burnable additives (activated carbon, cellulose and dolomite) to cordierite precursors in order to improve the porosity of cordierite could not result in higher surface area of product. Meanwhile, the treatment of cordierite surface by strong acid as HCl for a suitable time increase significantly surface area of cordierite (from lower than $1m^2/g$ to about 20 m^2/g. When a suitable amount of dolomite (16.27 wt.%) was added to cordierite precursors, cordierite content was not influenced significantly. Moreover, when the sample was treated with HCl, surface area increased to 138.7 m^2/g for a better impregnation of support and active phase while the mechanical strength was still enough to use in motorbike

2. Original FeCr substrates exhibited high wetness contact angle, leading to worse deposition of support and active phase. The treatment of FeCr substrate's surface by thermal and chemical treatments have been performed which shows that the first treatment of the surface by calcinations at 800^{o}C, followed by chemical treatment decrease more significant wetness contact angle than the reverse treatment procedure. The surface treatment procedure was optimized as thermal treatment at 800^{o}C for 3 hour, afterward chemical etching in solution NaOH 10 wt.% for 10 min. The obtained wetness contact angle was 6^o, which meet the requirement for the wetting of support and active phase precursor solution afterward.

3. The support materials as γ-Al_2O_3, $Ce_{0.2}Zr_{0.8}O_2$ and $AlCe_{0.2}Zr_{0.05}O_2$ were prepared successfully. The γ-Al_2O_3 was prepared from boehmite, and possessed surface area of 207 m^2/g. The $Ce_{0.2}Zr_{0.8}O_2$ sample possessed highest surface area and most stable is $Ce_{0.2}Zr_{0.8}O_2$ synthesized by hydrothermal synthesis at 160^{o}C using CTAB template. The sample had surface area of 90 m^2/g after calcined at 550^{o}C while its precursor (before calcinations) had surface area of 85.57 m^2/g. The $AlCe_{0.2}Zr_{0.05}O_2$ sample possessed highest surface area is $AlCe_{0.2}Zr_{0.05}O_2$ synthesized by hydrothermal synthesis at 160^{o}C using precipitant NH_4HCO_3, and SDS template. The sample had surface area of 397.3 m^2/g.

4. The supports was deposited successfully on the substrates by suspension, hybrid deposition, direct combustion, secondary growth on seeding, the double depositions with the combination of wet impregnation and suspension. Among these methods, the double deposition produced the catalyst with the most homogeneous surface and stable adhesion of the support layer on the substrate. Both the suspension and direct combustion were produced the thick layer with high content of support material, but the layer was easy to detach from the substrate. The hydrid deposition and secondary growth on seeding produced a thin layer with low content of support material. The double depositions method was chosen to prepared complete catalyst.

5. The catalysts which MnO_2-Co_3O_4-NiO and MnO_2-Co_3O_4-CeO_2 was loaded on the support-substrate system by wet impregnation method and were characterized by XRD, SEM, EDX, XPS and BET. The results show that the active phase layer covered

completely on the surface of support-substrate. With the presence of support, the active phase was dispersed finer than that of non support sample, with nano particles.

6. The complete catalyst MnO_2-NiO-Co_3O_4 / $Ce_{0.2}Zr_{0.8}O_2$ / cordierite was able to treat 100% CO at 250^{o}C, 80-100% C_3H_6 at temperatures from 400^{o}C onward. Whereas the catalysts MnO_2-Co_3O_4-CeO_2 / γ-Al_2O_3/cordierite and MnO_2-Co_3O_4-CeO_2 / $AlCe_{0.2}Zr_{0.05}O_2$ /cordierite treated 80% of CO and C_3H_6 at 250^{o}C. The MnO_2-Co_3O_4-CeO_2 / $AlCe_{0.2}Zr_{0.05}O_2$ / FeCr substrates had lower catalytic activities than that on cordierite due to low content of active phase. These mixed oxides catalysts did not treat CO and C_3H_6 completely as the commercial noble catalyst but was able to convert high amount of CO and C_3H_6 at lower temperature than the noble catalyst.

7. The installation of MnO_2-Co_3O_4-CeO_2 / $AlCe_{0.2}Zr_{0.05}O_2$ / honeycomb cordierite in the exhaust tube of a motorbike Vespa LX shows that the concentration of CO and HC decreased significantly compared to the case without catalyst. The concentration of CO and HC emitted from that motorbike after the installation of MnO_2-Co_3O_4-CeO_2 catalyst meet Euro 3 standard. The motorbike running for 110 km on the road still exhibited the same behaviot, proving the positive possibility to apply non noble catalyst MnO_2-Co_3O_4-CeO_2 on a motorbike using Electric Fuel Injection.

REFERENCES

1. Qingyu Zhang, Guojin Sun, Simai Fang, Weili Tian, Xiaoxiao Li, Huiyu Wang (2013), *Air pollutant emissions from vehicles in China under various energy scenarios*, Science of the Total Environment 450–451, pp. 250– 258.
2. "Control the emission from vehicles for environmental protection" – June 4th 2013 – Ministry of Transport.
   http://moitruong.mt.gov.vn/Default.aspx?tabid=2&catid=325&articleid=6300
3. 2010 National State of Environmental Report - Ministry of Natural Resource and Environment - 2010
   http://quantracmoitruong.gov.vn/VN/BAOCAO_Content/tabid/356/cat/176/nfriend/2418001/language/vi-VN/Default.aspx
4. https://en.wikipedia.org/wiki/European_emission_standards
5. http://transportpolicy.net/index.php?title=Vietnam:_Motorcycles:_Emissions
6. R. W. Boubel, D. L. Fox, D. B. Turner, A. C. Stern (1994) *Fundamental of air pollution*, third edition, Academic press, America, pp. 25-37.
7. Dieter Schwela, Olivier Zali and Philipp Schwela, *Motor Vehicle Air Pollution*, 1997, World Health Organization and ECOTOX.
8. Ronald M. Heck, Robert J. Farrauto. (2001), *Automobile exhaust catalysts*, Applied Catalysis A: General, 221 (1-2), pp. 443–457.
9. W. Walerczyk, M. Zawadzki (2011) *Structural and catalytic properties of Pt/ZnAl2O4 as catalyst for VOC total oxidation.* Catalysis Today 176, pp. 159– 162.
10. G. Neri , G. Rizzo , F. Corigliano, I. Arrigo, M. Caprı`, L. De Luca, V. Modafferi, A. Donato (2009) *A novel Pt/zeolite-based honeycomb catalyst for selective CO oxidation in a H_2-rich mixture*. Catalysis Today 147, pp. 210–S214.
11. Y. Hasegawa, K. Fukumoto, T. Ishima, H. Yamamoto, M. Sano, T. Miyake (2009) *Preparation of copper-containing mesoporous manganese oxides and their catalytic performance for CO oxidation*. Applied Catalysis B: Environmental, 89 (3-4), pp. 420–424.
12. H. Zou, S. Chen, Z. Liu, W. Lin (2011) *Selective CO oxidation over CuO–CeO_2 catalysts doped with transition metal oxides.* Powder Technology 207, pp. 238–244.
13. S. Lim, J. Bae, K. Kim (2009) *Study of activity and effectiveness factor of noble metal catalysts for water–gas shift reaction.* International journal of hydrogen energy 34 (2), pp. 870 – 876
14. L. M. Thang (1999) *Preparation of the catalyst for the total oxidation hydrocarbon applying for treatment of exhaust automobile gas*. Master thesis, Hanoi University of science and technology, pp. 1-26
15. I. Heo, J. W. Choung, P. S. Kim, I. Nam, Y. I. Song, C. B. In, G. K. Yeo (2009) *The alteration of the performance of field-aged Pd-based TWCs towards CO and C_3H_6 oxidation.* Applied Catalysis B: Environmental 92, pp.114–125.
16. C.A. Miller. (1995), *Air pollution-control technologies*, United States Environmental Protection Agency Research Triangle Park, North Carolina, Chapter 65, pp. 120-172

17. J. Xu, M. P. Harold, V. Balakotaiah (2011) *Modeling the effects of Pt loading on NO_x storage on $Pt/BaO/Al_2O_3$ catalysts.* Applied Catalysis B: Environmental 104, pp. 305–315
18. F.E. López-Suárez, M.J. Illán-Gómez, A. Bueno-López, James A. Anderson (2011) *NO_x storage and reduction on a $SrTiCuO_3$ perovskite catalyst studied by operando DRIFTS*. Applied Catalysis B: Environmental 104, pp. 261–267
19. J. Chen, J. Zhu, Y. Zhan, X. Lin, G. Cai, K. Wei, Q. Zheng (2009) *Characterization and catalytic performance of Cu/CeO_2 and Cu/MgO-CeO_2 catalysts for NO reduction by CO.* Applied Catalysis A: General 363, pp. 208–215
20. N. D. Khien. (1997), *Study on produce catalytic converters to treat automobile exhaust gases*. Ministry of Science Technology and Environment
21. J. Kašpar, P. Fornasiero, N. Hickey (2003) *Automotive catalytic converters: current status and some perspectives*. Catalysis Today 77 (4), pp. 419–449
22. P. KOČÍ, M. KUBÍČEK, M. MAREK (2004), *Multifuntional aspect of three-way catalyst. Effects of Complex Washcoat Composition*, Chemical Engineering Research and Design, 82(A2), pp. 284–292
23. Pedro Avila, Mario Montes, Eduardo E. Miró (2005), *Monolithic reactor for environment applications. A review on preparation technologies*, Chemical Engineering Journal 109, pp. 11–36
24. T. Alexander Nijhuis, Annemarie E. W. Beers, Theo Vergunst, Ingrid Hoek, Freek Kapteijn, Jacob A. Moulijn (2001), *Preparation of monolithic catalysts*, Catalysis reviews 43(4), pp. 345–380.
25. Barbara Kasprzyk-Hordern (2004), *Chemistry of alumina, reactions in aqueous solution and its application in water treatment*, Advances in Colloid and Interface Science 110, pp. 19–48.
26. G. COCITO and V. PATIERNO (1978), *Chemical – physical characterization of aluminas in the car exhaust gas treatment*, Materials Chemistry 3, pp.233 – 254.
27. Sudhanshu Sharma, M.S. Hegde, Ratindra Nath Das, Manish Pandey (2008), *Hydrocarbon oxidation and three-ways catalytic activity on a single step directly coated on cordierite monolith. $Ce_{0.98}Pd_{0.02}O_{2-\delta}$,* Applied Catalysis A: General 337, pp. 130–137
28. Sonia Letichevsky, Claudio A. Tellez, Roberto R. de Avillez (2005), *Obtaining CeO2–ZrO2 mixed oxides by coprecipitation, role of preparation conditions*, Applied Catalysis B: Environmental 58, pp.203–210
29. J. Kašpar, P. Fornasiero, M. Graziani (1999), *Use of CeO_2-based oxides in the three-way catalysis*, Catalysis Today 50 , pp. 285±298.
30. Masakuni Ozawa (1998), *Role of Ce-Zr mixed oxides as catalyst for car pollution. A short review*, Journal of Alloys and Compounds 275–277, pp. 886–890.
31. Eduardo L. Crepaldi (2003), *Controlled formation of highly ordered cubic and hexagonal mesoporous nanocrystalline Y-Zr and Ce-Zr thin films exhibiting high thermal stability*, Angew. Chem. Int . Ed.2003, 42 , No. 3.
32. J. Kearney, R.T.Baker (2011), *Redox and catalytic properties of Ce-Zr mixed oxides nanopowders for fuel cell applications*, Catalysis Today.

33. G. Ranga Rao (1996), *Reduction of NO over Partially Reduced Metal-Loaded CeO2-ZrO2 solid solution*, JOURNAL OF CATALYSIS 162, pp. 1–9
34. P. Fornasiero (1995), *Rh loaded CeO2-ZrO2 solid solution as high efficient oxygen exchange*, JOURNAL OF CATALYSIS 151, pp.168 – 177
35. Guo Jiaxiu, Shi Zhonghua, Wu Dongdong (2013), *Study of Pt-Rh over CeO2-ZrO2 -MxOy (M = Y, La)/Al2O3 three ways catalyst*, Applied Surface Science 273 , pp.527– 535
36. H. Chunming, Z. Ming, W. Hairong, C. Shanhu, G. Maochu, S. Zhonghua, C. Yaoqiang (2008) *Three-Way Catalyst Meeting Euro III Emission Standards for Motorcycles*. Chin J Catal 29(8), pp. 677–679
37. G. Jiaxiu, Y. Shuhua, G. Maochu, S. Mei, Z. Junbo, C. Yaoqiang (2007) *Influence of $Ce_{0.35}Zr_{0.55}Y_{0.10}$ solid solution performance Pt-Rh three-way catalyst*. Journal of Rare Earths, 25 (2), pp. 179-183
38. Zhenling Wei, Hongmei Li, Xiaoyu Zhang, Shenghui Yan, Zhen Lv (2008), *Preparation and property investigation of CeO2–ZrO2–Al2O3 oxygen-storage compounds*, Journal of Alloys and Compounds 455 , pp. 322–326.
39. Roberta Di Monte, Jan J. Kašpar (2005), *Heterogeneous environmental catalysis – a gentle art. CeO2–ZrO2 mixed oxides as a case history*, Catalysis Today 100 , pp. 27–35.
40. LI Hongmei, ZHU Qingchao, LI Yile (2010), *Effect of Ce-Zr ratio on properties of mixed CeO2 - ZrO2 - Al2O3 compound*, JOURNAL OF RARE EARTHS, Vol. 28, No. 1, pp. 79
41. Akira Morikawa, Tadashi Suzuki, Takaaki Kanazawa, Koichi Kikuta, Akihiko Suda, Hirofumi Shinjo (2008), *A new concept in high performance ceria-zirconia oxygen storage capacity material with Al2O3 as a diffusion barrier*, Applied Catalysis B: Environmental 78 , pp. 210–221.
42. ZHANG Qingwei, WEN Jing, SHEN Meiqing, WANG Jun (2008), *Effect of different mixing ways in palladium/ceria-zirconia/alumina preparation on partial oxidation of methane*, JOURNAL OF RARE EARTH S, Vol.26 , No.5 , pp .700.
43. CAI Li, ZHAO Ming, PI Zhan, GONG Maochu, CHEN Yaoqiang (2008), *Preparation of Ce-Zr-La-Al2O3 and supported singles Palladium 3-way Catalyst*, CHINESE JOURNAL OF CATALYSIS, 29(2), pp. 108–112.
44. Bo Zhao, Chunqing Yang, Qiuyan Wang, Guangfeng Li, Renxian Zhou (2010), *influence of thermal treatment on catalytic performance of Pd.Ce.Zr.Ox-Al2O3 TWCs*, Journal of Alloys and Compounds, Volume 494, Issues 1–2, Pages 340-346.
45. X. Zhang, E. Long, Y. Li, J. Guo, L. Zhang, M. Gong, M. Wang, Y. Chen (2009) *CeO_2-ZrO_2-La_2O_3-Al_2O_3 composite oxide and its supported palladium catalyst for the treatment of exhaust of natural gas engined vehicles*. Journal of Natural Gas Chemistry 17 (1), pp. 139–144
46. S.Y. Christou, S. Garcia-Rodriguez, J.L.G. Fierro, A.M. Efstathiou (2012) *Deactivation of $Pd/Ce_{0.5}Zr_{0.5}O_2$ model three-way catalyst by P, Ca and Zn deposition*. Applied Catalysis B: Environmental 111– 112, pp. 233– 245.

47. T. Masui, H. Imadzu, N. Matsuyama, N. Imanaka (2010) *Total oxidation of toluene on $Pt/CeO_2–ZrO_2–Bi_2O_3$-Al_2O_3 catalysts prepared in the presence of polyvinyl pyrrolidone*. Journal of Hazardous Materials 176, pp. 1106–1109
48. J. Wang, M. Shen, Y. An, J. Wang (2008) *Ce–Zr–Sr mixed oxide prepared by the reversed microemulsion method for improved Pd-only three-way catalysts*. Catalysis Communications 10 (1), pp. 103–107
49. U. Lassi, R. Polvinen, S. Suhonen, K. Kallinen, A. Savimäki, M. Härkönen, M. Valden, R.L. Keiski (2004) *Effect of ageing atmosphere on the deactivation of Pd/Rh automotive exhaust gas catalysts: catalytic activity and XPS studies*. Applied Catalysis A: General, 263 (2), pp. 241–248.
50. A. Iglesias-Juez, A. B. Hungria, A. M. Arias, J. A. Anderson, M. Fernandes-Garcia (2009). *Pd-based $(Ce,Zr)O_x$- supported catalyst: promoting effect of base metals (Cr,Cu,Ni) in CO and NO elimination*. Catalysis Today, 143 (3-4), pp.195–202
51. H. J. Kwon, J. H. Baik, Y. T. Kwon, I. Nam, Se H. Oh (2008) *Enhancement effect of water on oxidation reactions over commercial three-way catalyst*. Chemical Engineering Journal, 141 (1-3), pp.194–203
52. L. T. H. Nam, N. T. Minh, N. D. Tuyen, V. A. Tuan, D. X. Dong, L. T. K. Lan, T. T. Khanh, T. T. N. Mai, H. D. Lanh, J. Radnik, E. Roduner (2007) *Research on Au-ZSM5 catalyst for carbon monoxide oxidation to carbon oxide*, 4th Vietnam National Conference on Catalysis and Adsorption HCM city proceedings, pp. 529-534.
53. Tran Que Chi, Tran Thi Minh Nguyet, Luu Tien Hung, Quach Thi Hoang Yen, Nguyen Thi Toan, Nguyen Doan Thai, Nguyen Quoc Trung, Do The Chan, Le Phuc Son (2011), *Preparation of nanoparticle gold over support Co_3O_4 and catalytic activity of Au/Co_3O_4*, Journal of Chemistry, vol 49-5AB, pp. 201-206 .
54. B. Levasseur, S. Kaliaguine (2009), *Effects of iron and cerium in $La_{1-y}Ce_yCo_{1-x}Fe_xO_3$ perovskites as catalysts for VOC oxidation*, Applied Catalysis B: Environmental 88 , pp. 305–314
55. D. Fino, N. Russo, G. Saracco, V. Specchia (2007) *Supported Pd-perovskite catalyst for CNG engines' exhaust gas treatment.* Progress in Solid State Chemistry, 35 (2-4), pp. 501-511
56. L. Forni, C. Oliva, F.P. Vatti a, M.A. Kandala, A.M. Ezerets, A.V. Vishniakov (1996) *La-Ce-Co perovskites as catalysts for exhaust gas depollution*. Applied Catalysis B: Environmental, 7(3-4), pp. 269-284
57. H. Tanaka, N. Mizuno, M. Misono (2003) *Catalytic activity and structural stability of $La_{0.9}Ce_{0.1}Co_{1-x}Fe_xO_3$ perovskite catalysts for automotive emissions control*. Applied Catalysis A: General, 244 (2), pp. 371–382
58. T. T. M. Nguyet, N. Q. Huan, L. V. Tiep, N. V. Quy, N. C. Trang, T. Q. Chi, N. D. Thai, D. T. Chan, N. Q. Trung (2007) *$DeNO_x$ properties of $La_{1-x}Sr_xCoO_3$ perovskite/complex oxides*. 4th Vietnam National Conference on Catalysis and Adsorption HCM city proceedings, pp.511-517
59. Quach Thi Hoang Yen, Tran Thi Minh Nguyet, Nguyen Thi Toan, Tran Que Chi (2011), *Synthesis of nanoparticles of perovskite $La_{1-x}Na_xCoO_3$ using citric acid sol-gel method and its catalytic activity*, Journal of Chemistry, vol 49-5AB , pp. 535-541.

60. A. De Lucas, J.L. Valverde, F. Dorado, A. Romero, I. Asencio (2005), *Influence of the ion exchanged metal (Cu, Co, Ni and Mn) on the selective catalytic reduction of NOX over mordenite and ZSM-5,* Journal of Molecular Catalysis A: Chemical 225 , pp. 47–58.
61. Le Thanh Son, Tran Van Nhan (2007), *The role of oxygen in selective reduction of NOx by C_3H_6 over Cu/ZSM5 catalyst*, 4th Vietnam National Conference on Catalysis and Adsorption HCM city proceedings, pp.494-498.
62. Hoang Tien Cuong, Nguyen Tri, Nguyen Phuc Hoang Duy, Nguyen Thi Thuy Van, Pham Thi Thuy Phuong, Duong Huynh Thanh Linh (2011), *Preparation of catalysts applied for treatment of carbon monoxide in charcoal kilns*, Journal of Chemistry, 49-5AB,pp. 219-227.
63. Le Phuc Nguyen, Tran Hon Quoc, Nguyen Van Hieu, Nguyen Minh Huy (2011), *Study on treatment of NOx in excess oxygen over catalyst MnOx/BaO/Al2O3 by direct thermal decomposition*, Journal of Chemistry, vol.49-5AB,pp. 408-414.
64. Tran Thi Minh Nguyet, Tran Que Chi, Quach Thi Hoang Yen, Nguyen Thi Toan, Nguyen Doan Thai, Nguyen Quoc Trung, Do The Chan, Le Phuc Son (2011), *Study on catalytic activity on oxidation of CO of Co_3O_4-ZrO_2 over cordierite*, Journal of Chemistry, 49-5AB, pp.415-419.
65. Karthik Ramanathan, Vemuri Balakotaiah, David H. West (2003), *Light-off criterion and transient analysis of catalytic monoliths*, Chemical Engineering Science 58, pp. 1381 – 1405
66. J. M. A. Harmsen, J. H. B. J. Hoebink, J. C. Schouten (2001), *Acetylene and carbon monoxide oxidation over a Pt/Rh/CeO2/gamma-Al2O3 automotive exhaust gas catalyst: kinetic modelling of transient experiments,* Chemical Engineering Science 56 , pp. 2019- 2035
67. J.M.A. Harmsen, J.H.B.J. Hoebink, J.C. Schouten (2001), *NO reduction by CO over automotive exhaust gas catalysts in the present of O2*, Catalysis Letters Vol. 71, No. 1-2.
68. Hyuk Jae Kwon, Joon Hyun Baik, Yong Tak Kwon, In-Sik Nam, SeH.Oh (2007), *Detailed reaction kinetics over commercial three-way catalysts,* Chemical Engineering Science 62 , pp. 5042 – 5047
69. E.I. Basaldella, A. Kikot, J.F. Bengoa, J.C. Tara (2002), *ZSM-5 zeolite films on cordierite modules. Effect of dilution on the synthesis medium*, Materials Letters 52, pp. 350–354
70. Juan M. Zamaro, Marı´a A. Ulla, Eduardo E. Miro (2006), *Growth of mordenite on monoliths by secondary synthesis Effects of the substrate on the coating structure and catalytic activity,* Applied Catalysis A: General 314 , pp. 101–113
71. S. Biamino, P. Fino, D. Fino, N. Russo, C. Badini (2005), *Catalyzed traps for diesel soot abatement: In situ processing and deposition of perovskite catalyst*, Applied Catalysis B: Environmental 61 , pp.297–305
72. Valérie Meille (2006), *Review on methods to deposit catalysts on structured surfaces*, Applied Catalysis A: General 315, pp. 1–17.

73. C. Agrafiotis, A. Tsetekou, A. Ekonomakou (1999), *The effect of particle size on the adhesion properties of oxide washcoats on cordierite honeycombs*, JOURNAL OF MATERIALS SCIENCE LETTERS 18, pp.1421 – 1424
74. L. Villegas, F. Masse, N. Guilhaume (2007), *Wet impregnation of alumina - washcoated monoliths. Effect of the drying preocedure on Ni distribution and on autothermal reforming activity*, Applied Catalysis A: General 320, pp. 43–55.
75. C. Agrafiotis, A. Tsetekou (2002), *Deposition of meso-porous γ -alumina coatings on ceramic honeycombs by sol-gel methods*, Journal of the European Ceramic Society 22, pp. 423–434
76. R.Zapf, C.Becker-Williger, K.Berresheim (2003), *Detained characterization of various porous alumina-based catalyst coatings within microchannels and their testing for methanol steam reforming*, Trans IChemE, Vol 81, Part A..
77. P. Pfeifer, K. Schubert, G. Emig (2005), *Preparation of copper catalyst washcoats for methanol steam reforming in microchannels based on nanoparticles*, Applied Catalysis A: General 286 , pp. 175–185.
78. P. Pfeifer, K. Schubert, M.A. Liauw, G. Emig (2004), *PdZn catalysts prepared by washcoating microstructured reactors*, Applied Catalysis A: General 270, pp. 165–175.
79. Dimitris K. Liguras, Katerina Goundani, Xenophon E. Verykios (2004) , *Production of hydrogen for fuel cells by catalytic partial oxidation of ethanol over structured Ni catalysts*, Journal of Power Sources 130, pp. 30–37.
80. L.F. Liotta, A. Longo, G. Pantaleo, G. Di Carlo, A. Martorana, S. Cimino, G. Russo, G. Deganello (2009), *Alumina supported Pt 1%-Ce 0.6Zr0.4O2 monolith: Remarkable stabilization of ceria–zirconia solution towards CeAlO3 formation operated by Pt under redox conditions*, Applied Catalysis B: Environmental 90, pp. 470–477.
81. A. Rouge, B. Spoetzl, K. Gebauer, R. Schenk, A. Renken (2001), Microchannel *reactors for fast periodic operation: the catalytic dehydration ofisopropanol*, Chemical Engineering Science 56 , pp.1419-1427.
82. Joan Papavasiliou, George Avgouropoulos, Theophilos Ioannides (2006), *In situ combustion synthesis of structured Cu-Ce-O and Cu-Mn-O catalysts for the production and purification of hydrogen*, Applied Catalysis B: Environmental 66 , pp. 168–174
83. Albert N. Shigapov, George W. Graham, Robert W. McCabe, Michellene Paputa Peck, H. Kiel Plummer Jr. (1999), *The preparation of high-surface-area cordierite monolith by acid treatment*, Applied Catalysis A: General 182, pp. 137±146.
84. Zeger Hens, Pascal Vandervoort, Isabel Vandriessche (2010), Solid state chemistry 2010, Ghent University, 176-177
85. Ye Liu, Ding Ma, Xiuwen Han, Xinhe Bao, Wiebke Frandsen, Di Wang, Dangsheng Su (2008,), *Hydrothermal synthesis of microscale boehmite and gamma nanoleaves alumina*, Materials Letters, Volume 62, Issues 8–9, Pages 1297–1301
86. Seung-Moon Kim, Yun-Jo Lee, Ki-Won Jun, Jo-Yong Park, H.S. Potdar (2007), *Synthesis of thermo-stable high surface area alumina powder from sol–gel*

derived boehmite, Materials Chemistry and Physics, Volume 104, Issue 1, , Pages 56–61.

87. N. Lepot, M.K. Van Bael, H. Van den Rul, J. D'Haen, R. Peeters, D. Franco, J. Mullens (2008), *Synthesis of platelet-shaped boehmite and γ-alumina nanoparticles via an aqueous route*, Ceramics International, Volume 34, Issue 8, , Pages 1971–1974.
88. R. Di Monte, P. Fornasiero, J. Kaˆspar, M. Graziani, J. M. Gatica, S. Bernal, A. G ómez-Herrero (2000), *Stabilisation of nanostructured $Ce_{0.2}Zr_{0.8}O_2$ solid solution by impregnation on Al_2O_3: a suitable method for the production of thermally stable oxygen storage/release promoters for three-way catalysts*, Chem. Commun., pp. 2167–2168
89. Rui Si, Ya-Wen Zhang, Chao-Xian Xiao, Shi-Jie Li, Bing-Xiong Lin, Yuan Kou, Chun-Hu a Yan (2004), *Non-template hydrothermal route derived mesoporous $Ce_{0.2}Zr_{0.8}O_2$ nanosized powders with blue-shifted UV absorption and high CO conversion activity*, Phys. Chem. Chem. Phys. 6, pp. 1056–1063
90. Qiuyan Wang, Guangfeng Li, Bo Zhao, Renxian Zhou (2011), *Investigation on properties of a novel ceria–zirconia–praseodymia solid solution and its application in Pd-only three-way catalyst for gasoline engine emission control*, Fuel 90, pp. 3047–3055.
91. Qiuyan Wang, Guangfeng Li, Bo Zhao, Renxian Zhou (2011), *The effect of Nd on the properties of ceria–zirconia solid solution and the catalytic performance of its supported Pd-only three-way catalyst for gasoline engine exhaust reduction*, Journal of Hazardous Materials 189,pp. 150–157
92. Qiuyan Wang, Guangfeng Li, Bo Zhao, Renxian Zhou (2010), *The effect of La doping on the structure of $Ce_{0.2}Zr_{0.8}O_2$ and the catalytic performance of its supported Pd-only three-way catalyst*, Applied Catalysis B: Environmental 101, pp. 150–159.
93. Yucheng Du, Shuli Shi, Hong He, Hongxing Dai (2011), *Fabrication and characterization of Ce0.7Zr0.3O2 nanorods having high specific surface area and large oxygen storage capacity*, Particuology 9 , pp. 63–68
94. Michael J. Hudson* and James A. Knowles (1996), *Preparation and characterisation of mesoporous, high-surface-area zirconium (IV) oxide*, J. Muter. Chem., 6(l), pp. 89-95
95. Gu Yingying, Feng Shengsheng, Li Jinlin, Gu Xiangkui, Wang M anjuan (2007), *Preparation of Mesoporous $Ce_{0.5}Zr_{0.5}O_2$ Mixed Oxide by Hydrothermal Templating Method*, JOURNAL OF RARE EARTHS 25, pp. 710 - 714.

PUBLISHED REPORTS:

1) **Phạm Thị Mai Phương**, Nguyễn Thế Tiến, Đặng Lý Nhân, Isabel van Driessche, Lê Minh Thắng, *Tổng hợp hệ chất mang và chất nền của hệ xúc tác ba chức năng, xử lý khí thải động cơ đốt trong*, Tạp chí hóa học, số T49 (5AB), tr. 432-438, 2011

2) **Phạm Thị Mai Phương**, Nguyễn Thị Hồng Ngân, Nguyễn Quang Minh, Nguyễn Thế Tiến, Isabel Van Driessche, Lê Minh Thắng (2012) *Nghiên cứu xử lý khí thải động cơ đốt trong trên hệ xúc tác Mn, Co, Ce trên oxit γ-Al_2O_3*, Tạp chí Hóa học, số T.50 (4A) tr. 355-358

3) **Phạm Thị Mai Phương**, Nguyễn Quang Minh, Nguyễn Thế Tiến, Isabel Van Driessche, Lê Minh Thắng, *Nghiên cứu các phương pháp tổng hợp Cordierite để ứng dụng trong chế tạo xúc tác ba chức năng*, Tạp chí hóa học T50 (5B), tr 135-138, 2012

4) **Phạm Thị Mai Phương,** Lê Khắc Thiện, Nguyễn Thế Tiến, Isabel Van Driessche, Lê Minh Thắng (2013) *Nghiên cứu tổng hợp cordierite từ cao lanh, nhom hydroxit và dolomite, ứng dụng trong chế tạo xúc tác ba chức năng*, Tạp chí Hóa học T.51 (2AB), tr. 238-242

APPENDIX

Appendix 1: BET results

1. Sample γ-Al_2O_3

Micromeritics Instrument Corporation

Gemini VII 2390 V1.02 (V1.02 t) Unit 1 Serial #: 188 Page 1

Sample: phuong- gamma Al2O3 Pore 24.05.2013
Operator:
Submitter:
File: D:\HUNGDO\BETFIL~1\001-147.SMP

Started: 5/24/2013 12:54:00PM Analysis Adsorptive: N2
Completed: 5/25/2013 10:45:44AM Equilibration Time: 10 s
Report Time: 9/6/2013 1:53:41PM Sat. Pressure: 101.9630 kPa
Free Space Diff.: -0.3025 cm^3 Sample Mass: 0.2138 g
Free Space Type: Measured Sample Density: 1.000 g/cm^3
Evac. Rate: 133.32 kPa/min Gemini Model: 2390 t

Summary Report

Surface Area

Single point surface area at p/p° = 0.299918955: 243.6937 m^2/g

BET Surface Area: 249.3060 m^2/g

t-Plot Micropore Area: 5.1875 m^2/g

t-Plot External Surface Area: 244.1185 m^2/g

BJH Adsorption cumulative surface area of pores
between 17.000 Å and 3000.000 Å width: 299.744 m^2/g

Pore Volume

t-Plot micropore volume: 0.001037 cm^3/g

BJH Adsorption cumulative volume of pores
between 17.000 Å and 3000.000 Å width: 0.920919 cm^3/g

Pore Size

BJH Adsorption average pore width (4V/A): 122.894 Å

BJH Desorption average pore width (4V/A): 122.618 Å

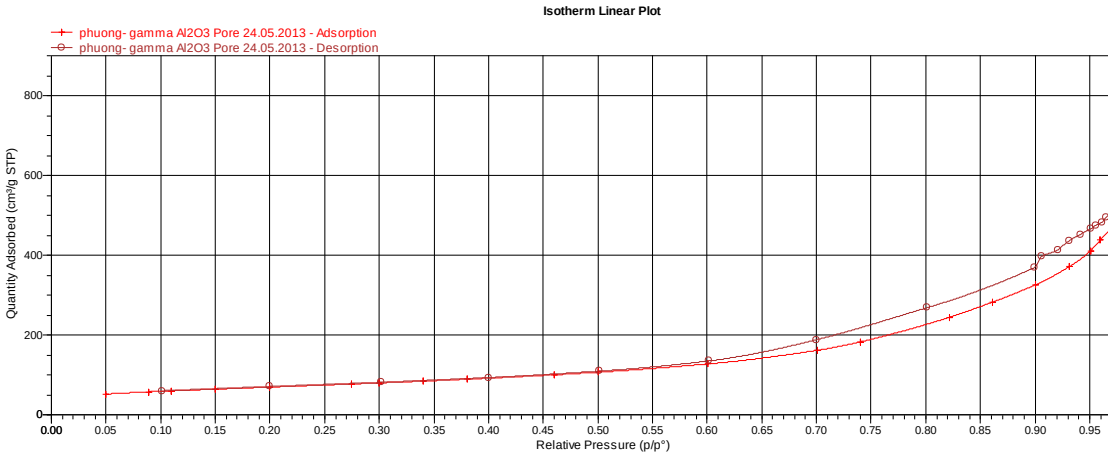

Isotherm Linear Plot

phuong- gamma Al2O3 Pore 24.05.2013 - Adsorption

Relative Pressure (p/p°)	Quantity Adsorbed (cm³/g STP)
0.049631	51.7563
0.0894063	57.4684
0.109387	59.8708
0.149604	64.2874
0.199726	69.4898
0.274826	77.2863
0.299919	79.9627
0.34019	84.4829
0.3805	89.3103
0.460293	100.19
0.499992	106.538
0.600164	127.217
0.700571	161.596
0.740602	182.873
0.82157	244.465
0.860684	282.223
0.900418	325.679
0.931527	371.514
0.950528	411.286
0.959831	437.274
0.972023	473.804
0.979457	504.698
0.990693	569.308
0.994619	597.19
0.999709	689.51
1.00171	855.132

phuong- gamma Al2O3 Pore 24.05.2013 - Desorption

Relative Pressure (p/p°)	Quantity Adsorbed (cm³/g STP)
1.00171	855.132
0.996289	735.497
0.994793	704.614
0.993172	668.24
0.988757	613.803

0.986608	588.105
0.981001	552.493
0.978716	534.541
0.970736	509.292
0.965463	495.14
0.961141	482.749
0.955695	475.172
0.951062	465.987
0.94118	452.426
0.930963	436.216
0.920653	414.02
0.90584	396.579
0.898994	369.015
0.801493	268.25
0.700103	188.002
0.601162	134.828
0.501197	109.293
0.399965	92.8355
0.301602	81.1591
0.199911	70.5619
0.101366	59.9957

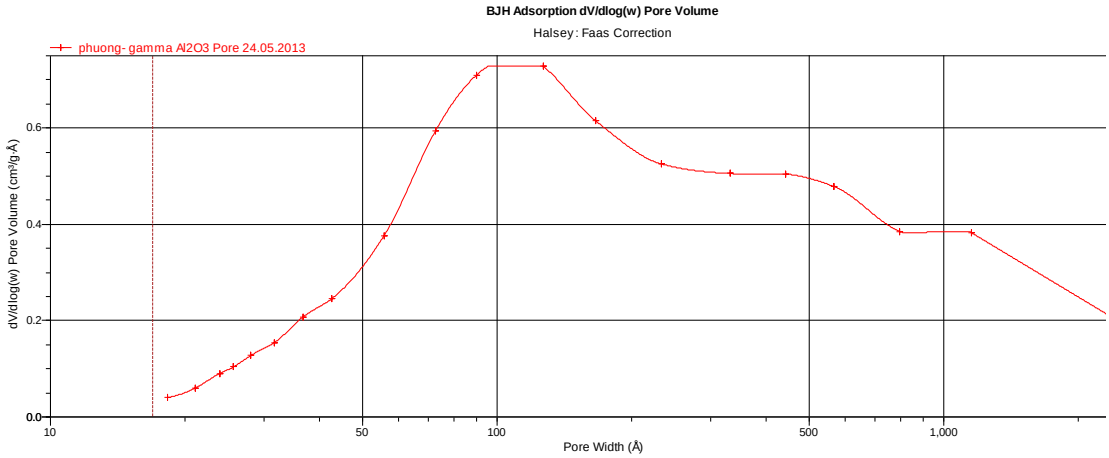

BJH Adsorption dV/dlog(w) Pore Volume

phuong- gamma Al2O3 Pore 24.05.2013

Pore Width (Å)	dV/dlog(w) Pore Volume (cm³/g·Å)
2469.63	0.197631
1151.43	0.382602
796.32	0.38526
565.978	0.478612
441.99	0.504257
332.812	0.505559
233.306	0.525244
166.211	0.61494
127.049	0.727641
89.9269	0.710111
72.6173	0.594113
55.8979	0.376865
42.6158	0.245587

36.7006	0.207616
31.6807	0.15455
28.0277	0.127497
25.6566	0.10364
23.9285	0.0906068
21.0618	0.0598852
18.2345	0.0397202

Appendix 2: Catalytic activity of complete catalyst

1. Ca.2: MnO_2-NiO-Co_3O_4 / cordierite

TEMP (oC)	NO	C3H6	CO
0	0	0	0
150	0.818263	0.17566	0.04493
200	4.540558	1.291127	3.308896
250	4.015678	6.752768	93.41245
300	7.265809	42.4512	96.00409
350	17.77029	69.31209	97.01037
400	28.76298	79.26724	97.86116
450	39.29496	85.20906	98.39581
500	44.02805	89.65607	98.35978
550	56.88991	92.90477	98.17637

2. Ca.3: MnO_2-NiO-Co_3O_4 / $Ce_{0.2}Zr_{0.8}O_2$ / cordierite

TEMP (oC)	NO	C3H6	CO
0	0	0	0
150	0.16336	1.051633	0.20209
200	4.332924	3.069786	1.847914
250	22.45395	76.49654	97.63681
300	24.89408	82.67938	99.5201
350	37.2894	89.19118	99.7433
400	26.22923	97.51294	99.93822
450	31.81905	99.15781	99.80283
500	41.1643	100	99.89653
550	47.16348	100	99.9109

3. Ca.5: MnO_2-Co_3O_4-CeO_2 / γ-Al_2O_3/cordierite

TEMP (oC)	C3H6	CO
150	1.18	0
200	1.23	0
250	70.86	92.88
300	76.06	94.11
350	81.09	95.5
400	85.09	97.04

450	88.42	97
500	91.24	97.68

4. Ca.6: MnO_2-Co_3O_4 – CeO_2 / $Ce_{0.2}Zr_{0.8}O_2$ / cordierite

TEMP (oC)	C3H6	CO
150	1.22	2.59
200	1.98	2.12
250	2.33	96.88
300	83.88	97.2
350	86.21	98
400	88.67	98.59
450	90.54	98.74
500	98.77	98.77

5. Ca.7: MnO_2-Co_3O_4-CeO_2 / $AlCe_{0.2}Zr_{0.05}O_2$ /cordierite

TEMP (oC)	C3H6	CO
150	2.16	0.5
200	42.78	2.81
250	79.85	83.45
300	82.86	87.17
350	85.24	89.33
400	87.73	94.76
450	89.47	95.76
500	91.17	96.84

Appendix 3: Emission results tested by **National Motor Vehicle Emission Test Center** - NETC

Table 1: Emission of Vespa LX motorbike using prepared MnO_2-Co_3O_4-CeO_2 / $AlCe_{0.2}Zr_{0.05}O_2$ / honeycomb cordierite

Speed	CO (%)	CO_2 (%)	HC(ppm)
Nomal ideal mode (1704r/min)	0,484	4,2	84
High ideal mode (3269 r/min)	0,528	6,3	99

Table 2: Emission of Vespa LX motorbike using commercial catalyst

Speed	CO (%)	CO_2 (%)	HC(ppm)
Nomal ideal mode (1827r/min)	0,208	7,1	113
High ideal mode (2204 r/min)	0,12	15,4	72